University of Alberta

Structural Characterization of Protein-Protein Interactions for the Uev/Ubc13 Heterodimer: Insights into Lys63-Linked Polyubiquitin Chain Assembly

by

Michael Lewis 

A thesis submitted to the Faculty of Graduate Studies and Research in partial fulfillment of the requirements for the degree of **Master of Science**.

Department of Biochemistry

Edmonton, Alberta
Spring, 2006

Your file Votre référence
ISBN: 0-494-13841-6
Our file Notre référence
ISBN: 0-494-13841-6

Abstract

Protein ubiquitination is a biochemical strategy exercised by eukaryotes that signals for a wide variety of downstream events. Selectivity of downstream effects largely depends on the topology of the ubiquitin signal employed. Polyubiquitin chains are created through the formation of an isopeptide bond between the C-terminus of one ubiquitin, and a side chain lysine of a second ubiquitin.

Assembly of lysine 63-linked polyubiquitin chains is catalyzed by a Uev/Ubc protein complex. Using solution state nuclear magnetic resonance spectroscopy, we have characterized the interaction between Mms2, a member of the Uev family, and ubiquitin. The structure provides insights into the selective assembly of lysine 63-linked polyubiquitin chains that ultimately signal for activation of DNA repair enzymes. Nuclear magnetic resonance was also employed to probe the interaction between Ubc13 and the ubiquitination target protein Traf6, a vital signalling component of the NF-κB pathway.

Acknowledgements

I would like to thank the following people and organizations:

(i) The Canadian Institutes of Health Research (CIHR), and the Alberta Heritage Foundation for Medical Research (AHFMR) for funding this research.

(ii) Members of the Spyracopoulos and Sykes labs for their valuable input with respect to experimental design, as well as assistance with respect to NMR spectral acquisition, Unix scripting, and software usage.

(iii) Dr. Leo Spyracopoulos for providing an educational and enjoyable laboratory experience, and for his support and direction throughout my graduate career.

(iv) The Canadian National High Field NMR Centre (NANUC) for their assistance and use of the facilities.

(v) Deryk Webb for spectrometer maintenance, Yanni Batsiolas and Dean Schieve for computer support, and Sue Smith for secretarial assistance.

(vi) Dr. Wei Xiao from the University of Saskatchewan for providing DNA clones used in my research.

(vii) David Hau, Haley Cleary, Heather McMurtrie, and the regular crew of "Open Mike" Night for keeping me from taking things too seriously.

(viii) My family, as well as Oriana Pegoraro, Joseph Henke, and Shaun Goodhope for balancing my life outside of the lab, and for their support over the years.

Contents

List of Figures

List of Tables

List of Symbols

AIR - Ambiguous Interaction Restraint

BB - Backbone

Chfr - Checkpoint Containing FHA and RING finger

CR - Cysteine Rich

CSI - Chemical Shift Index

CUE - Homologous to yeast Cue1p

diUb - Di-Ubiquitin

dsDNA - Double-Stranded DNA

E1 - Ubiquitin Activating Enzyme

E2 - Ubiquitin Conjugating Enzyme

E3 - Ubiquitin Ligase

ERAD - Endoplasmic Reticulum-Associated Degradation

FHA - Forkhead-Associated

IκB - Inhibitor of NF-κB

IKK - IκB Kinase

IPTG - Isopropyl β-D-thiogalactopyranoside

ISG15 - Interferon-Stimulating Gene 15

LIST OF SYMBOLS

ITC - Isothermal Titration Calorimetry

LRR - Leucine-Rich Repeat

MMS - Methyl Methane Sulfonate

MoCo - Molybdenum Cofactor

mono-Ub - Mono-Ubiquitin

MVB - Multivesicular Body

NMR - Nuclear Magnetic Resonance

NOE - Nuclear Overhauser Effect

NZF - Novel Zinc Finger

PCNA - Proliferating Cell Nuclear Antigen

PDB - Protein Data Bank

Pol δ - DNA polymerase δ

Pol η - DNA polymerase η

Pol ζ - DNA polymerase ζ

poly-Ub - Poly-Ubiquitin

PRR - Post-Replication Repair

RMSD - Root Mean Squared Deviation

ssDNA - Single-Stranded DNA

SUMO - Small Ubiquitin-Like Modifier

TAB - TAK1-Binding Protein

TAK1 - TGFβ-Activating Kinase 1

TKB - Tyrosine Kinase Binding

TLS - Translesion Synthesis

TNF - Tumor Necrosis Factor

LIST OF SYMBOLS

TRAF - TNF Receptor-Associated Factor

TSG101 - Tumor Susceptibility Gene 101

Ub - Ubiquitin

Ub_2 - Di-Ubiquitin Conjugate

Ub_4 - Tetra-Ubiquitin Conjugate

UBA - Ubiquitin Associated Domain

UBC - Ubiquitin Conjugating Domain

Ubl - Ubiquitin-Like Modifier

UFD - Ubiquitin Fold Domain

UIM - Ubiquitin Interacting Motif

UV - Ultra-Violet

VHL - von Hippel-Lindau

VPS - Vacoule Protein Sorting

List of Software Programs

Adobe Acrobat 5.0
PDF preparation (Mac OS X)
`www.adobe.com`

Adobe Photoshop 7.0
Graphics editing and figure preparation (Mac OS X)
`www.adobe.com`

Aqua 3.2
NOE restraint plotting and violation computation (Linux)
`tang.bmrb.wisc.edu/~jurgen/aqua/`

CorelDraw 11
Graphics editing and figure preparation (Mac OS X)
`www.corel.com`

CNS 1.1
Simulated annealing and energy minimization (Linux)
`cns.csb.yale.edu/v1.1/`

HADDOCK 1.3
Data-driven docking (Linux)
`www.nmr.chem.uu.nl/haddock/`

KaleidaGraph 3.6
Data graphing and analysis (Mac OS X)
`www.synergy.com`

NMRDraw 2.3
Companion graphical interface for NMRPipe (Linux)
`spin.niddk.nih.gov/bax/software/NMRPipe/`

NMRPipe
NMR spectrum processing (Linux)
`spin.niddk.nih.gov/bax/software/NMRPipe/`

NMRView 5.2.2
NMR spectrum visualization and assignment (Linux)
`onemoonscientific.com/nmrview/`

Procheck-NMR 3.5.4
NMR ensemble quality analysis (Linux)
`www.biochem.ucl.ac.uk/~roman/procheck_nmr/procheck_nmr.html`

Pymol 0.98
PDB visualization (Linux, Mac OS X)
`pymol.sourceforge.net/`

Sparky 3.110
NMR spectrum visualization and assignment (Linux, Mac OS X)
`www.cgl.ucsf.edu/home/sparky/`

STC 5.0
Free energy calculations for protein-ligand interactions (Mac OS X)
`www.bionmr.ualberta.ca/bds/software/stc/latest/index.html`

TeXShop 1.40
LaTeX editor and typesetter (Mac OS X)
`www.uoregon.edu/~koch/texshop/`

Chapter 1

Introduction to Ubiquitin Biochemistry

1.1 Ubiquitin Biology

The post-translational modification of proteins is an efficient mechanism for altering the physical and chemical characteristics of a protein. Post-translational modifications take a variety of forms, including phosphorylation, glycosylation, acetylation, lipidation, methylation, and the topic of this thesis, ubiquitination. Compared to smaller modifications, ubiquitination is a high-energy, resource-heavy process, but a ubiquitin tag also has a much larger and more chemically varied surface available for protein-protein interactions. Indeed, there are several ubiquitin-binding proteins that recognize ubiquitin and ubiquitin-related modifiers through ubiquitin-binding motifs. The diversity in the number of protein-protein interactions at the surface of ubiquitin reflects the biochemical diversity observed in ubiquitin signalling.

Since its discovery in 1978 [19], ubiquitin has been implicated in a wide array of eukary-

otic cell processes, such as proteolysis [29], endocytosis [36], and DNA repair [4]. Given the wide variety of biological consequences of ubiquitination, the number of diseases caused by defects in the process is not surprising. Liddle's Syndrome, Angelman Syndrome, Cystic Fibrosis, neurodegenerative diseases such as Alzheimer's Disease, and some cancers have implicated the ubiquitination system as a causative factor [29].

The first role assigned to ubiquitination has been termed the "classical", or "canonical", pathway and signals for protein degradation [35]. It is now clear that many of the new roles assigned to ubiquitin are derived from "non-canonical", or "variant" ubiquitin signals, and as such, the construction of these variant ubiquitin signals is of great interest. One of these signals is involved in post-replicative DNA repair and immune response activation, and is the subject of this dissertation.

1.2 The Protein Ubiquitination Cascade

Protein ubiquitination involves the mechanistic action of a cascade of three enzymes [35], reviewed in references [29, 86, 85] (Figure 1.1). First, a Ub-activating enzyme, or E1, forms a thiolester bond between an E1 cysteine and the C-terminal Gly76 of Ub in an ATP-dependent manner. The activated Ub is subsequently transferred from the E1 to a cysteine residue of a Ub-conjugating enzyme, or E2, in a transthiolesterification reaction. A Ub-ligase, or E3, then localizes the E2 to a target protein, where the C-terminus of Ub is conjugated to either an ϵ-NH_3^+ group, or the α-NH_3^+ terminus on the target through an isopeptide linkage. Multi-Ub chains can be built up by the formation of isopeptide bonds between the ϵ-NH_3^+ of one Ub and the C-terminus of the next Ub, through a mechanism that is presently unclear [29].

In spite of the breadth of downstream consequences of protein ubiquitination, most eu-

karyotes (plants are an exception) possess only a single ubiquitin activating enzyme (UBA1 in yeast). This enzyme transfers activated Ub to all known ubiquitin conjugating enzymes, of which there are eleven known in yeast, and many more have been discovered in higher organisms [86]. Of the known enzymes, most E2s interact with multiple E3s, and most E3s have several known target substrates [29]. Exceptions to this rule include substrate targetting by more than one E3, and E3 targetting by more than one E2. Nevertheless, the organization of the system allows for a large diversity of signalling responses [29].

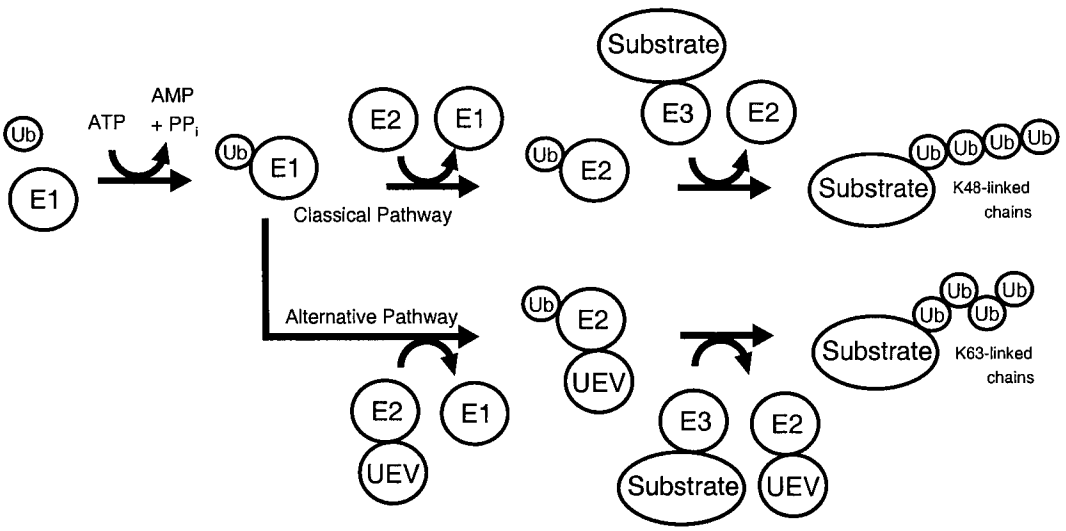

Figure 1.1: **The Ubiquitination Cascade.** Pathway of ubiquitin transfer for both the "classical", Lys48-linked polyubiquitin chain formation pathway, and the "alternative", Lys63-linked polyubiquitin chain formation pathway. Linkage specificity is determined by the E2/UEV heterodimer.

1.3 Ubiquitin and Ubiquitin-Like Modifiers

Ubiquitin is a heat stable [19], 76 amino acid protein that is found throughout the eukaryotic kingdom. It is highly conserved, showing only a three residue difference between the yeast and human sequences [86], for example. The structure contains three α-helices and

five β-strands. These secondary structural elements form the commonly occuring "Ubiquitin fold", where the β-sheet packs against a twelve residue α-helix (Figure 1.2A). The C-terminus contains two glycine residues, which are solvent exposed and accessible for chain elongation. Additionally, of the seven lysine residues in the sequence, three are fully exposed (6, 33, and 63) and four are partially exposed (11, 27, 29, and 48), and therefore likely available for poly-Ub chain extension [113].

The charge distribution on the surface of Ub includes a basic "stripe" formed by Arg42, Arg72, and Arg74 [21], and a hydrophobic "patch" formed primarily by Ile44, Val70, and Leu8 [6]. These surface regions may partly explain the evolutionary conservation of the Ub sequence, as they are known to interact with a wide range of targets, including Ub E1, E2s, the proteasome, and the other ubiquitin-binding domains [86].

There are other Ub-like modifier proteins (Ubls), such as SUMO (Small Ub-Like Modifier) and NEDD8 (Rub1 in yeast) (Figure 1.2). Other less-well known Ubls include the interferon-stimulating gene 15 (ISG15), and the autophagy-associated Ubls AUT7 and APG12 (reviewed in [95]).

SUMOlation occurs in all eukaryotes, playing essential roles in many areas including nuclear transport, transcriptional regulation, cell-cycle control, and DNA repair (SUMO is reviewed in [67], see section 1.8.2 for details regarding DNA repair). Four SUMO isoforms have been discovered in humans, and solution structures have been solved for two of them: SUMO-1 [5] and SUMO-3 [26]. Interestingly, SUMO-1 and Ub share the same protein fold, though they are only 18% identical in sequence. SUMO-1 differs from Ub in surface charge distribution and it contains an additional N-terminal extension. Additionally, SUMO-1 does not contain any of the conserved Ub lysines except that corresponding to Lys6 [5].

SUMO isoforms -2 and -3 are nearly identical in sequence ($\sim$97% identity between

SUMO-2 and -3), but only ~47% identical to SUMO-1. Interestingly, SUMO-3 is only 14% identical to Ub, but is structurally more similar to Ub than to SUMO-1 [26] (Figure 1.2B). The most striking difference between isoforms, however, is that both SUMO-2 and -3 contain the consensus SUMOylation motif ψKXE (where ψ is large and hydrophobic) at their N-termini, and have been observed to form poly-SUMO chains *in vivo* (SUMO-2) and *in vitro* (SUMO-3), whereas this functionality is absent in SUMO-1 [106].

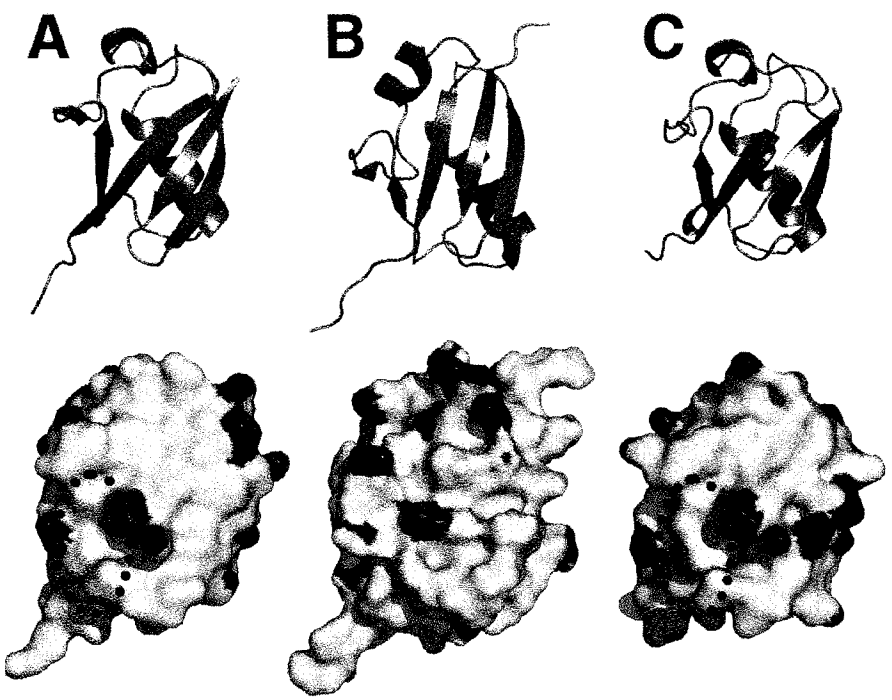

Figure 1.2: **Ubiquitin-Like Folds.** Ubiquitin-like folds shown in cartoon (top) and surface representation (bottom). Positively charged atoms are colored in blue, negatively charged atoms are colored in red, aliphatic atoms from hydrophobic residues (Ala, Ile, Leu, Val, Phe, Tyr, Met, Pro) are colored in yellow, and atoms from polar residues are colored in white. The conserved Ile44, Val70, Leu8 hydrophobic patch is encircled. Shown are (A) Ubiquitin [1UBQ], (B) SUMO-3 [1U4A], and (C) NEDD8 [1NDD].

The Ubl NEDD8 is most similar in sequence to Ub (60% identical), and plays a key role in cell-cycle control. Specifically, NEDD8 modifies and thereby regulates the SCF family of ubiquitin ligases [95] (SCF complexes are covered in detail in section 1.6.2). The crystal

structure of NEDD8 shows a similar charge distribution as Ub across its surface, and displays a hydrophobic surface "patch" that is identical in both sequence and solvent accessibility (Figure 1.2C). Several of the lysine residues, including Lys48, are conserved [118], though poly-NEDD8 chains have yet to be observed *in vivo*.

1.4 Ubiquitin-Activating Enzymes

The ubiquitin activating enzyme, E1, is the first enzyme in the protein ubiquitination cascade and catalyzes an ATP-dependent, two-step reaction to form a E1-Ub thiolester intermediate [31]. In the first step, the E1 binds ATP, then Ub, and subsequent ATP hydrolysis drives formation of the Ub-adenylate intermediate at the Ub C-terminus:

$$E1_{SH} + Ub + ATP \cdot Mg \rightleftharpoons E1_{SH}^{\cdot AMP\text{-}Ub} + PP_i \tag{1.1}$$

In the second step, the adenylate donates Ub to the active site cysteine residue of the E1, resulting in the formation of a high-energy thiolester intermediate:

$$E1_{SH}^{\cdot AMP\text{-}Ub} \rightleftharpoons E1_{S\text{-}Ub} + AMP \tag{1.2}$$

With the adenylation site free, the E1-Ub thiolester can initiate a second adenylation:

$$E1_{S\text{-}Ub} + Ub + ATP \cdot Mg \rightleftharpoons E1_{S\text{-}Ub}^{\cdot AMP\text{-}Ub} + PP_i \tag{1.3}$$

Generally, different Ubls are activated by specific activating enzymes [86], regardless of the structural similarity of some Ubls. The discriminating factor on Ub, previously implicated by mutational analysis [15], appears to be a single residue, Arg72. The Ub R72L mu-

tation enables activation by the NEDD8 E1 (APPBP1-UBA3) [8, 115], and likewise, the NEDD8 A72R mutation enables NEDD8 activation by the Ub E1 [118].

The structural basis for the E1-Ub interaction is currently unknown, but has been inferred by analogy to the crystal structures of NEDD8 in complex with its E1 (APPBP1-UBA3-NEDD8-ATP) [115], and MoeB in complex with MoaD [60]. In the APPBP1-UBA3-NEDD8-ATP structure (Figure 1.3A), NEDD8 binds to a large cleft on the cognate E1 through two faces on its globular domain: an acidic face, and a hydrophobic face which contains the conserved Leu8, Ile44, Val70 hydrophobic patch (residue numbering identical to ubiquitin). The seven residue, hydrophobic C-terminal tail extends along a groove on the E1, and the terminus is positioned 4 Å away from the α-phosphate of bound ATP [115]. The high sequence conservation of the E1-interacting residues of NEDD8 and Ub (aside from the "specificity determining" residue 72, the tail is completely conserved [118, 115]), and the complete conservation of the ATP binding sites of both E1s, suggest that Ub interacts with its E1 in an analogous manner, and it is likely that other Ubls bind their cognate E1s similarily as well [115].

The mechanism of adenylation revealed by the E1-NEDD8-ATP structure is consistent with the adenylation mechanism that was proposed based upon the MoeB-MoaD-ATP structure (Figure 1.3B). In *Escherichia coli*, MoeB activates MoaD to form a MoaD acyl-adenylate, which is then converted to a thiocarboxylate by a sulphurtransferase, thus allowing it to act as a sulphur donor during MoCo (Molybdenum Cofactor) biosynthesis [60]. The proposed mechanism predicts that the C-terminus of MoaD/Ubl is brought within catalytic distance of the α-phosphate of ATP, with Mg^{2+} positioned to alleviate electrostatic repulsion between the two groups. The C-terminal carboxylate oxygen attacks the α-phosphate to form a trigonal bi-pyramidal intermediate, followed by strain-facilitated cleavage of the

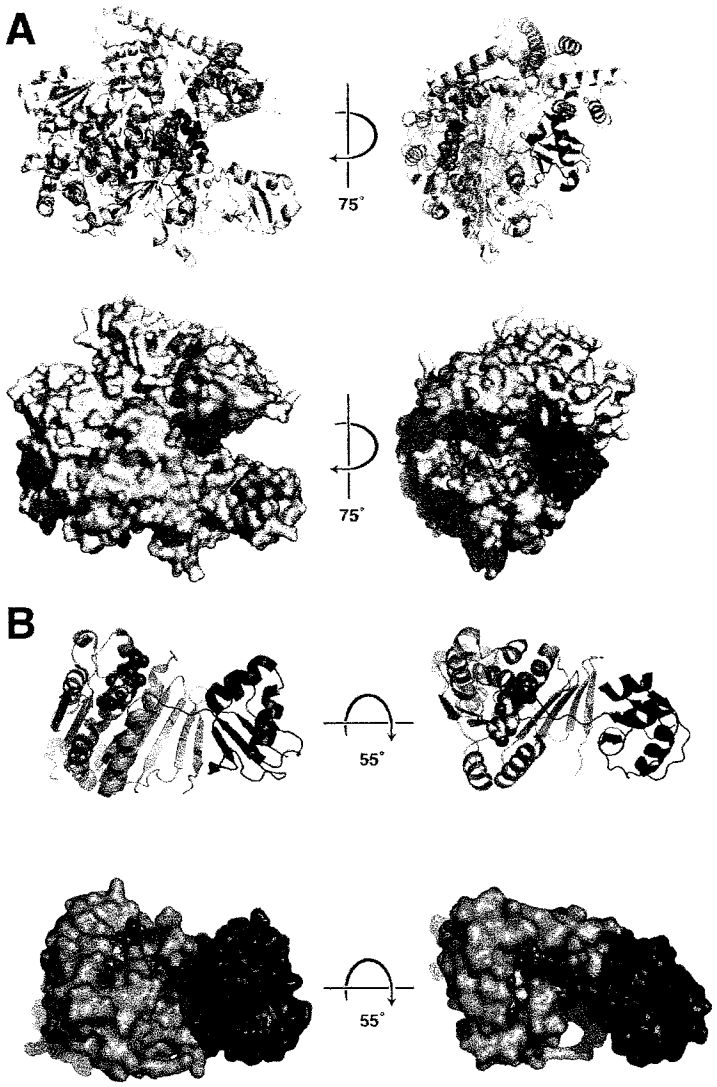

Figure 1.3: **Structural Basis for Peptide Adenylation.** (A) Crystal structure of APPBP1-UBA3-NEDD8-ATP [1R4N] in cartoon (top) and surface (bottom) representation. APPBP1, the catalytic domain, is shown in green, and UBA3, the adenylation domain, is shown in gold. A cleft in the adenylation domain incorporates the C-terminal tail of NEDD8 (pink), placing it in close proximity to the bound ATP (blue spheres). Bound zinc is shown in grey. (B) Crystal structure of the MoeB-MoaD-ATP complex [1JWA] in cartoon (top) and surface (bottom) representation. MoeB (grey) coordinates the C-terminal tail of MoaD (pink) across a cleft towards the bound ATP (spheres, colored by element).

bond between the α- and β-phosphates [60].

Details about the second step in the reaction are currently a mystery, although protein flexibility is expected to play a role. In the case of E1-NEDD8, this certainly appears to be the case; NEDD8 is able to bind to its E1 such that its C-terminus is only 4 Å away the ATP α-phosphate, but the adenylation reaction leaves the C-terminus-AMP ~35 Å away from the catalytic cysteine residue of the E1. In order to close the gap, the E1 catalytic domain would have to undergo a 10° rotation with respect to the adenylation domain [115].

1.5 Ubiquitin-Conjugating Enzymes

1.5.1 Conventional ubiqutin-conjugating enzymes

After activation, ubiquitin is transferred from the E1 to the active site cysteine of an E2, or ubiquitin conjugating enzyme, in a transthiolesterification reaction [35]:

$$E1^{\cdot AMP\text{-}Ub}_{S\text{-}Ub} + E2_{SH} \rightleftharpoons E1^{\cdot AMP\text{-}Ub}_{SH} + E2_{S\text{-}Ub} \tag{1.4}$$

In yeast, there are 13 known E2s: 11 conjugate ubiquitin, one conjugates SUMO, and another conjugates NEDD8. E2s contain a conserved, ~150 residue UBC domain, which consists of four anti-parallel β-strands packed against four α-helices [22]. The active site cysteine is positioned along a loop region, inside a shallow cleft on the E2 surface (reviewed in references [86, 85, 29]).

Ubiquitin-conjugating enzymes can be further sub-divided into three categories, based on existing extensions to the core domain. Class I E2s consist of just the UBC core, Class II E2s contain a C-terminal extension, and Class III E2s contain an N-terminal extension [69]. These tails have been proposed to play a variety of roles, and are reviewed in reference [85].

At least twelve class II E2s, including yeast Ubc1, contain ubiquitin-binding UBA domains in their extensions [119], suggesting a role in orienting Ub molecules for nucleophilic attack by the thiolester-bound Ub [69]. Other proposed roles include inhibiting excessive chain elongation [37], directing alternative chain assembly [37], and membrane-localization [102].

Recently, the structural basis for E2 recruitment by E1 enzymes was determined through crystallographic studies of the C-terminal domain of the NEDD8 E1 (APPBP1-UBA3) in complex with the catalytic core of the NEDD8 E2 (Ubc12) [41] (Figure 1.4A). The C-terminal domain of the NEDD8 E1 forms a ubiquitin fold domain (UFD) that structurally resembles ubiquitin but has low sequence similarity. This UFD binds to Ubc12 in a manner similar to the interaction of Ub with ubiquitin binding motifs (discussed in section 1.9). The E1 UFD binds primarily to the N-terminal helix of Ubc12 through interactions at its variant hydrophobic patch. This interaction also allows Ubc12 to selectively distinguish APPBP1-UBA3 from other Ubls. Interestingly, this structure places the two active site cysteine residues 50 Å away from each other, suggesting that Ubc12, just like the E1s, must undergo significant structural changes in order to drive Ub transthiolesterification [41].

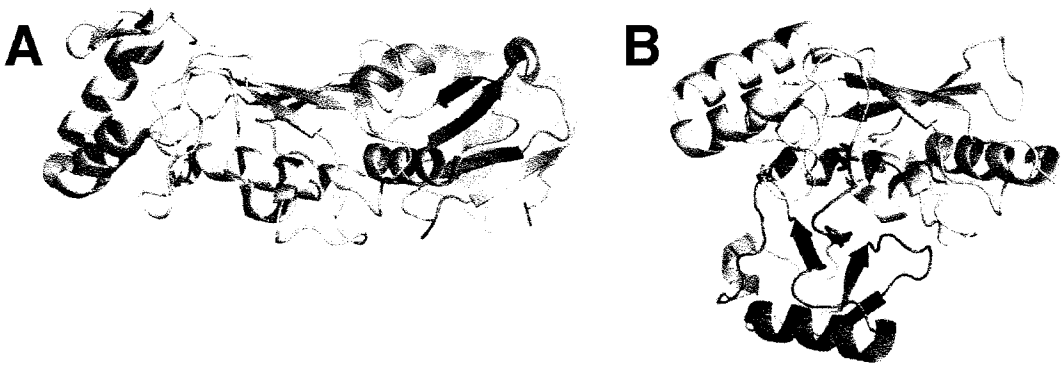

Figure 1.4: **E2 Interactions With Ubiquitin Folds.** (A) Recognition of the UFD of NEDD8 E1 (blue) by the N-terminal helix of Ubc12 (green) [1Y8X], as determined crystallographically, shown in cartoon. (B) Chemical shift-based model of the Ubc1 (green)-ubiquitin (blue) thiolester [1FXT], also as a cartoon. The active site cysteine is depicted in red in stick representation.

Although the APPBP1-UBA3-Ubc12 structure is the only E1-E2 interaction known at atomic resolution, it is likely that similar modes of interaction exist for other E1-E2 pairings. For example, the N-terminal helix of the Ubc domain is highly conserved among E2s [119], and mutagenesis studies have implicated this region in binding to the SUMO E1 [7]. Furthermore, the E2 N-terminal helices differ amongst E2s that are specific for different Ubls, suggesting that this interaction likely distinguishes the downstream pathways for each Ubl [119, 41].

The post-transthiolesterification interaction between E2 and Ub has been probed through solution-state NMR studies of the yeast Ubc1-Ub complex [33] (Figure 1.4B). In this binding mode, Ubc1 interacts with the Leu8, Ile44, Val70 hydrophobic face of Ub through α-helix-2 (the central helix that packs against the UBC β-sheet face). The C-terminus of Ub binds to a shallow cleft, proximal to helix-2, which contains the active site cysteine. It is interesting to note that, while this structure is consistent with the chemical shift map data that was previously reported for the class I HsUbc2b interaction with Ub [70], it is not consistent with the chemical shift map data that has been reported for the Ubc9 interaction with SUMO. It does appear that all three SUMO paralogues bind to Ubc9 through a site analogous to the hydrophobic patch of Ub [26], however the interacting surface of Ubc9 is primarily α-helix-1, rather than α-helix-2 [107].

1.5.2 Ubiquitin conjugating enzyme variants

Ubiquitin conjugating enzyme variants (UEVs) resemble typical E2s but lack the active site cysteine required for thiolester formation. Two UEVs, MMS2 and UEV1a, are known to form heterodimeric complexes with the conventional E2, Ubc13, to produce Lys63-linked polyubiquitin chains [40, 23] (Figure 1.1). MMS2 and UEV1a are similar in sequence (~90%

core identity) [123], but UEV1a contains an additional 20 residue N-terminal tail, typical of class III E2s [11]. The biological role of the N-terminal tail is currently unknown.

Details of the Mms2-Ubc13 interaction were first elucidated through the crystal structures of both the human [73] and yeast [111] Mms2-Ubc13 complex. Mms2 interacts with the β-sheet face of Ubc13 through its N-terminal α-helix, which shifts to a partially-extended conformation upon binding [73]. Further insights provided by mutational analysis established Phe13 as the key interacting residue of hMms2, which fits into a hydrophobic pocket formed by E55, F57 and R70 of hUbc13 [82, 111] (Figure 1.5B). These contacts, which are conserved from yeast to human, are necessary for both heterodimer formation and subsequent K63-linked di-Ub formation [82].

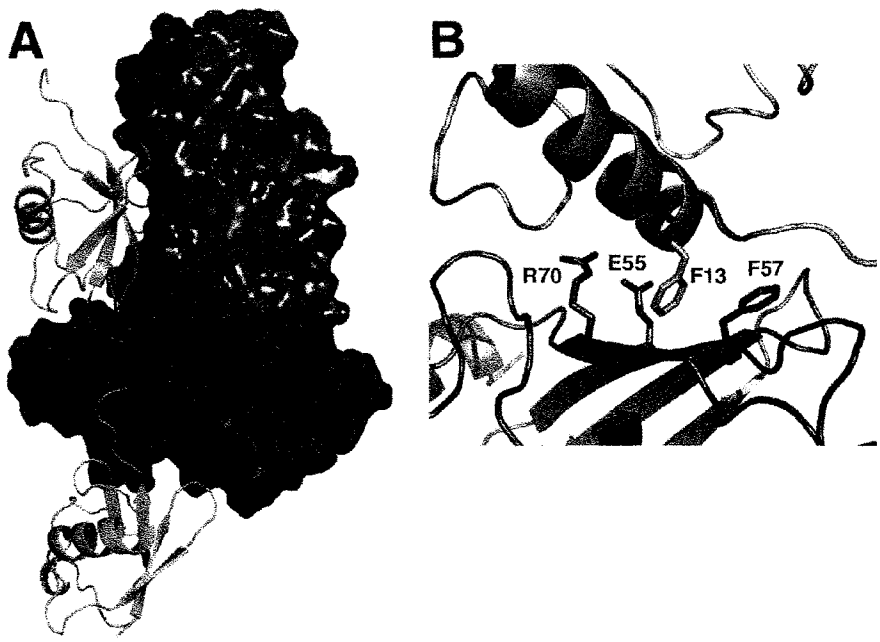

Figure 1.5: **Model for the Ub_2-Mms2-Ubc13 Tetramer.** (A) Chemical shift-based model of the Ub_2-Mms2-Ubc13 tetramer, adapted from [65]. Acceptor (top) and donor (bottom) Ubs are shown in cartoon representation (green). Mms2 (orange) and Ubc13 (purple) are shown in the surface representation. (B) Key interactions at the interface of the Mms2-Ubc13 heterodimer [1J7D]. The main chain atoms of hMms2 are shown as an orange cartoon, and hUbc13 by a purple cartoon, with the "key" interacting residues represented as sticks. Adapted from [82].

The mechanism of K63-Ub_2 formation involves the transfer of the E2-Ub (donor Ub) to Lys63 of a free, or acceptor, Ub [66]. A model based on chemical shift mapping data indicates that the acceptor Ub interacts non-covalently with Mms2 through the hydrophobic patch on its β-sheet. This model, depicted in Figure 1.5A, positions the acceptor Ub such that the side chain of Lys63 is placed within catalytic distance of the active site Cys87 of Ubc13 [65].

A mechanism for di-Ub formation was proposed based on mutational analysis of suspected residues around the active site Cys87. The mechanism, depicted in Figure 1.6, involves Asp89 acting as a general base to prime Lys63 for nucleophilic attack on the carbonyl carbon of the thiolester bond at the side chain of Cys87. The resulting oxyanion transition state is proposed to be stabilized by the side chain of Gln79 [121, 72].

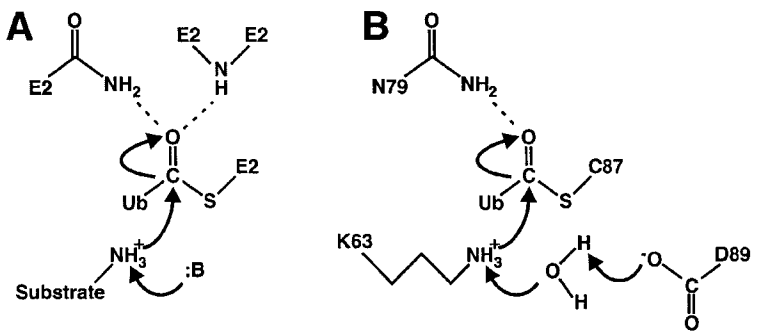

Figure 1.6: **Proposed Ubiquitination Mechanisms.** (A) Proposed thiolesterification mechanism, adapted from [86]. :B denotes a general base. Oxyanion hole is formed by a main chain and/or a side chain amide. (B) Proposed catalysis of Lys63-linked polyubiquitin chains by Mms2-Ubc13, adapted from [72].

1.6 Ubiquitin Ligase Enzymes

In the final stage of the ubiquitination cascade, an E3, or ubiquitin ligase, mediates the transfer of ubiquitin from an E2 to a specific substrate, where conjugation occurs either

at the ϵ-NH_3^+ of a lysine side chain, or the α-NH_3^+ of the main chain. Ubiquitin ligases can be classified under two groups: HECT (Homologous to E6AP C-Terminus) domain E3s catalyze an additional Ub-conjugation step to an active site cysteine within the HECT domain prior to isopeptide bond formation with the substrate peptide. RING (Really Interesting New Gene) domain E3s, on the other hand, do not form thiolesters with Ub. Rather, they act as scaffolds to bring the E2 and the substrate together (reviewed in references [29, 85, 110, 86]). Our structural understanding of the process comes from two crystallographically determined complexes: The HECT-containing E6AP in complex with UbcH7 [42], and the RING-containing c-Cbl in complex with UbcH7 and a fragment from the substrate ZAP-70 [127].

1.6.1 HECT domain ubiquitin ligases

The HECT domain is a ~350 amino acid domain that is typically located at the C-terminus of E3 ubiquitin ligases. The N-terminal regions from E3 Ub ligases are unique and likely involved in substrate targetting [44]. HECT domains form a thiolester bond with Ub [94] through an active site cysteine ~32-36 amino acids from the C-terminus; this thiolester intermediate is required for substrate ubiquitination [44]. HECT domains have been further divided into two subdomains, based on the presence or absence of WW domains. Both subdomains structurally resemble each other, and share 33% sequence identity and 53% sequence similarity [42, 112].

The non-WW containing E6-AP HECT domain consists of an N- (242 residue) and a C- (111 residue) terminal lobe. The structure of E6AP bound to UbcH7 resembles a U-shape (Figure 1.7A). The N-terminal lobe, which also binds E2 enzymes, is primarily α-helical, whereas the catalytic C-terminal lobe contains both α-helices and β-sheets. The two lobes

are connected via a hinge containing three-residues [42]. The HECT-E2 interaction involves association of the conserved residue Phe63 [79], within loop 1 of the E2, with a surface groove containing both hydrophobic and aromatic side chains on the HECT domain. The binding face on UbcH7 consists of the N-terminal helix and the first two loop regions. The hydrophobic surface groove on E6AP is situated between two α-helices and two β-strands. The HECT active site cysteine is part of a conserved loop that is positioned between the N- and C-lobes. The positioning of the active site loop is such that the E2-E3 active site cysteines are 41 Å apart. This suggests that a conformational change is likely required to catalyse the transfer of ubiquitin from the E2 to the E3 [42].

Insight into the required conformational changes is provided by the structure of the WW-containing HECT domain WWP1/AIP5, which structurally resembles E6-AP, but contains additional α-helix and β-strand secondary structure in both the N- and C-terminal lobes [112]. Unlike the E6AP structure, in which the C-lobe is connected to the N-lobe to form an L-shaped structure (Figure 1.7A), the C-lobe of WWP1/AIP5 is closer to the middle of the N-lobe, creating a T-shaped structure (Figure 1.7B). The difference between the two observed orientations can be attributed to rotations around the hinge that connects the C- and N-terminal lobes: A 100° rotation followed by a 30° tilt of the C-terminal lobe would be nearly sufficient to change between the "L" and "T" conformations. Modelling UbcH5 to WWP1/AIP5 places the distance between the E2 and E3 catalytic cysteines within 17 Å, a distance which can be further reduced to 5 Å by allowing for additional rotations around the hinge residues [112]. It has been suggested that given the absence of Ub in the HECT-E2 structure, that Ub conjugation may serve to trigger the changes between the "L" and "T" states. In addition, progressive cycles of E3 ubiquitination and poly-Ub chain elongation could be promoted by flexibility of the C-lobe [42]. This is supported by the observation

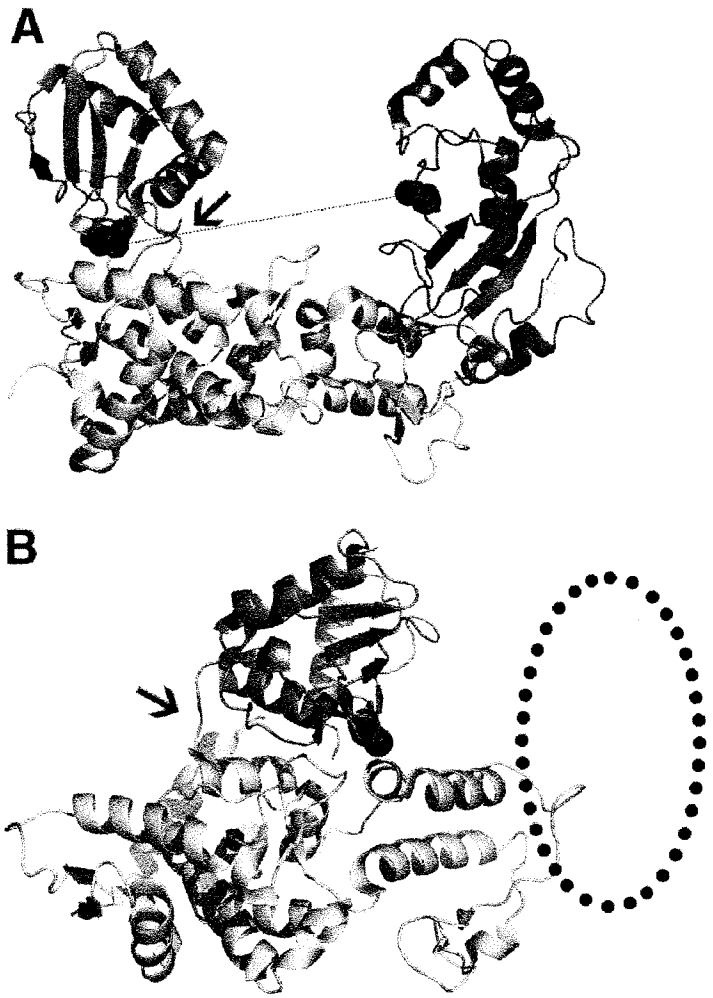

Figure 1.7: **Structures of HECT Domain E3s.** (A) Crystal structure of UbcH7-E6AP HECT domain [1C4Z] in the cartoon representation. The E6AP C-terminal (forest green) and N-terminal lobes (pale green) are connected to form an "L"-shaped structure. The N-terminal lobe recruits UbcH7 (blue) to form a "U"-shaped complex. The two active site cysteines are represented as red spheres, and are separated by a distance of ~41 Å. (B) Crystal structure of the WWP1/AIP5 HECT domain [1ND7] in cartoon representation. The C-terminal lobe (forest green) interacts with the N-terminal lobe (pale green) to form an inverted "T"-shaped structure, thus positioning the active site cysteine (red spheres) closer to the putative UbcH5 binding region (encircled). Differences between the orientation of the C-terminal lobes in each structure are attributed to rotations around the hinge region (arrows).

that mutations that restrict flexibility in the hinge region also restrict Ub transfer between the E2 and E3 [112].

1.6.2 RING domain ubiquitin ligases

RING domains are small, zinc binding motifs that promote substrate ubiquitination by localizing the E2 to the target (reviewed in [49]). RING domains contain the consensus sequence C-X_2-C-$X_{(9-39)}$-C-$X_{(1-3)}$-H-$X_{(2-3)}$-C/H-X_2-C-$X_{(4-48)}$-C-X_2-C, where the Cys and His residues are responsible for zinc binding [49]. Zinc is required for RING-dependent ubiquitination, and in some cases, RING domains are required for poly-Ub chain extension [63].

The first published RING-E2 structure was the crystallographically-determined complex consisting of the RING E3 c-Cbl, UbcH7, and a fragment of ZAP-70 (a known substrate of c-Cbl). Unlike E6-AP-UbcH7, the c-Cbl-UbcH7-ZAP-70 complex forms a rigid and compact structure [127] (Figure 1.8A). c-Cbl binds to ZAP-70 through the SH2 domain of its tyrosine kinase binding (TKB) domain [50, 68]. The TKB domain consists of a four-helix bundle, two EF hands, an SH2 domain [68], and is connected to the RING domain through an α-helix. The α-helix packs against the TKB domain and forms some contacts with UbcH7, although most of the interface consists of residues from the RING domain. UbcH7 loops 1 and 2 bind a shallow groove on the surface of c-Cbl formed by the α-helical linker and the two zinc-chelating loops of the RING domain [127]. Notably, there is a conserved Trp in the RING domain that is found in the interface [50]. It is interesting to note that the shallow groove also accommodates Phe63, the conserved residue from loop 1 of UbcH7. This residue is also required for the UbcH7 interaction with the E6AP HECT domain [127, 42]. It is also interesting that the tight association of the c-Cbl-UbcH7 complex suggests a rigid overall arrangement. This rigidity may enable the complex to serve as a scaffold, which would in

turn allow the complex to selectively target a substrate lysine residue for ubiquitination. This mode of binding may not be unique to c-Cbl-UbcH7, as sequence alignment suggests that similar binding modes are also likely to exist for other RING-E2 pairs, including Rad6-Rad18 and Ubc9-Pml [127].

RING domains are sometimes also part of large, multi-unit complexes, such as SCF complexes. SCF complexes are highly elongated structures comprised of a RING-containing protein, a scaffolding protein from the cullin family, and an F-box protein, which is responsible for substrate recognition [49, 128]. In the structure of the Cul1-Rbx1-Skp1-F box^{Skp2} SCF complex, Cul1 acts as a scaffold between the variant RING protein Rbx1 and the F-box-binding Skp1 (Figure 1.8B). Like the c-Cbl complex, the SCF complex may function as a rigid scaffold. UbcH7 was modelled to the SCF complex based on analogy to the c-Cbl-UbcH7 interaction. The span of the SCF complex, from the active site cysteine of UbcH7, to the substrate recognition leucine-rich repeat (LRR) domain of Skp2, is ~50 Å. This distance could span the region of p27 between the phosphothreonine E3 binding site, and the candidate ubiquitination target residues. To investigate this hypothesis, a flexible linker was introduced between the N- and C-domains of Cul1. The mutant SCF complex was unable to ubiquitinate p27 *in vitro*, suggesting that spatial restraints may be important for RING domain-mediated substrate ubiquitination [128].

1.6.3 Substrate recognition and regulation

There is no known consensus motif for protein ubiquitination, and E3s may have evolved a variety of strategies for targeting specific substrates. Consider the following F-box proteins for example: Cdc4 is known to bind Sic1 through WD-40 repeats [101]. On the other hand, Grr1 binds Cln2 through LRR regions [57], as does Skp2 when binding to p27 [128, 71].

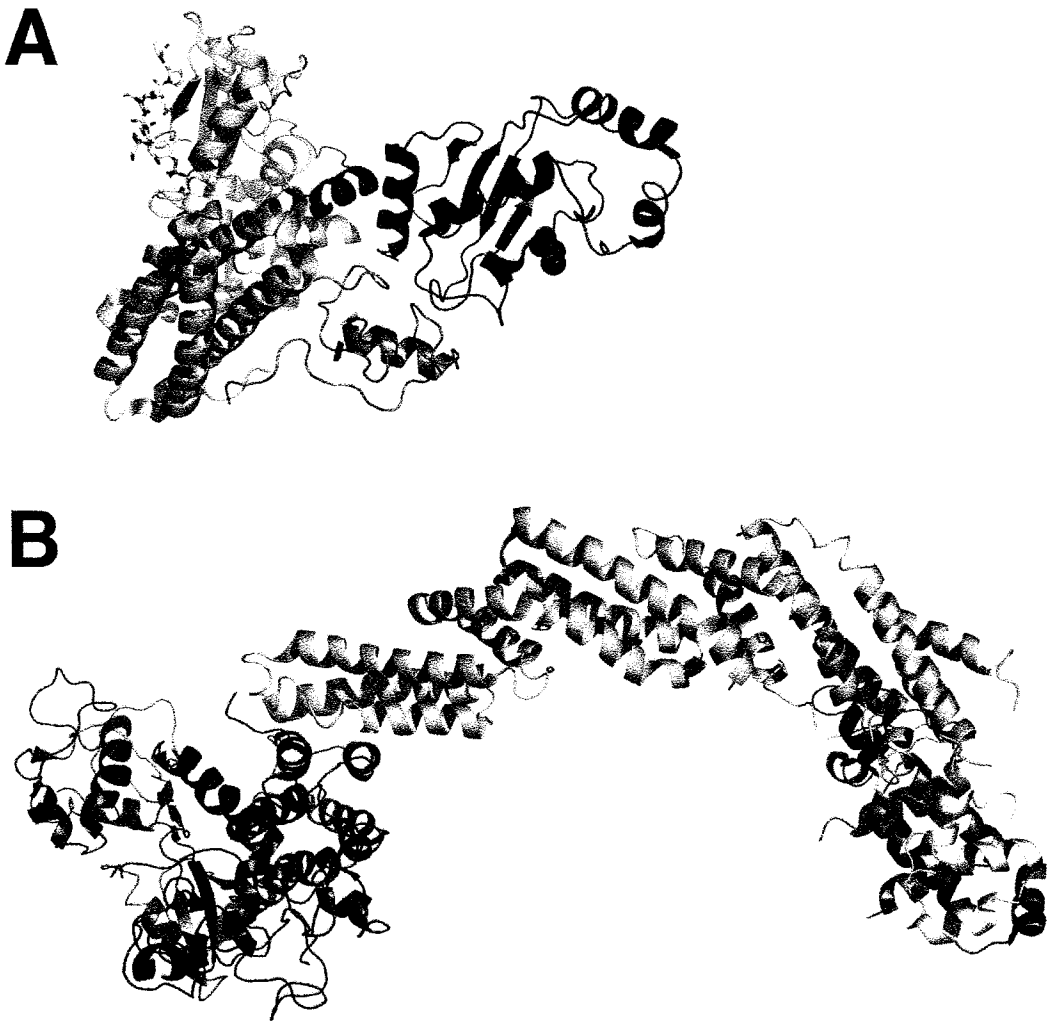

Figure 1.8: **RING Domain-Mediated Scaffolding.** (A) Crystal structure of c-Cbl-UbcH7 (cartoon representation) in complex with a fragment of ZAP-70 (stick representation) [1FBV]. The c-Cbl TKB domain (light blue) is connected to the RING domain (marine blue) through an α-helical linker (deep blue). The RING domain and the linker region form contacts to UbcH7 (pink). The active site cysteine is depicted as red spheres. (B) Crystal structure of the Cul1-Rbx1-Skp1-F box^{Skp2} SCF complex [1LDK] in the cartoon representation. Cul1 (C-domain in deep blue, N-domain in light blue) acts as a scaffold between the RING protein Rbx1 (red) and Skp1 (orange). Skp1 binds Skp2 (cyan), which contains the substrate binding LRR domain.

Phosphorylation of the substrate is often a prerequisite, and occurs in many cell cycle control pathways, such as the examples listed above. In the case of Sic1, six sites must be phosphorylated before Cdc4 will trigger its degradation. This is an example of the elegant control of protein ubiquitination.

Each phosphoylation site of Sic1 is embedded in a sequence that has poor affinity for Cdc4. Therefore each interaction of the SCF^{Cdc4} complex with a given phosphorlyation site is weak, and it has been observed that it takes the combined interactions to trigger substrate ubiquitination [76]. In an interesting experiment by Nash *et al.* [76], the weak phosphorylation sites of Sic1 were substituted for a single phosphorylation site embedded in a sequence optimized for high affinity Cdc4 binding. The substitution enabled SCF^{Cdc4} binding to Sic1, but resulted in premature entry of the cell into S phase and subsequent chromosome damage. Thus, it appears that having six weak-affinity phosphorylation sites provides a time delay for Sic1 degradation [76, 24].

Phosphorylation is not the only post-translational modification involved in regulation of ubiquitination. For example, hypoxia-induced HIFα degradation is regulated by prolyl hydroxylation, which is recognized by an E3 complex known as the von Hippel-Lindau (VHL) complex [45, 46]. Acetylation of a specific lysine residue is also a requirement for HIFα degradation [48], though interactions between the acetyl-group modification and the VHL complex have yet to be shown. Another example is the F-box protein Fbx2, which recognizes *N*-linked glycosylated substrates, and may play an important role in ER-associated degradation (ERAD) [124].

Ubiquitination is also regulated by cross-talk from other Ubl pathways. Proteolysis of p27 by the SCF^{Skp2} complex requires the activation of NEDD8, and although the target of this required modification has not been identified, evidence suggests that it is cullin-1 of the

SCF^{Skp2} complex [74], and not p27 [90]. In the NF-κB activation pathway, ubiquitination of NEMO requires that SUMO first be conjugated to NEMO at the ubiquitination site [43]. The role of SUMOlation in this pathway is discussed in section 1.8.2.

Finally, regulation of ubiquitination can occur through E3-E3 associations. For example, the association of MDMX with MDM2 occurs through their RING domains, and inhibits MDM2-mediated proteolysis of p53 [98]. RAD18 and RAD5 also associate, though not through their RING domains, and the interaction serves to localize RAD5 to the ubiquitination site (discussed in section 1.8.2) [109].

1.7 Mono-Ub Signalling

The existence of a signalling pathway that utilizes non-polymerized Ub was proposed based on the observation that mono-Ub has no inhibitory effect on the 26 S proteasome [87]. Monoubiquitination is known to play a major role in the regulation of protein transport, both by regulating transport machinery, and functioning as a sorting signal (reviewed in [36, 32]).

Monoubiquitin signaling is accomplished through non-covalent recognition of Ub by a variety of ubiquitin binding motifs, including CUE (similar to yeast Cue1p), UBA (ubiquitin associated domain), UIM (ubiquitin interacting motif), and UEV.

For example, endocytosis in yeast cells can be triggered by ligand-induced ubiquitination of several plasma membrane receptors, including the α-receptor Ste2p. Internalization of Ste2p requires the epsins Ent1 and Ent2 (also known as Ub receptors), both of which contain UIMs for recognition of ubiquitinated Ste2p [99, 32]. After internalization, Ste2p-Ub is dependent on Vps9p (Vacuole Protein Sorting 9p) for delivery to the endosome. Vps9p contains an auto-inhibitory CUE domain, whose inhibition can be lifted by the preferential

binding of Ste2p-Ub to CUE. Active Vps9p then promotes fusion of internalized Ste2p-Ub with the endosome [27]. Further downstream of these events, after maturation of the late endosome, regions of the membrane invaginate to form the multivesicular body (MVB), which is later destined for breakdown at the lysosome. Vps27 functions as a sorting signal for receptors destined for the MVB. Like the epsins, Vps27 also contains a UIM, and disruption of this motif results in deficiencies in cargo transport [99].

In human cells, protein sorting in the endosome also involves Tsg101 (Tumor Susceptibility Gene 101), a protein that contains a UEV domain that may perform a similar role as the UIM domain of Vps27 [28]. Tsg101 can also be "hijacked" in the HIV-1 budding pathway [28], where the UEV domain recruits Tsg101 to the HIV-1 assembly protein, Gag [89].

1.7.1 Ubiquitin recognition by ubiquitin binding motifs

CUE

The CUE domain is a ~50 residue motif [100] that forms a compact, three helix bundle [55]. CUE domains contain a conserved Met-Phe-Pro sequence followed by a downstream di-Leu motif [100]. The interaction between the CUE domain of CUE2 and Ub has been elucidated by NMR [55] (Figure 1.9A). CUE contains a hydrophobic pocket, formed by Met19 and Phe20 from the Met-Phe-Pro sequence, and Leu47 from the di-Leu sequence, which interacts with the Ub hydrophobic pocket formed by Ile44, Val70, and Leu8 [55].

In comparison to CUE2-Ub, a different structure for the CUE-Ub interaction was observed for the CUE domain from Vps9 (Figure 1.9B). In this case, the CUE domain dimerizes through domain swapping, but leaves the hydrophobic surface exposed. One of the CUE units interacts with Ub in a mode identical to that of CUE2. Additional contacts are formed between the second CUE-unit and a region on Ub proximal to the Ile44, Val70,

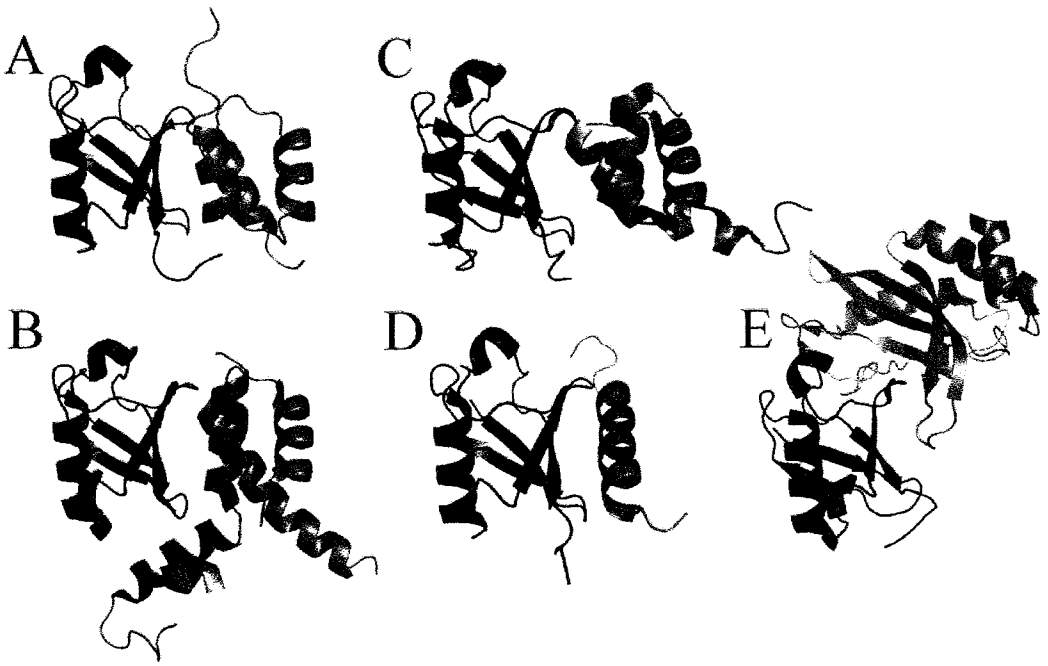

Figure 1.9: **Ubiquitin Recognition by Ubiquitin Binding Motifs.** Cartoon representations of Ub (red) bound to known ubiquitin binding motifs (blue, violet), including: (A) The CUE domain from CUE2 [1OTR]. (B) The domain-swapped CUE domain dimer from Vps9p [1P3Q]. (C) The UBA domain from Dsk2p [1WR1]. (D) The UIM domain from Vps27 [1Q0W]. (E) The UEV domain from Tsg101 [1S1Q].

Leu8 hydrophobic patch [91]. Functional data in support of these two structures is given by the observation that Ub has a stronger affinity for Vps9 ($K_D = 20 \pm 1$ μM) [100] than it does for CUE2 ($K_D = 155 \pm 9$ μM) [55].

UBA

UBA domains are structurally similar to CUE (1.8 Å C_α rmsd) [55], and interact with Ub in an analogous manner [80]. The solution structure of Dsk2p-UBA-Ub (Figure 1.9C) reveals that the UBA domain interacts with the Ub hydrophobic patch through a conserved Met-Gly-Phe motif (in place of the Met-Phe-Pro motif in CUE), as well as the di-Leu motif [80].

UIM

UIM is the smallest of the ubiquitin binding domains, consisting of a short, fifteen residue α-helix defined by the amino acid sequence E-E-E-X-ϕ-X-X-A-X-X-X-S-X-X-E, where ϕ denotes a hydrophobic residue and X denotes any residue [39]. The UIM-Ub interface, characterized through the solution structure of Vps27 UIM-Ub, interacts with Ub through the Ile44, Val70, Leu8 hydrophobic patch (Figure 1.9D). The UIM helix packs against the solvent exposed surface of the β-sheet from Ub, through hydrophobic and electrostatic interactions [105].

UEV

UEV domains (section 1.5.2), are structurally similar to conventional E2 enzymes [73]. A unique feature of the Tsg101 UEV domain is the existence of an extended β-hairpin between β-strands 1 and 2, which has been termed a β-tongue motif [88]. Tsg101 utilizes the extended β-tongue to interact with Ub through the Ile44, Val70, Leu8 hydrophobic

patch [104] (Figure 1.9E). It is important to note that this mode of interaction is distinct from that seen for other UEV domains, which are described in detail in Chapter 3.

1.8 Poly-Ub Signalling

Polyubiquitin chains, linked through the C-terminus of one Ub, and Lys48 on a sequential Ub, have classically been characterized as proteolytic signals. However, novel polyubiquitin chains, linked through lysine residues other than 48, have been observed either *in vivo* or *in vitro*, and the biological consequences of the observed linkage topologies (48, 63, 29, 6) are discussed below [29, 40, 51, 75]. The existence of novel chains in yeast raise the question of whether or not other polyubiquitin linkages exist in eukaryotes; a question that has recently been answered through a proteomics study in which all seven possible linkage types were observed in yeast cells, marking the first *in vivo* observation of Lys11, Lys33, Lys27, and Lys6-linked chains. Additionally, the study analyzed the relative order of abundance of each chain linkage, finding quantitatively that linkages involving Lys48 > Lys63, Lys11 >> Lys33, Lys27, Lys6 (abundance of K29 is unclear) [83]. The surprising result here is that Lys11-linked chains, previously unobserved *in vitro* and *in vivo*, share a similar abundance to Lys63-linked chains, which have been studied extensively. It is also surprising that Lys6-linked chains, which have been the subject of numerous studies, are among the lowest abundance chains. It is clear that future research will be dedicated to the study of newly discovered poly-Ub chain topologies.

1.8.1 Lys48-linked polyubiquitin chains

The 26S proteasome is a ~2.5 MDa complex that cleaves proteins tagged with Lys48-linked polyubiquitin chains (reviewed in [29]). The proteasome consists of two subunits:

The 20S subunit, which is responsible for proteolyis, consists of a series of repeating subunits that form a barrel structure with four rings [61]. The 19S subunit, which plays a regulatory role, consists of a variety of ATPases and deubiquitinating enzymes [30], and interacts with a variety of auxilliary factors, including ubiquitinating enzymes and chaperones [29].

The proteolytic requirement for a four-unit Lys48-polyubiquitin chain [25] has been addressed through two polyubiquitin structures determined by x-ray crystallography (Figure 1.10). The structure of tetraubiquitin is compact and asymmetric, with the Ile44, Val70, Leu8 hydrophobic patches exposed [21]. The exposure of these patches is necessary for binding subunit 5 of the proteasome [25, 6]. The structure of diubiquitin reveals an alternative packing through an interface containing the Ile44, Val70, Leu8 hydrophobic patch [20], providing a structural explanation for why the proteasome binds Ub_2 with an affinity ~100-fold weaker than for Ub_4 [108].

It has been observed that the binding affinity for polyubiquitin to subunit 5 increases with chain length [87]. For example, Ub_8 displays a ~6-fold higher binding affinity for the proteasome than Ub_4 [108]. A mode of long chain interaction has been inferred from the tetraubiquitin structure, where additional Ub units can be added to create a structure where repeating units of Ub_2 differ by a 24 Å translation. This structure ensures that each Ile44, Val70, Leu8 hydrophobic patch from Ub is exposed, thereby increasing the surface area available for proteasome recognition [21].

1.8.2 Lys63-linked polyubiquitin chains

Lys63-linked poly-Ub chains are the most highly studied of the alternative Ub chains. They have been implicated in two eukaryotic pathways, both involving a UEV-Ubc pairing. Mms2 binds Ubc13 and functions with RAD5 in error-free DNA damage repair, and Uev1a

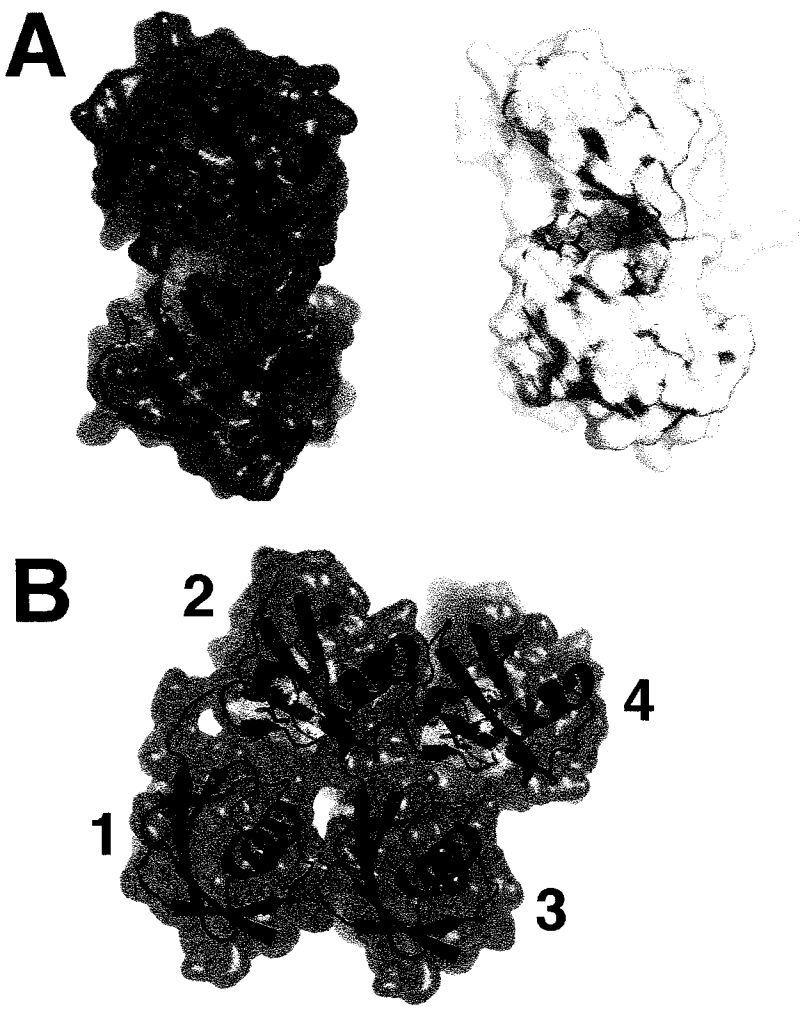

Figure 1.10: **Lys48-Linked Poly-Ub Chain Packing.** (A) Adjacent Ubs from the Lys48-linked tetraubiquitin structure [1TBE] shown in red. The structure of Lys48-linked diubiquitin [1AAR] is shown in green. (B) Structure of Lys48-linked tetraubiquitin, adapted from [21]. Structures are shown in the cartoon representation with a semi-transparent surface. Each hydrophobic patch (Leu8, Ile44, Val70) is shown in blue in the stick representation.

binds Ubc13 and functions with TRAF6 in NF-κB activation [1]. Additionally, evidence exists for Mms2 and Ubc13 participation with Chfr in mitotic stress signalling [9], though alternative models exist for this pathway as well [16, 126].

Post-replicative DNA repair

Extensive research into post-replicative DNA repair in eukaryotes has elucidated three sub-pathways for bypassing replication blocks, all of which require *RAD6* and *RAD18*, the genes which encode an E2 (Ubc2) [47] and an E3 respectively (reviewed in [4]). Two of the sub-pathways have been classified as translesion synthesis (TLS) pathways. One of these involves the action of DNA polymerase ζ (pol ζ), which promotes slow and error-prone replication past DNA lesions [77]. The other involves the action of DNA polymerase η (pol η), which is capable of efficient and accurate replication past thymine dimers [52]. The third *RAD6* sub-pathway is the damage-avoidance, or error-free pathway, which replicates past DNA damage lesions using newly synthesized sister strands as a template [62, 4, 10].

Genetic analysis has identified both Mms2 [11] and Ubc13 [14] as part of the damage-avoidance pathway. Further research has shown that Mms2 and Ubc13 interact, and that the UEV-Ubc heterodimer is responsible for the production of non-canonical, Lys63-linked di-Ub chains which are essential for post-replicative DNA repair in yeast [40].

The substrate for covalent modification through attachment of Lys63-linked poly-Ub chains by Mms2-Ubc13 was recently revealed to be PCNA (Proliferating Cell Nuclear Antigen) [38]; a part of the DNA polymerase δ (pol δ) complex. PCNA forms a closed circular, trimeric ring structure that acts as a sliding clamp around dsDNA [59]. Each monomer consists of two antiparallel β-sheets and three α-helices, which are arranged to form a circular collar. The β-sheets wrap around the outside of the collar, supporting the

α-helices that form the inner lining of the collar and the DNA binding site [59].

In the current model for post-replication repair (PRR), RAD18 single-stranded DNA binding activity allows the recruitment of the Ubc2-RAD18 complex to ssDNA regions [3] that arise as a result of stalled replication machinery [4]. The presence of Mms2, Ubc13, and the ubiquitin ligase RAD5 directs PCNA into the damage-avoidance pathway [14] (Figure 1.11). The two E3 enzymes RAD18 and RAD5 have been observed to interact through yeast-two hybrid analysis to form a multimeric complex. In this way, recruitment by the RING domain of RAD5 localizes Ubc13-Mms2 to the DNA damage site [109]. The mechanism of PCNA recruitment is unclear, although both RAD18 and RAD5 have been shown to interact with PCNA using a yeast two-hybrid screen [38]. PCNA is first mono-ubiquitinated by Ubc2-RAD18 at K164 [38]; a highly conserved residue, present in yeast and higher eukaryotes (including humans) [38], which is required for DNA repair during replication stress [38, 10]. The K164-Ub is subsequently extended by Mms2-Ubc13, resulting in a di-Ub chain linked through Lys63 [38]. Polyubiquitinated PCNA is hypothesized to initiate template switch DNA synthesis, where the stalled replication machinery disassembles itself from the damaged strand, and uses the daughter strand to code past the lesion. The mechanism by which polyubiquitin chains promote template swapping is, as of yet, unknown.

As shown in Figure 1.11, PCNA can also undergo SUMOlation at Lys164 and at Lys127 [38] (reviewed in [117]). Unlike ubiquitination, the SUMO modification at Lys164 is not required for DNA damage repair during replication stress [10], and the sharing of Lys164 by both modifications led to the proposal of an antagonistic relationship between PCNA SUMOlation and ubiquitination [38]. This hypothesis has since been refuted by genetic analysis [81], in favor of a new model where PCNA SUMOlation occurs independent of ubiq-

uitination to recruit Srs2 [84, 81], a DNA helicase that has been shown to inhibit *RAD52*-dependent recombinational repair [34]. The interplay between the *RAD52*-dependent and *RAD6*-dependent repair pathways can be considered as a type of switchboard, where PCNA-SUMO-Srs2 facilitates channelling to *RAD6*-dependent damage bypass, and guards against unwanted *RAD52*-dependent recombination during DNA replication [12, 84, 81]. The biological details surrounding the switchboard interplay are still largely unclear.

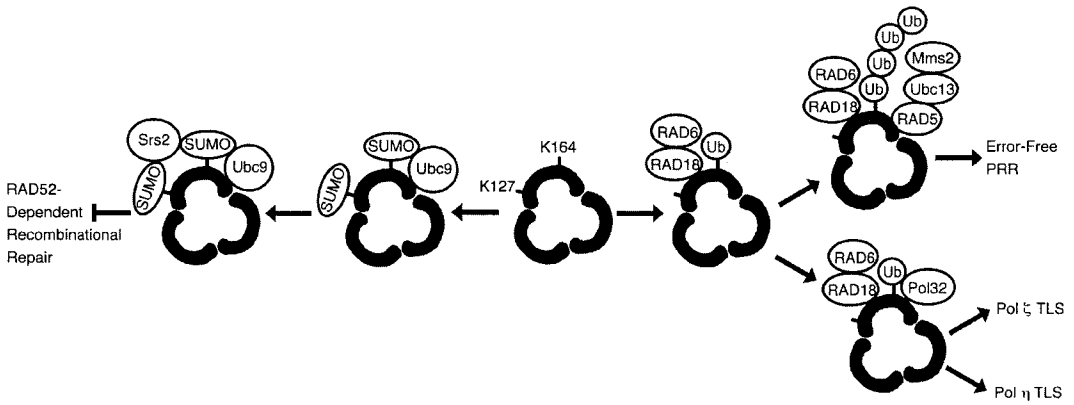

Figure 1.11: **Ubl Modification of PCNA.** Ubiquitination of PCNA (black ring) by RAD6-RAD18 funnels PCNA into either the translesion synthesis pathways, or the post-replicative DNA repair pathway mediated by Mms2-Ubc13. SUMOlation by Ubc9 leads to recognition of PCNA by Srs2, which in turn inhibits RAD52-dependent recombinational repair. All of these modifications require the trimerization of PCNA as a prerequisite [38].

One of the primary motives for elucidating PRR pathways is the hope that cancer therapeutics can be developed in the long-term. One established hallmark of cancer is the ability for a cell to replicate continuously in spite of growing genomic instability and DNA damage [4]. Therefore any relevance of the yeast model to human biochemistry is of great interest. While the human model has yet to be studied in comparable detail, research has noted the high conservation of the Mms2-Ubc13 pathway, not only between yeast and humans, but among other eukaryotes as well [13, 114]. The observation that human Mms2 can rescue $\Delta mms2$ yeast cells from MMS and UV exposure suggested a

functional conservation between yeast and humans [123]; this hypothesis was later verified by survivorship assays of $\Delta hmms2$ human fibroblast cells [62]. Recently, genetic analysis has also shown that both $spm2^{+}$, the *mms2* homologue in *Schizosaccharomyces pombe* [13], and shUEV, the mms2 homologue in a ciliated protist *Sterkiella histriomuscorum* [114], can rescue $\Delta mms2$ yeast cells from MMS exposure. These results suggest that the UEV and Ubc families are highly conserved across the eukaryotic kingdom, since UEV function requires a specific Ubc-UEV interaction [13, 114]. Other aspects of PRR in human cells are less clear. Neither polyubiquitinated nor SUMOlated forms of human PCNA have been detected, and a human homologue of Srs2 has not been identified [117]. It is possible that Srs2 functions may have been taken over by mammalian helicases not present in yeast strains [117], though further research is required to substantiate this hypothesis.

NF-κB activation

Alternative Lys63-linked polyubiquitin chains play a role in the activation of NF-κB; a composite of Rel family, dimeric transcription factors that upregulate immunological responses (reviewed in [18]). The E2 that catalyzes the synthesis of these poly-Ub chains is the Uev1a-Ubc13 heterodimer [1], and the E3 is a RING domain ligase from the TRAF (TNF Receptor-Associated Factor) family of proteins [23, 92].

TRAF6-dependent NF-κB activation (Figure 1.12) is initiated through antigenic stimulation of cells through the toll-like receptor or the interleukin-1β receptor. Following receptor stimulation, TRAF6 oligomerizes [120] and polyautoubiquitinates [116] through interaction with the Uev1a-Ubc13 heterodimer [1]. The Ub chains are subsequently recognized by the TAB (TAK1-binding) family of proteins, through a novel zinc finger (NZF) domain that preferentially binds Lys63-linked poly-Ub chains [53]. Ubiquitin-associated

TABs then promote the autophosphorylation and activation of TAK1 (TGFβ-activating kinase), which in turn phosphorylates IKKβ, causing the activation of the IKK (IκB Kinase) complex [116].

IKK consists of two catalytic subunits, α and β, and a regulatory subunit, γ, which is widely referred to as NEMO. The target of IKK phosphorylation activity is the inhibitor of NF-κB, IκB. IκB inhibits NF-κB transcriptional activity by binding to its nuclear translocation/DNA binding sequence, thus trapping it in the cytoplasm [18]. Activated IKKβ phosphorylates IκB at two N-terminal serine residues, initiating a cascade that triggers IκB proteolysis [17]. With the removal of its inhibitor, NF-κB is free to translocate into the nucleus, where it upregulates the transcription of genes involved in the autoimmune response [18].

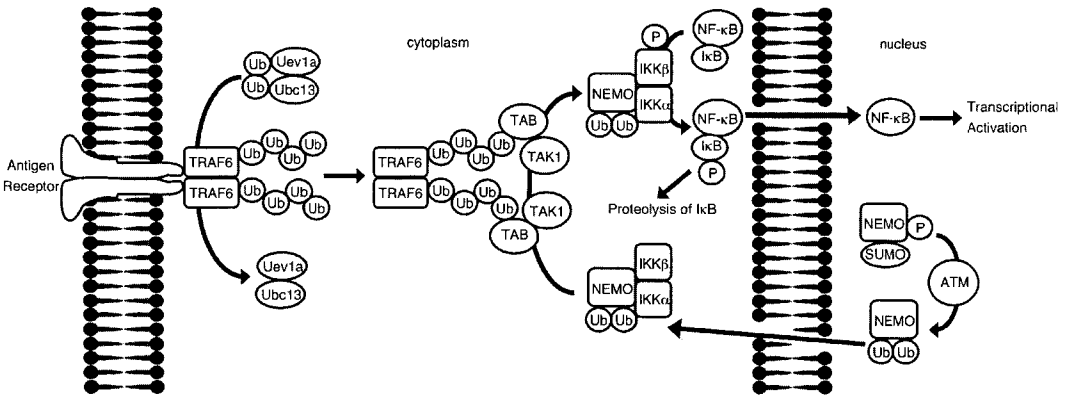

Figure 1.12: **TRAF6-Dependent Activation of NF-κB.** Schematic diagram of NF-κB activation by the polyubiquitination of TRAF6 in conjunction with NEMO activation by ATM.

Activation of the IKK complex also involves the activation of NEMO. DNA damage triggers the SUMOlation of nuclear NEMO, and activation of the nuclear kinase ATM. SUMOlation traps NEMO in the nucleus of the cell, whereas activated ATM phosphorylates SUMOlated NEMO, resulting in the replacement of SUMO with two Ub tags; one

at Lys277 and one at Lys309 [43]. Ubiquitinated NEMO is able to leave the nucleus, and association with the IKKα and IKKβ subunits in the cytoplasm results in activation of the IKK complex [43]. Notably, activation of NF-κB through B- and T-cell receptors requires the Lys63-linked polyubiquitination of NEMO by Uev1a-Ubc13 [129, 1]. The structural basis for this requirement is still unclear.

Chfr, mitotic checkpoint protein

Recently, it has been proposed that the mitotic checkpoint protein Chfr (Checkpoint containing FHA and RING finger) is regulated by attachment of Lys63-linked polyUb chains [9]. Chfr is a 664 residue protein that contains an N-terminal FHA (forkhead-associated) domain, a central RING domain, and a C-terminal cysteine-rich (CR) domain. Chfr functions as a checkpoint for entry of the cell into metaphase, delaying mitotic progression in mitotically-stressed cells [16]. Chfr has also been implicated in cancer, as Chfr inactivation is observed in some human cancer cell lines [97].

The *in vivo* role of Chfr is contentious. The first role assigned to Chfr involved regulation of the protein kinase Plk1. Chfr was shown to be autoubiquitinated with Ub from both Ubc4 and Ubc5 [16, 54], and that Chfr polyubiquitinates Plk1, leading to its degradation, in *Xenopus* cell-free extracts. Plk1 degradation results in downregulation of the protein phosphatase Cdc25C and upregulation of the protein kinase Wee1, which in turn leads to the prolonged phosphorylation of the Cdc2 kinase. The net regulatory effect of Plk1 degradation is a prolonged entry of the cell into metaphase [54] (reviewed in [56]). However, while this is an attractive model for Chfr function, *in vivo* evidence for this functionality is weak, and irreproducible in other cell lines [9].

A second hypothesis is that the Mms2-Ubc13 heterodimer acts as the E2 for Chfr. While

Ubc5 appears to be the relevant E2 in *Xenopus* cell-free extracts, it is also a promiscuous E2 [79, 122, 96], and ubiquitination assays show that Chfr preferentially binds Mms2-Ubc13. Mms2-Ubc13 has been shown to function with Chfr to produce Lys63-linked poly-ubiquitin chains *in vitro*, and it is suggested that this alternative chain is involved in signalling mitotic stress [9].

Chfr is also believed to play a role as a tumor suppressor. Using a mouse model system, Yu *et al.* found that Chfr was vital for tumor suppression, and that the *in vivo* target of its ubiquitin ligase activity is the proto-oncoprotein Aurora A [126].

It is clear that further research is required to provide a complete picture of *in vivo* Chfr function. While many models have been proposed, it is possible that they are all, to some extent, correct. The existence two protein-binding domains, an FHA and a CR domain, on Chfr suggests that it has more than one protein target. The CR region has already been shown to mediate Aurora A ubiquitination [126], and a structure of the FHA domain with tungstate, a PO_4^- mimic, reveals that Chfr has the potential to bind phosphoproteins as well [103].

1.8.3 Lys29-linked polyubiquitin chains

The E2-HECT E3 pairs Ubc4p-Ufd4p [58] and UbcH5-KIAA10 are the only known proteins that assemble Lys29-linked polyUb chains [125]. Functionally, Lys29-linked chains have only been observed as part of the ubiquitin-fusion degradation pathway [51], however domain analysis of Ufd3, a Lys29-linked poly-Ub binding protein, revealed homology to phospholipase A2 activating protein (PLAP), thus suggesting that these chains could conceivably play a role in vesicle or membrane trafficking [93].

Another interesting observation is that UbcH5A-KIAA10 has been shown to produce

poly-Ub with hetero-linkages (mixed Lys29- and Lys48- linkages) as well as homo-linked poly-Ub, with a similar propensity for linking through Lys48 and Lys29 for either linkage type. This result not only shows that mixed chains are possible, but also implies that Lys29 of the terminating Ub remains solvent exposed in canonical, Lys48-linked chains [64].

1.8.4 Lys6-linked polyubiquitin chains

Currently the only known substrate for Lys6-linked chains *in vivo* is the auto-ubiquitinated form of BRCA1, a tumor suppressor that forms a heterodimer with the RING E3 BARD1 [75, 78]. *In vitro* studies have suggested that Lys6-linked chains can be produced by the E2 UbcH5, though only when the BRCA1-BARD1 heterodimer is present [122]. Interestingly, UbcH5 produces Lys48-linked chains in the absence of BRCA1-BARD1, suggesting that catalytic context is a strong determinant of linkage specificity [122, 2].

The role that Lys6-chains play *in vivo* is just beginning to be realized. It has been shown that these chains are produced by BRCA1-BARD1 during S-phase, and are localized at sites of DNA damage, implicating Lys6-linked chains in DNA repair [75]. Interestingly, BRCA1-BARD1 can produce both Lys6- and Lys29-linked chains with equal preference *in vivo*, and this activity is thought to be enhanced by the autoubiquitination of BRCA1 [78].

Though much of the biology surrounding Lys6-linked chains is unclear, recent work has shed some light on the degradation of non-proteolytic Ub signals. *In vitro* evidence suggests that, while Lys6-linked chains do not signal for degradation, they do bind the 26 S proteasome for de-ubiquitination, though the molecular details are unclear [78].

1.9 Thesis Overview

The research described in this dissertation is focused on determining the structural basis for selective assembly of Lys63-linked polyubiquitin chains by Uev/Ubc13 heterodimeric enzymes. Using nuclear magnetic resonance as the primary methodology, we have focused on the protein-protein interactions that direct this alternative chain synthesis. The next chapter discusses the chemical shift assignment for hMms2 and Ub in the bound state, as well as the preliminary NOE-based structure determination for each individual component of the complex. Chapter 3 describes the structure of the hMms2-Ub complex determined using a protein docking protocol driven by NOE-based restraints. Chapter 4 discusses the chemical shift assignment of the E2 hUbc13, and possible modes of interaction between hUbc13 and the RING domain from Traf6. Finally, Chapter 5 provides a brief summary of the dissertation, and future directions for research.

Bibliography

[1] Parker L. Andersen, Honglin Zhou, Landon Pastushok, Trevor Moraes, Sean McKenna Barry Ziola, Michael J. Ellison, Vishva M. Dixit, and Wei Xiao. Distinct regulation of Ubc13 functions by the two ubiquitin-conjugating enzyme variants Mms2 and Uev1A. *J Cell Biol*, 170:745–755, 2005.

[2] Olga V. Baboshina and Arthur L. Haas. Novel Multiubiquitin Chain Linkages Catalyzed by the Conjugating Enzymes $E2_{EPF}$ and RAD6 Are Recognized by 26 S Proteasome Subunit 5. *J Biol Chem*, 271:2823–2831, 1996.

[3] Véronique Bailly, John Lamb, Patrick Sung, Satya Prakash, and Louise Prakash. Specific complex formation between yeast RAD6 and RAD18 proteins: a potential mechanism for targetting RAD6 ubiquitin-conjugating activity to DNA-damage sites. *Genes Dev*, 8:811–820, 1994.

[4] Leslie Barbour and Wei Xiao. Regulation of alternative replication bypass pathways at stalled replication forks and its effects on genome stability: a yeast model. *Mutat Res*, 532:137–155, 2003.

[5] Peter Bayer, Andreas Arndt, Susanne Metzger, Rohit Mahajan, Frauke Melchior, Rainer Jaenicke, and Jörg Becker. Structure Determination of the Small Ubiquitin-related Modifier SUMO-1. *J Mol Biol*, 280:275–286, 1998.

[6] Richard Beal, Quinn Deveraux, Gang Xia, Martin Rechsteiner, and Cecile Pickart. Surface hydrophobic residues of multiubiquitin chains essential for proteolytic targeting. *Proc Natl Acad Sci U S A*, 93:861–866, 1996.

[7] Kalman P. Bencsath, Michael S. Podgorski, Vishwajeeth R. Pagala, Clive A. Slaughter, and Brenda A. Schulman. Identification of a Multifunctional Binding Site on Ubc9p Required for Smt3p Conjugation. *J Biol Chem*, 277:47938–47945, 2002.

[8] Richard N. Bohnsack and Arthur L. Haas. Conservation in the Mechanism of Nedd8 Activation by the Human AppBp1-Uba3 Heterodimer. *J Biol Chem*, 278:26823–26830, 2003.

[9] John Bothos, Matthew K. Summers, Monica Venere, Daniel M. Scolnick, and Thanos D. Halazonetis. The Chfr mitotic checkpoint protein functions with Ubc13-Mms2 to form Lys63-linked polyubiquitin chains. *Oncogene*, 22:7101–7107, 2003.

[10] Dana Branzei, Masayuki Seki, and Takemi Enomoto. Rad18/Rad5/Mms2-mediated polyubiquitination of PCNA is implicated in replication completion during replication stress. *Genes Cells*, 9:1031–1042, 2004.

[11] Stacey Broomfield, Barbara L. Chow, and Wei Xiao. *MMS2*, encoding a ubiquitin-conjugating-enzyme-like protein, is a member of the yeast error-free postreplication repair pathway. *Proc Natl Acad Sci U S A*, 95:5678–5683, 1998.

[12] Stacey Broomfield and Wei Xiao. Suppression of genetic defects within the *RAD6* pathway by *srs2* is specific for error-free post-replication repair but not for damage-induced mutagenesis. *Nucleic Acids Res*, 30:732–739, 2002.

[13] Morgan Brown, Yu Zhu, Sean M. Hemmingsen, and Wei Xiao. Structural and functional conservation of error-free DNA postreplication repair in *Schizosaccharomyces pombe*. *DNA Repair*, 1:869–880, 2002.

[14] Janna Brusky, Yu Zhu, and Wei Xiao. UBC13, a DNA-damage-inducible gene, is a member of the error-free postreplication repair pathway in *Saccharomyces cerevisiae*. *Curr Genet*, 37:168–174, 2000.

[15] Timothy J. Burch and Arthur L. Haas. Site-Directed Mutagenesis of Ubiquitin. Differential Roles for Arginine in the Interaction with Ubiquitin-Activating Enzyme. *Biochemistry*, 33:7300–7308, 1994.

[16] Priya Chaturvedi, Valery Sudakin, Matthew L. Bobiak, Paul W. Fisher, Michael R. Mattern, Sandra A. Jablonski, Mark R. Hurle, Yuan Zhu, Tim J. Yen, and Bin-Bing S. Zhou. Chfr Regulates a Mitotic Stress Pathway through its RING-Finger Domain with Ubiquitin Ligase Activity. *Cancer Res*, 62:1797–1801, 2002.

[17] Zhijian J. Chen. Signal-induced site-specific phosphorylation targets IκBα to the ubiquitin-proteasome pathway. *Genes Dev*, 9:1586–1597, 1995.

[18] Zhijian J. Chen. Ubiquitin signalling in the NF-κB pathway. *Nat Cell Biol*, 7:758–765, 2005.

[19] Aharon Ciehanover, Yaacov Hod, and Avram Hershko. A HEAT-STABLE POLYPEPTIDE COMPONENT OF AN ATP-DEPENDENT PROTEOLYTIC SYSTEM FROM RETICULOCYTES. *Biochem Biophys Res Commun*, 81:1100–1105, 1978.

[20] William J. Cook, Leigh C. Jeffrey, Mike Carson, Zhijian Chen, and Cecile M. Pickart. Structure of a Diubiquitin Conjugate and a Model for Interaction with Ubiquitin Conjugating Enzyme (*E2*). *J Biol Chem*, 267:16467–16471, 1992.

[21] William J. Cook, Leigh C. Jeffrey, Eileen Kasperek, and Cecile M. Pickart. Structure of Tetraubiquitin Shows How Multiubiquitin Chains Can Be Formed. *J Mol Biol*, 236:601–609, 1994.

[22] William J. Cook, Leigh C. Jeffrey, Michael L. Sullivan, and Richard D. Vierstra. Three-dimensional Structure of a Ubiquitin-conjugating Enzyme (E2). *J Biol Chem*, 267:15116–15121, 1992.

[23] Li Deng, Chen Wang, Erika Spencer, Liyong Yang, Amy Braun, Jianxin You, Clive Slaughter, Cecile Pickart, and Zhijian J. Chen. Activation of the IκB Kinase Complex by TRAF6 Requires a Dimeric Ubiquitin-Conjugating Enzyme Complex and a Unique Polyubiquitin Chain. *Cell*, 103:351–361, 2000.

[24] Raymond J. Deshaies and James E. Farrell, Jr. Multisite Phosphorylation and the Countdown to S Phase. *Cell*, 107:819–822, 2001.

[25] Quinn Deveraux, Vicença Ustrell, Cecile Pickart, and Martin Rechsteiner. A 26S Protease Subunit That Binds Ubiquitin Conjugates. *J Biol Chem*, 269:7059–7061, 1994.

[26] Husheng Ding, Yingqi Xu, Quan Chen, Haiming Dai, Yajun Tang, Jihui Wu, and Yunyu Shi. Solution Structure of Human SUMO-3 C47S and Its Binding Surface for Ubc9. *Biochemistry*, 44:2790–2799, 2005.

[27] Kathryn M. Donaldson, Hongwei Yin, Nicholas Gekakis, Frantisek Supek, and Claudio A. P. Joazeiro. Ubiquitin Signals Protein Trafficking via Interaction with a Novel Ubiquitin Binding Domain in the Membrane Fusion Regulator, Vps9p. *Curr Biol*, 13:258–262, 2003.

[28] Jennifer E. Garrus, Uta K. von Schwedler, Owen W. Pornillos, Scott G. Morham, Kenton H. Zavitz, Hubert E. Wang, Daniel A. Wettstein, Kirsten M. Stray, Mélanie Côté, Rebecca L. Rich, David G. Myszka, and Wesley I. Sundquist. Tsg101 and the Vacuolar Protein Sorting Pathway Are Essential for HIV-1 Budding. *Cell*, 107:55–65, 2001.

[29] Michael H. Glickman and Aaron Ciechanover. The Ubiquitin-Proteasome Proteolytic Pathway: Destruction for the Sake of Construction. *Physiol Rev*, 82:373–428, 2002.

[30] Michael H. Glickman, David M. Rubin, Victor A. Fried, and Daniel Finley. The Regulatory Particle of the *Saccharomyces cerevisiae* Proteasome. *Mol Cell Biol*, 18:3149–3162, 1998.

[31] Arthur L. Haas and Irwin A. Rose. The Mechanism of Ubiquitin Activating Enzyme. *J Biol Chem*, 257:10329–10337, 1982.

[32] Kaisa Haglund, Pier Paolo Di Fiore, and Ivan Dikic. Distinct monoubiquitin signals in receptor endocytosis. *Trends Biochem Sci*, 28:598–603, 2003.

[33] Katherine S. Hamilton, Michael J. Ellison, Kathryn R. Barber, R. Scott Williams, John T. Huzil, Sean McKenna, Christopher Ptak, Mark Glover, and Gary S. Shaw. Structure of a Conjugating Enzyme-Ubiquitin Thiolester Intermediate Reveals a Novel Role for the Ubiquitin Tail. *Structure*, 9:897–904, 2001.

[34] Lajos Haracska, Carlos A. Torres-Ramos, Robert E. Johnson, Satya Prakash, and Louise Prakash. Opposing Effects of Ubiquitin Conjugation and SUMO Modification of PCNA on Replicational Bypass of DNA Lesions in *Saccharomyces cerevisiae*. *Mol Cell Biol*, 24:4267–4274, 2004.

[35] Avram Hershko, Hannah Heller, Sarah Elias, and Aaron Ciechanover. Components of Ubiquitin-Protein Ligase System. *J Biol Chem*, 258:8206–8214, 1983.

[36] Linda Hicke and Rebecca Dunn. Regulation of Membrane Protein Transport by Ubiquitin and Ubiquitin-Binding Proteins. *Annu Rev Cell Dev Biol*, 19:141–172, 2003.

[37] Robert Hodgins, Chantelle Gwozd, Terra Arnason, Maxwell Cummings, and Michael J. Ellison. The Tail of a Ubiquitin-conjugating Enzyme Redirects Multi-ubiquitin Chain Synthesis from the Lysine 48-linked Configuration to a Novel Nonlysine-linked Form. *J Biol Chem*, 271:28766–28771, 1996.

[38] Carsten Hoege, Boris Pfander, George-Lucian Moldovan, George Pyrowolakis, and Stefan Jentsch. *RAD6*-dependent DNA repair is linked to modification of PCNA by ubiquitin and SUMO. *Nature*, 419:135–141, 2002.

[39] Kay Hofmann and Laurent Falquet. A ubiquitin-interacting motif conserved in components of the proteasomal and lysosomal protein degradation systems. *Trends Biochem Sci*, 26:347–350, 2001.

[40] Roseanne M. Hofmann and Cecile M. Pickart. Noncanonical *MMS2*-Encoded Ubiquitin-Conjugating Enzyme Functions in Assembly of Novel Polyubiquitin Chains for DNA Repair. *Cell*, 96:645–653, 1999.

[41] Danny T. Huang, Amir Paydar, Min Zhuang, M. Brett Waddell, James M. Holton, and Brenda A. Schulman. Structural Basis for Recruitment of Ubc12 by an E2 Binding Domain in NEDD8's E1. *Mol Cell*, 17:341–350, 2005.

[42] Lan Huang, Elspeth Kinnucan, Guangli Wang, Sylvie Beaudenon, Peter M. Howley Jon M. Huibregtse, and Nikola P. Pavletich. Structure of an E6AP-UbcH7 Complex: Insights into Ubiquitination by the E2-E3 Enzyme Cascade. *Science*, 286:1321–1326, 1999.

[43] Tony T. Huang, Shelly M. Wuerzberger-Davis, Zhao-Hui Wu, and Shigeki Miyamoto. Sequential Modification of NEMO/IKKγ by SUMO-1 and Ubiquitin Mediates NF-κB Activation by Genotoxic Stress. *Cell*, 115:565–576, 2003.

[44] Jon M. Huibregtse, Martin Scheffner, Sylvie Beaudenon, and Peter M. Howley. A family of proteins structurally and functionally related to the E6-AP ubiquitin-protein ligase. *Proc Natl Acad Sci U S A*, 92:2563–2567, 1995.

[45] Mircea Ivan, Keiichi Kondo, Haifeng Yang, William Kim, Jennifer Valiando, Michael Ohh, Adrian Salic, John M. Asara, William S. Lane, and William G. Kaelin, Jr. HIFα Targeted for VHL-Mediated Destruction by Proline Hydroxylation: Implications for O_2 Sensing. *Science*, 292:464–468, 2001.

[46] Panu Jaakkola, David R. Mole, Ya-Min Tian, Michael I. Wilson, Janine Gielbert, Simon J. Gaskell, Alexander von Kriegsheim, Holger F. Hebestreit, Mridul Mukherji, Christopher J. Schofield, Patrick H. Maxwell, Christopher W. Pugh, and Peter J. Ratcliffe. Targetting of HIF-α to the von Hippel-Lindau Ubiquitylation Complex by O_2-Regulated Prolyl Hydroxylation. *Science*, 292:468–472, 2001.

[47] Stefan Jentsch, John P. McGrath, and Alexander Varshavsky. The yeast DNA repair gene *RAD6* encodes a ubiquitin-conjugating enzyme. *Nature*, 329:131–134, 1987.

[48] Joo-Won Jeong, Moon-Kyoung Bae, Mee-Young Ahn, Se-Hee Kim, Tae-Kwon Sohn, Myung-Ho Bae, Mi-Ae Yoo, Eun Joo Song, Kong-Joo Lee, and Kyu-Won Kim. Regulation and Destabilization of HIF-1α by ARD1-Mediated Acetylation. *Cell*, 111:709–720, 2002.

[49] Claudio A. P. Joazeiro and Allan M. Weissman. RING Finger Proteins: Mediators of Ubiquitin Ligase Activity. *Cell*, 102:549–552, 2000.

[50] Claudio A. P. Joazeiro, Simon S. Wing, Han kuei Huang, Joel D. Leverson, Tony Hunter, and Yun-Cai Liu. The Tyrosine Kinase Negative Regulator c-Cbl as a RING-Type, E2-Dependent Ubiquitin-Protein Ligase. *Science*, 286:309–312, 1999.

[51] Erica S. Johnson, Philip C. M. Ma, Irene M. Ota, and Alexander Varshavsky. A Proteolytic Pathway That Recognizes Ubiquitin as a Degradation Signal. *J Biol Chem*, 270:17442–17456, 1995.

[52] Robert E. Johnson, Satya Prakash, and Louise Prakash. Efficient Bypass of a Thymine-Thymine Dimer by Yeast DNA Polymerase, Pol η. *Science*, 283:1001–1004, 1999.

[53] Atsuhiro Kanayama, Rashu B. Seth, Lijun Sun, Chee-Kwee Ea, Mei Hong, Abdullah Shaito, Yu-Hsin Chiu, Li Deng, and Zhijian J. Chen. TAB2 and TAB3 Activate the NF-κB Pathway through Binding to Polyubiquitin Chains. *Mol Cell*, 15:535–548, 2004.

[54] Dongmin Kang, James Chen, Jim Wong, and Guowei Fang. The checkpoint protein Chfr is a ligase that ubiquitinates Plk1 and inhibits Cdc2 at the G2 to M transition. *J Cell Biol*, 156:249–259, 2002.

[55] Richard S. Kang, Cynthia M. Daniels, Smitha A. Francis, Susan C. Shih, William J. Salerno, Linda Hicke, and Ishwar Radhakrishnan. Solution Structure of a CUE-Ubiquitin Complex Reveals a Conserved Mode of Ubiquitin Binding. *Cell*, 113:621–630, 2003.

[56] Randall W. King, Peter K. Jackson, and Marc W. Kirschner. Mitosis in Transition. *Cell*, 79:563–571, 1994.

[57] Tsutomu Kishi and Fumiaki Yamao. An essential function of Grr1 for the degradation of Cln2 is to act as a binding core that links Cln2 to Skp1. *J Cell Sci*, 111:3655–3661, 1998.

[58] Manfred Koegl, Thorsten Hoppe, Stephen Schlenker, Helle D. Ulrich, Thomas U. Mayer, and Stefan Jentsch. A Novel Ubiquitination Factor, E4, Is Involved in Multiubiquitin Chain Assembly. *Cell*, 96:635–644, 1999.

[59] Talluru S. R. Krishna, Xiang-Peng Kong, Sonja Gary, Peter M. Burgers, and John Kuriyan. Crystal Structure of the Eukaryotic DNA Polymerase Processivity Factor PCNA. *Cell*, 79:1233–1243, 1994.

[60] Michael W. Lake, Margot M. Wuebbens, K. V. Rajagopalan, and Hermann Schindelin. Mechanism of ubiquitin activation revealed by the structure of a bacterial MoeB-MoaD complex. *Nature*, 414:325–329, 2001.

[61] Jan Löwe, Daniela Stock, Bing Jap, Peter Zwickl, Wolfgang Baumeister, and Robert Huber. Crystal Structure of the 20S Proteasome from the Archaeon *T. acidophilum* at 3.4 Å Resolution. *Science*, 268:533–539, 1995.

[62] Ziqiang Li, Wei Xiao, J. Justin McCormick, and Veronica M. Maher. Identification of a protein essential for a major pathway used by human cells to avoid UV-induced DAN damage. *Proc Natl Acad Sci U S A*, 99:4459–4464, 2002.

[63] Kevin L. Lorick, Jane P. Jenson, Shengyun Fang, Albert M. Ong, Shigetsugu Hatakeyama, and Allan M. Weissman. RING fingers mediate ubiquitin-conjugating enzyme (E2)-dependent ubiquitination. *Proc Natl Acad Sci U S A*, 96:11364–11369, 1999.

[64] Lucy D. Mastrandrea, Jianxin You, Edward G. Niles, and Cecile M. Pickart. E2/E3-mediated Assembly of Lysine 29-linked Polyubiquitin Chains. *J Biol Chem*, 274:27299–27306, 1999.

[65] Sean McKenna, Trevor Moraes, Landon Pastushok, Christopher Ptak, Wei Xiao, Leo Spyracopoulos, and Michael J. Ellison. An NMR-based Model of the Ubiquitin-bound Human Ubiquitin Conjugation Complex Mms2·Ubc13. The structural basis for lysine 63 chain catalysis. *J Biol Chem*, 278:13151–13158, 2003.

[66] Sean McKenna, Leo Spyracopoulos, Trevor Moraes, Landon Pastushok, Christopher Ptak, Wei Xiao, and Michael J. Ellison. Noncovalent Interaction between Ubiquitin and the Human DNA Repair Protein Mms2 Is Required for Ubc13-mediated Polyubiquitination. *J Biol Chem*, 276:40120–40126, 2001.

[67] Frauke Melchior. SUMO–Nonclassical Ubiquitin. *Annu Rev Cell Dev Biol*, 16:591–626, 2000.

[68] Wuyi Meng, Sansana Sawasdikosol, Steven J. Burakoff, and Michael J. Eck. Structure of the amino-terminal domain of Cbl complexed to its binding site on ZAP-70 kinase. *Nature*, 398:84–90, 1999.

[69] Nadine Merkley and Gary S. Shaw. Solution Structure of the Flexible Class II Ubiquitin-conjugating Enzyme Ubc1 Provides Insights for Polyubiquitin Chain Assembly. *J Biol Chem*, 279:47139–47147, 2004.

[70] Takaaki Miura, Werner Klaus, Bernard Gsell, Chikara Miyamoto, and Hans Senn. Characterization of the binding interface between ubiquitin and class I human ubiquitin-conjugating enzyme 2b by multidimensional heteronuclear NMR spectroscopy in solution. *J Mol Biol*, 290:213–228, 1999.

[71] Alessia Montagnoli, Francesca Fiore, Esther Eytan, Andrea C. Carrano, Giulio F. Draetta, Avram Hershko, and Michele Pagano. Ubiquitination of p27 is regulated by Cdk-dependent phosphorylation and trimeric complex formation. *Genes Dev*, 13:1181–1189, 1999.

[72] Trevor Moraes. *A Structural and Functional Characterization of Ubc13, Mms2, and Uev1a: Insights into the Mechanism of Alternative Ubiquitin Chain Synthesis.* PhD thesis, University of Alberta, 2004.

[73] Trevor F. Moraes, Ross A. Edwards, Sean McKenna, Landon Pastushok, Wei Xiao, J. N. Mark Glover, and Michael J. Ellison. Crystal structure of the human ubiquitin conjugating enzyme complex, hMms2-hUbc13. *Nat Struct Biol*, 8:669–673, 2001.

[74] Mitsuru Morimoto, Tamotsu Nishida, Reiko Honda, and Hideyo Yasuda. Modification of Cullin-1 by Ubiquitin-like Protein Nedd8 Enhances the Activity of SCF^{skp2} toward $p27^{kip1}$. *Proc Natl Acad Sci U S A*, 97:4579–4584, 2000.

[75] Joanna R. Morris and Ellen Solomon. BRCA1:BARD1 induces the formation of conjugated ubiquitin structures, dependent on K6 of ubiquitin, in cells during DNA replication and repair. *Hum Mol Genet*, 13:807–817, 2004.

[76] Piers Nash, Xiaojing Tang, Stephen Orlicky, Qinghua Chen, Frank B. Gertler, Michael D. Mendenhall, Frank Sicheri, Tony Pawson, and Mike Tyers. Multisite phosphorylation of a CDK inhibitor sets a threshold for the onset of DNA replication. *Nature*, 414:514–521, 2001.

[77] John R. Nelson, Christopher W. Lawrence, and David C. Hinkle. Thymine-Thymine Dimer Bypass by Yeast DNA Polymerase ζ. *Science*, 272:1646–1649, 1996.

[78] Hiroyuki Nishikawa, Seido Ooka, Ko Sato, Kei Arima, Joji Okamoto, Rachel E. Klevit, Mamoru Fukuda, and Tomohiko Ohta. Mass Spectrometric and Mutational Analyses Reveal Lys-6-linked Polyubiquitin Chains Catalyzed by BRCA1-BARD1 Ubiquitin Ligase. *J Biol Chem*, 279:3916–3924, 2004.

[79] Ulrike Nuber and Martin Scheffner. Identification of determinants in E2 ubiquitin-conjugating enzymes required for hect E3 ubiquitin-protein ligase interaction. *J Biol Chem*, 274:7576–7582, 1999.

[80] Ayako Ohno, JunGoo Jee, Kenichiro Fujiwara, Takeshi Tenno, Natsuko Goda, Hidehito Tochio, Hideki Kobayashi, Hidekazu Hiroaki, and Masahiro Shirakawa. Structure of the UBA Domain of Dsk2p in Complex with Ubiquitin: Molecular Determinants for Ubiquitin Recognition. *Structure*, 13:521–532, 2005.

[81] Efterpi Papouli, Shuhua Chen, Adelina A. Davies, Diana Huttner, Lumir Krejci, Patrick Sung, and Helle D. Ulrich. Crosstalk between SUMO and Ubiquitin on PCNA Is Mediated by Recruitment of the Helicase Srs2p. *Mol Cell*, 19:123–133, 2005.

[82] Landon Pastushok, Trevor F. Moraes, Michael J. Ellison, and Wei Xiao. A Single Mms2 "Key" Residue Insertion into a Ubc13 Pocket Determines the Interface Specificity of a Human $Lys^{6}3$ Ubiquitin Conjugation Complex. *J Biol Chem*, 280:17891–17900, 2005.

[83] Junmin Peng, Daniel Schwartz, Joshua E Elias, Carson C Thoreen, Dongmei Cheng, Gerald Marsischky, Jeroen Roelofs, Daniel Finley, and Steven P Gygi. A proteomics approach to understanding protein ubiquitination. *Nat Biotechnol*, 21:921–926, 2003.

[84] Boris Pfander, George-Lucien Moldovan, Meik Sacher, Carsten Hoege, and Stefan Jentsch. SUMO-modified PCNA recruits Srs2 to prevent recombination during S phase. *Nature*, 436:428–433, 2005.

[85] Cecile M. Pickart. Mechanisms Underlying Ubiquitination. *Annu Rev Biochem*, 70:503–533, 2001.

[86] Cecile M. Pickart and Michael J. Eddins. Ubiquitin: structures, functions, mechanisms. *Biochim Biophys Acta*, 1695:55–72, 2004.

[87] Julia Piotrowski, Richard Beal, Laura Hoffman, Keith D. Wilkinson, Robert E. Cohen, and Cecile M. Pickart. Inhibition of the 26 S Proteasome by Polyubiquitin Chains Synthesized to Have Defined Lengths. *J Biol Chem*, 272:23712–23721, 1997.

[88] Owen Pornillos, Steven L. Alam, Rebecca L. Rich, David G. Myszka, Darrell R. Davis, and Wesley I. Sundquist. Structure and functional interactions of the Tsg101 UEV domain. *Embo J*, 21:2397–2406, 2002.

[89] Owen Pornillos, Daniel S. Higginson, Kirsten M. Stray, Robert D. Fisher, Jennifer E. Garrus, Marielle Payne, Gong-Ping He, Hubert E. Wang, Scott G. Morham, and Wesley I. Sundquist. HIV Gag mimics the Tsg101-recruiting activity of the human Hrs Protein. *J Cell Biol*, 162:425–434, 2003.

[90] Vladimir N. Postust, James E. Brownell, Tatiana B. Gladysheva, Rong-Shu Luo, Chunhua Wang, Michael B. Coggins, Jacqueline W. Pierce, Eric S. Lightcap, and Vincent Chau. A Nedd8 conjugation pathway is essential for proteolytic targetting of $p27^{Kip1}$ by ubiquitination. *Proc Natl Acad Sci U S A*, 97:4579–4584, 2000.

[91] Gali Prag, Saurav Misra, Eudora A. Jones, Rodolfo Ghirlando, Brian A. Davies, Bruce F. Horazdovsky, and James H. Hurley. Mechanism of Ubiquitin Recognition by the CUE Domain of Vps9p. *Cell*, 113:609–620, 2003.

[92] Mike Rothe, Suzy C. Wong, William J. Henzel, and David V. Goeddel. A Novel Family of Putative Signal Transducers Associated with the Cytoplasmic Domain of the 75 kDa Tumor Necrosis Factor Receptor. *Cell*, 78:681–692, 1994.

[93] Nathaniel S. Russell and Keith D. Wilkinson. Identification of a Novel 29-Linked Polyubiquitin Binding Protein, Ufd3, Using Polyubiquitin Chain Analogues. *Biochemistry*, 43:4844–4854, 2004.

[94] Martin Scheffner, Ulrike Nuber, and Jon M. Huibregtse. Protein ubiquitination involving an E1-E2-E3 enzyme ubiquitin thioester cascade. *Nature*, 373:81–83, 1995.

[95] David C. Schwartz and Mark Hochstrasser. A superfamily of protein tags: ubiquitin, SUMO and related modifiers. *Trends Biochem Sci*, 28:321–328, 2003.

[96] Sylvia E. Schwartz, José L. Rosa, and Martin Scheffner. Characterization of Human hect Domain Family Members and Their Interaction with UbcH5 and UbcH7. *J Biol Chem*, 273:12148–12154, 1998.

[97] Daniel M. Scolnick and Thanos D. Halazonetis. Chfr defines a mitotic stress checkpoint that delays entry into metaphase. *Nature*, 406:430–435, 2000.

[98] Darcie A. Sharp, Stephen A. Kratowicz, Michael J. Sank, and Donna L. George. Stabilization of the MDM2 Oncoprotein by Interaction with the Structurally Related MDMX Protein. *J Biol Chem*, 274:38189–38196, 1999.

[99] Susan C. Shih, David J. Katzmann, Joshua D. Schnell, Myra Sutanto, Scott D. Emr, and Linda Hicke. Epsins and Vps27p/Hrs contain ubiquitin-binding domains that function in receptor endocytosis. *Nat Cell Biol*, 4:389–393, 2002.

[100] Susan C. Shih, Gali Prag, Smitha A. Francis, Myra A. Sutanto, James H. Hurley, and Linda Hicke. A ubiquitin-binding motif required for intramolecular monoubiquitylation, the CUE domain. *Embo J*, 22:1273–1281, 2003.

[101] Dorota Skowrya, Karen L. Craig, Mike Tyers, Stephen J. Elledge, and J. Wade Harper. F-Box Proteins Are Receptors that Recruit Phosphorylated Substrates to the SCF Ubiquitin-Ligase Complex. *Cell*, 91:209–219, 1997.

[102] Thomas Sommer and Stefan Jentsch. A protein translocation defect linked to ubiquitin conjugation at the endoplasmic reticulum. *Nature*, 365:176–179, 1993.

[103] Elena S. Stavridi, Yentram Huyen, Ivy R. Loreto, Daniel M. Scolnick, Thanos D. Halazonetis, Nikola P. Pavletich, and Philip D. Jeffrey. Crystal Structure of the FHA Domain of the Chfr Mitotic Checkpoint Protein and Its Complex with Tungstate. *Structure*, 10:891–899, 2002.

[104] Wesley I. Sundquist, Heidi L. Schubert, Brian N. Kelly, Gina C. Hill, James M. Holton, and Christopher P. Hill. Ubiquitin Recognition by the Human TSG101 Protein. *Mol Cell*, 13:783–789, 2004.

[105] Kurt A. Swanson, Richard S. Kang, Svetoslava D. Stamenova, Linda Hicke, and Ishwat Radhakrishnan. Solution structure of Vps27 UIM-ubiquitin complex important for endosomal sorting and receptor downregulation. *Embo J*, 22:4597–4606, 2003.

[106] Michael H. Tatham, Ellis Jaffray, Owen A. Vaughan, Joana M. P. Desterro, Catherine H. Botting, James H. Naismith, and Ronald T. Hay. Polymeric Chains of SUMO-2 and SUMO-3 Are Conjugated to Protein Substrates by SAE1/SAE2 and Ubc9. *J Biol Chem*, 276:35368–35374, 2001.

[107] Michael H. Tatham, Suhkmann Kim, Bin Yu, Elis Jaffrey, Jing Song, Jian Zheng, Manuel S. Rodriguez, Ronald . Hay, and Yuan Chen. Role of an N-Terminal Site of Ubc9 in SUMO-1, -2, and -3 Binding and Conjugation. *Biochemistry*, 42:9959–9969, 2003.

[108] Julia S. Thrower, Laura Hoffman, Martin Rechsteiner, and Cecile M. Pickart. Recognition of the polyubiquitin proteolytic signal. *Embo J*, 19:94–102, 2000.

[109] Helle D. Ulrich and Stefan Jentsch. Two RING finger proteins mediate cooperation between ubiquitin-conjugating enzymes in DNA repair. *Embo J*, 19:3388–3397, 2000.

[110] Andrew P. VanDemark and Christopher P. Hill. Structural basis of ubiquitylation. *Curr Opin Struct Biol*, 12:822–830, 2002.

[111] Andrew P. VanDemark, Roseanne M. Hofmann, Colleen Tsui, Cecile M. Pickart, and Cynthia Wolberger. Molecular Insights into Polyubiquitin Chain Assembly: Crystal Structure of the Mms2/Ubc13 Heterodimer. *Cell*, 105:711–720, 2001.

[112] Mark A. Verdecia, Claudio A. P. Joazeiro, Nicholas J. Wells, Jean-Luc Ferrer, Marianne E. Bowman, Tony Hunter, and Joseph P. Noel. Conformational Flexibility Underlies Ubiquitin Ligation Mediated by the WWP1 HECT Domain E3 Ligase. *Mol Cell*, 11:249–259, 2003.

[113] Senadhi Vijay-Kumar, Charles E. Bugg, and William J. Cook. Structure of Ubiquitin Refined at 1.8 Å Resolution. *J Mol Biol*, 194:531–544, 1987.

[114] Eduardo Villalobo, Loïc Morin, Clara Moch, Rachel Lescasse, Michelle Hanna, Wei Xiao, and Anne Baroin-Tourancheau. A Homologue of CROC-1 in a Ciliated Protist (*Sterkiella histriomuscorum*) Testifies to the Ancient Origin of the Ubiquitin-conjugating Enzyme Variant Family. *Mol Biol Evol*, 19:39–48, 2002.

[115] Helen Walden, Michael S. Podgorski, Danny T. Huang, David W. Miller, Rebecca J. Howard, Daniel L. Minor Jr., James M. Holton, and Brenda A. Schulman. The Structure of the APPBP1-UBA3-NEDD8-ATP Complex Reveals the Basis for Selective Ubiquitin-like Protein Activation by an E1. *Mol Cell*, 12:1427–1437, 2003.

[116] Chen Wang, Li Deng, Mei Hong, Giridhar R. Akkaraju, Jun-Ichiro Inoue, and Zhijian J. Chen. TAK1 is a ubiquitin-dependent kinase of MKK and IKK. *Nature*, 412:346–351, 2001.

[117] Felicity Z. Watts. Sumoylation of PCNA: Wrestling with recombination at stalled replication forks. *DNA Repair*, 0:In Press, 2005.

[118] Frank G. Whitby, Gang Xia, Cecile M. Pickart, and Christopher P. Hill. Crystal Structure of the Human Ubiquitin-like Protein NEDD8 and Interactions with Ubiquitin Pathway Enzymes. *J Biol Chem*, 273:34983–34991, 1998.

[119] Peter J. Winn, Tomasz L. Religa, James N. D. Battey, Amit Banerjee, and Rebecca C. Wade. Determinants of Functionality in the Ubiquitin Conjugating Enzyme Family. *Structure*, 12:1563–1574, 2004.

[120] Jill Wooff, Landon Pastushok, Michelle Hanna, Yu Fu, and Wei Xiao. The TRAF6 RING finger domain mediates physical interaction with Ubc13. *FEBS L*, 566:229–233, 2004.

[121] Pei-Ying Wu, Mary Hanlon, Michael Eddins, Colleen Tsui, Richard S. Rogers, Jane P. Jensen, Michael J. Matunis, Allan M. Weisman, Cynthia P. Wolberger, and Cecile M. Pickart. A conserved catalytic residue in the ubiquitin-conjugating enzyme family. *Embo J*, 22:5241–5250, 2003.

[122] Foon Wu-Baer, Karen Lagrazon, Wei Yuan, and Richard Baer. The BRCA1/BARD1 Heterodimer Assembles Polyubiquitin Chains through an Unconventional Linkage Involving Lysine Residue K6 of Ubiquitin. *J Biol Chem*, 278:34743–34746, 2003.

[123] Wei Xiao, Stanley L. Lin, Stacey Broomfield, Barbara L. Chow, and Ying-Fei Wei. The products of the yeast *MMS2* and two human homologs (*hMMS2* and *CROC-1*) define a structurally and functionally conserved Ubc-like protein family. *Nucleic Acids Res*, 26:3908–3914, 1998.

[124] Yukiko Yoshida, Tomoki Chiba, Fuminori Tokunaga, Hiroshi Kawasaki, Kazuhiro Iwai, Toshiaki Suzuki, Yukishige Ito, Koji Matsuoka, Minoru Yoshida, Keiji Tanaka, and Tadashi Tai. E3 ubiquitin ligase that recognizes sugar chains. *Nature*, 418:438–442, 2002.

[125] Jianxin You and Cecile M. Pickart. A HECT Domain E3 Enzyme Assembles Novel Polyubiquitin Chains. *J Biol Chem*, 276:19871–19878, 2001.

[126] Xiaochun Yu, Katherine Minter-Dykhouse, Liviu Malureanu, Wei-Meng Zhao, Dongwei Zhang, Carolin J. Merkle, Irene M. Ward, Hideyuki Saya, Guowei Fang, Jan van Deursen, and Junjie Chen. Chfr is required for tumor suppression and Aurora A regulation. *Nat Genet*, 37:401–406, 2005.

[127] Ning Zheng, Ping Wang Philip D. Jeffrey, and Nicola P. Pavletich. Structure of a c-Cbl-UbcH7 Complex: RING Domain Function in Ubiquitin-Protein Ligases. *Cell*, 102:533–539, 2000.

[128] Ning Zheng, Brenda A. Schulman, Langzhou Song, Julie J. Miller, Philip D. Jeffrey, Ping Wang, Claire Chu, Deanna M. Koepp, Stephen J. Elledge, Michele Pagano, Ronald C. Conaway, Joan W. Conaway, J. Wade Harper, and Nikola P. Pavletich. Structure of the Cul1-Rbx1-Skp1-F box^{Skp2} SCF ubiquitin ligase complex. *Nature*, 416:703–709, 2002.

[129] Honglin Zhou, Ingrid Wertz, Karen O'Rourke, Mark Ultsch, Somasekar Seshagiri, Michael Eby, Wei Xiao, and Vishva M. Dixit. Bcl10 activates the NF-κB pathway through ubiquitination of NEMO. *Nature*, 427:167–171, 2004.

Chapter 2

Main Chain and Side Chain Chemical Shift Assignment for the hMms2-Ub Complex

2.1 Introduction

The post-translational addition of ubiquitin (Ub) to a target protein plays a pivotal role in the regulation of cell processes in eukaryotes [6, 2, 12]. In the most studied pathway, polyubiquitin chains linked through Lys48 serve to target proteins for degradation by the 26S proteasome [12]. The first step of this process involves the covalent attachment of the C-terminus of Ub (Gly76) to the active site cysteine of a ubiquitin activating enzyme (E1), where it is subsequently transferred as a thiolester intermediate to a ubiquitin conjugating enzyme (E2). Finally, Ub is attached to a target protein through the activity of a ubiquitin ligase (E3). Ultimately, polyubiquitin chains are built up by the formation of isopeptide bonds between Lys48 of one Ub and the C-terminus of a sequential Ub, through a mechanism

for which the details are presently unknown.

Ubiquitin is involved in regulatory mechanisms in eukaryotes that are distinct from signaling for proteolysis. For example, protein mono-ubiquitination is involved in vesicle budding, transcriptional regulation, and receptor endocytosis [15, 14]. Polyubiquitin chains linked through Lys63 have been implicated in error-free DNA repair [3, 18, 17], and NF-κB activation [9, 39].

Lys63-linked polyubiquitin chains are covalently assembled by a protein heterodimer consisting of an E2 and a ubiquitin E2 variant, or UEV. UEVs are structurally similar to E2s, but lack the canonical active site cysteine residue that is necessary to catalyze isopeptide bond formation with the C-terminus of Ub. UEV domains comprise one type of structurally distinct ubiquitin binding motifs. Other ubiquitin binding motifs include CUE (similar to yeast Cue1p), UBA (Ub associated domain), and UIM (Ub interacting motif) [35]. The ubiquitin binding properties of these motifs are variable, and have been recently reviewed in [16].

In yeast, Lys63-linked polyubiquitin chains function in the post-transcriptional DNA repair pathway [3, 18]. The chains are assembled by a heterodimer consisting of Ubc13, a typical class I E2, and Mms2, a UEV. The human homologue of the Mms2-Ubc13 complex has been identified, and shown to complement DNA repair defects in yeast, implicating this complex for DNA repair in humans [42].

A mechanism for Lys63-linked chain catalysis has been proposed based on a combination of X-ray crystallography [30], NMR [28, 27, 26], and ITC [26] studies. For this model, the active site cysteine of hUbc13 is covalently attached to the C-terminus of a "donor" Ub, and hMms2 is non-covalently associated with an "acceptor" Ub whose Lys63 is proximal to the active site cysteine of hUbc13. Of the three major protein-protein interactions

in the tetramer (E2-UEV, UEV-Ub, and E2-Ub), only the hMms2-hUbc13 complex has been characterized at high resolution using X-ray crystallography [30]. Crystallization of hMms2-hUbc13 with acceptor and/or donor Ub is difficult, presumably due to the low binding affinity between hMms2 and the acceptor Ub ($K_D = 98 \pm 15$ μM) [26], and the instability of the thiolester bond between hUbc13 and the donor Ub [29]. The present study outlines NMR chemical shift assignment for hMms2 and acceptor Ub in the bound state, and a preliminary *de novo* NOE-based solution structure for the hMms2-Ub complex.

2.2 Materials and Methods

2.2.1 Protein expression and purification

In order to determine the structure of the hMms2-Ub complex using solution state NMR spectroscopy, three NMR samples containing various proteins or combinations of proteins were prepared: ~2.0 mM [*U*-^{15}N; *U*-^{13}C]-Ubiquitin K48R and ~0.5 mM hMms2; ~0.5 mM [*U*-^{15}N; *U*-^{13}C]-hMms2 and ~2.0 mM Ubiquitin; and ~0.6 mM [*U*-^{15}N; *U*-10% ^{13}C]-hMms2.

Ubiquitin

[*U*-^{15}N; *U*-^{13}C]-Ubiquitin K48R was expressed in *E. coli* strain BL21(DE3)-RIL in the following manner: 50 mL of LB medium (10 g/L bacto-tryptone, 5 g/L bacto-yeast extract and 10g/L NaCl, pH 7.5) containing ~50 μg/mL ampicillin and ~25 μg/mL chloramphenicol was inoculated with a single colony and allowed to grow to A_{600} ~0.9. 2 mL of this culture was used to inoculate 2 L of M9 minimal media [34] containing 2 g/L [$^{13}C_6$, 99%] D-glucose as the sole carbon source and 1 g/L [^{15}N, 98%] ammonium sulfate as the sole nitrogen source. The media also contained 2 mM $MgSO_4$, 2 μM $FeSO_4$, 5 mg/L thiamine, 1 mL/L vitamin solution [36], 50 μg/mL ampicillin, and 25 μg/mL chloramphenicol.

The cells were grown at 25 °C with aeration to A_{600} ~0.8, and induced with 0.4 mM IPTG. The cells were grown for an additional 4 hours and harvested by centrifugation. The cell pellet was resuspended in lysis buffer (140 mM NaCl, 2.7 mM KCl, 10 mM Na_2HPO_4, 1.8 mM KH_2PO_4, 100 μg/mL DNase I, 1 mM DTT, 10 mM $MgSO_4$, 0.5% protease inhibitor cocktail II (Calbiochem catalog #538132)) and lysed by two passes through a French press. The lysate was clarified by centrifugation at 25,000 rpm in a Beckman JA 25.5 rotor, and the supernatant was filtered through a Millipore steriflip 0.45 μm vacuum filtration device. The filtrate was loaded onto a HiLoad 26/10 Q-Sepharose column equilibrated with 50 mM TRIS, 1 mM EDTA, and 1 mM DTT, pH 7.0. Fractions eluting between 50-127 mL were pooled and passed over the Q-Sepharose column a second time. Fractions eluting between 50-200 mL were collected, concentrated to a volume of ~1.4 mL, and loaded onto a Hiload 26/60 Superdex 30 column. Fractions eluting at ~150 mL were collected and concentrated to ~2 mL using Amicon Ultra15 5K and Millipore Ultrafree 0.5 BioMax 5K centrifugal membrane filtration devices.

Ubiquitin K48R was expressed in *E. coli* strain BL21(DE3)-RIL. 2 L cultures of LB media containing ~50 μg/mL ampicillin were grown at 37 °C to A_{600} ~1.3, subsequently induced with 0.4 mM IPTG, and allowed to grow ~12 hours. Bacterial cells were subjected to centrifugation at 5000 rpm in a Beckman JLA 10.5 rotor for 15 minutes and re-suspended in buffer containing 140 mM NaCl, 2.7 mM KCl, 10 mM Na_2HPO_4, 1.8 mM KH_2PO_4. Clarification of the cell lysate was achieved by centrifugation at 25000 rpm in a Beckman JA-25.5 rotor for 20 minutes followed by filtration through a Millipore steriflip 0.45 μm vacuum filtration unit. The filtered solution was passed two times through a Q-Sepharose HiLoad 26/10 ion-exchange column equilibrated in pH 7.0 buffer containing 50 mM TRIS, 1 mM DTT, and 1 mM EDTA. The flow-through was lyophilized, dry protein was dissolved in

distilled H_2O, and this solution was passed over a Superdex 30 HiLoad 26/60 size-exclusion column equilibrated with pH 7.0 buffer containing 50 mM sodium phosphate, 50 mM NaCl, and 1 mM DTT. Column fractions eluting at ~150 mL were collected and buffer-exchanged using a series of three HiPrep 26/10 desalting columns equilibrated with pH 8.0 buffer containing 25 mM ammonium bicarbonate. The flow-through was collected and lyophilized to yield dry protein that was used in subsequent NMR studies.

hMms2

Human Mms2 was cloned as a GST fusion protein as previously described [28]. [*U*-^{15}N; *U*-^{13}C]-Mms2 protein was expressed in *E. coli* strain BL21(DE3)RIL as follows: 50 mL of LB containing 50 μg/mL ampicillin and 25 μg/mL chloramphenicol was inoculated with a single colony and grown at 37 °C with aeration to A_{600} ~0.8. 2 L of M9 media was prepared in an identical fashion as that for production of [*U*-^{15}N; *U*-^{13}C]-Ub. The M9 media was inoculated with 2 mL of LB culture and grown overnight (~16 hours) at 25 °C with aeration to A_{600} ~0.8, induced with 0.4 mM IPTG, and incubated for an additional 9 hours.

Cells were harvested by centrifugation, the cell pellets were resuspended in ~70 mL lysis buffer (as prepared for Ub). Cells were lysed by two passes through a French press and the lysate was clarified by centrifugation. The supernatant was then filtered through a Millipore steriflip 0.45 μm vacuum filtration device. The filtered lysate was loaded onto a GSTprep FF 16/10 column equilibrated in pH 7.4 buffer containing 140 mM NaCl, 2.7 mM KCl, 10 mM Na_2HPO_4 and 1.8 mM KH_2PO_4. GST-fusion protein was eluted from the column with buffer containing 50 mM TrisHCl, 10 mM reduced glutathione, pH 8.0. Fractions eluting with glutathione buffer were collected, pooled, and buffer exchanged by passage through three HiPrep 26/10 desalting columns equilibrated with pH 7.0 buffer containing 50 mM

TRIS, 150 mM NaCl, 1 mM EDTA, and 1 mM DTT. The flow-through was collected and concentrated to ~5 mL. 10 μL (20 units) of PreScission protease was added to the concentrated protein and the cleavage reaction was allowed to proceed for 24 hours at 4 °C. The cleaved protein was then purified with a GSTprep FF 16/10 column as described above for the intact fusion protein. The flow-through was collected and further purified by loading 9 mL of protein solution twice onto a HiLoad 26/60 Superdex 75 column equilibrated with buffer containing 50 mM sodium phosphate, 50 mM NaCl, and 1 mM DTT, pH 7.0. The peak fractions eluting at 185–210 mL were pooled and concentrated for NMR studies. In order to stereospecifically assign the methyl groups of hMms2, [*U*-^{15}N; *U*-10% ^{13}C]-Mms2 was expressed in *E. coli* strain BL21(DE3)-RIPL using the protocol described by Neri et al [32].

Expression of unlabeled hMms2 was accomplished in a similar fashion as Ub-K48R. Purification of unlabeled hMms2 was identical to [*U*-^{15}N; *U*-^{13}C]-Mms2.

2.2.2 NMR spectroscopy

All NMR spectra were obtained using either Varian Unity INOVA 600, or 800 MHz NMR spectrometers. For [*U*-^{15}N; *U*-^{13}C]-hMms2 and [*U*-^{15}N; *U*-^{13}C]-Ub, NMR samples were 600 μL for standard 5 mm i.d. NMR tubes, and 300 μL for SHIGEMI microcell NMR tubes, and contained 9:1 H2O/D2O with 50 mM phosphate (pH 7.5) 150 mM NaCl, 1 mM DTT, 1 mM DSS, 3 mL of 100x stock protease inhibitor cocktail I (Calbiochem catalog #539131), with ~0.5 mM hMms2 and ~2.0 mM Ub. For [*U*-^{15}N; *U*-10% ^{13}C]-hMms2, samples were 600 μL in 5 mm i.d. NMR tubes with sample conditions same as above, with the exception that the protein concentration used was ~0.6 mM hMms2.

Chemical shift assignment of Ub - Unambiguous assignment of the Ub main chain atoms was completed at 30 °C using a combination of the HNCACB [41, 31] and (H)CCTOCSY(CO)NNH experiments [24, 11]. Non-aromatic side chain atoms were assigned using the H(CC)TOCSY(CO)NNH and (H)CCTOCSY(CO)NNH experiments [25, 24, 11], and the HCCH-TOCSY experiment [1, 22]. Aromatic side chains were assigned using a constant-time [38] ^{13}C-edited NOESY-HSQC experiment. All spectra were processed using the program NMRPipe [7], and chemical shift assignment was accomplished using the program NMRView [19].

Chemical shift assignment of hMms2 bound to Ub - NMR experiments for chemical shift assignment of hMms2 bound to Ub were collected using a 1:4 [*U*-^{13}C; *U*-^{15}N]-hMms2:unlabelled Ub sample ([hMms2] ~0.5 mM). The main chain atoms of hMms2 were unambiguously assigned using a combination of the HNCA [20, 5, 21, 31] and HN(CO)CA [20, 43] experiments at 30 °C. Methyl group ^{1}H and ^{13}C assignments were accomplished using the MQ-(H)CC$_m$H$_m$-TOCSY experiment at 30 °C [44]. Partial assignments for non-methyl and non-aromatic side chain atoms were obtained in the same fashion as the side chain atoms for Ub, with the exception that the spectra were obtained at 40 °C. The prochiral Val and Leu methyl groups of hMms2 were stereospecifically assigned using a non-constant time ^{1}H-^{13}C-HSQC spectrum obtained from a 1:4 [*U*-^{15}N; *U*-10% ^{13}C]-hMms2:unlabelled Ub sample at 30 °C [32]. hMms2 main chain chemical shift assignment was accomplished using the program NMRview [19], and side chain assignment was subsequently accomplished using the program Sparky [13].

Structure Determination - Interproton distance restraints were obtained from the ^{15}N-separated 3D NOESY HSQC [45] and ^{15}N-^{13}C-separated 3D NOESY HSQC [33] experiments. A total of 610 NOEs were assigned for Ub and 579 NOEs were assigned for Mms2. The NOE resonance peak intensities were calibrated to distance restraints in the range of

1.8 – 6.0 Å. Simulated annealing was performed using CNS (Crystallography and NMR System) [4]. Each protein was subjected to 50 simulated annealing trials, using intramolecular NOEs as restraints, and the structures were refined using an iterative approach. The top five lowest energy structures were included in each ensemble. The quality of the structures was assessed using the program Procheck [23].

Molecular Graphics - Protein structure graphics (Figures 2.4 and 2.5) were produced using the program Pymol [8].

2.3 Results and Discussion

2.3.1 Chemical shift assignment of hMms2 and Ub

Preliminary assignment of hMms2 in the Ub-bound state was accomplished by saturating [*U*-^{15}N; *U*-^{13}C]-hMms2 with a fourfold excess of Ub and collecting spectra at 30 °C. The large size of the complex (~26 kDa) is likely responsible for the poor signal to noise in the ^{13}C-TOCSY-based experiments. Thus, while the main chain (^{15}N, $^{1}H_N$, $^{13}C_\alpha$, $^{1}H_\alpha$) was 85.3% assigned, it was not possible to obtain substantial chemical shift assignments for the side chain atoms of hMms2 at 30 °C. However, nearly complete chemical shift assignment for the methyl groups of hMms2 was obtained using the MQ-(H)CC$_m$H$_m$-TOCSY experiment. In an effort to increase signal/noise ratio through an increased rate of rotational tumbling, the temperature at which NMR spectra were acquired was raised to 40 °C. As a result of this change, nearly double the number of assigned side chain ^{1}H and ^{13}C atoms was attained (from 233 to 412).

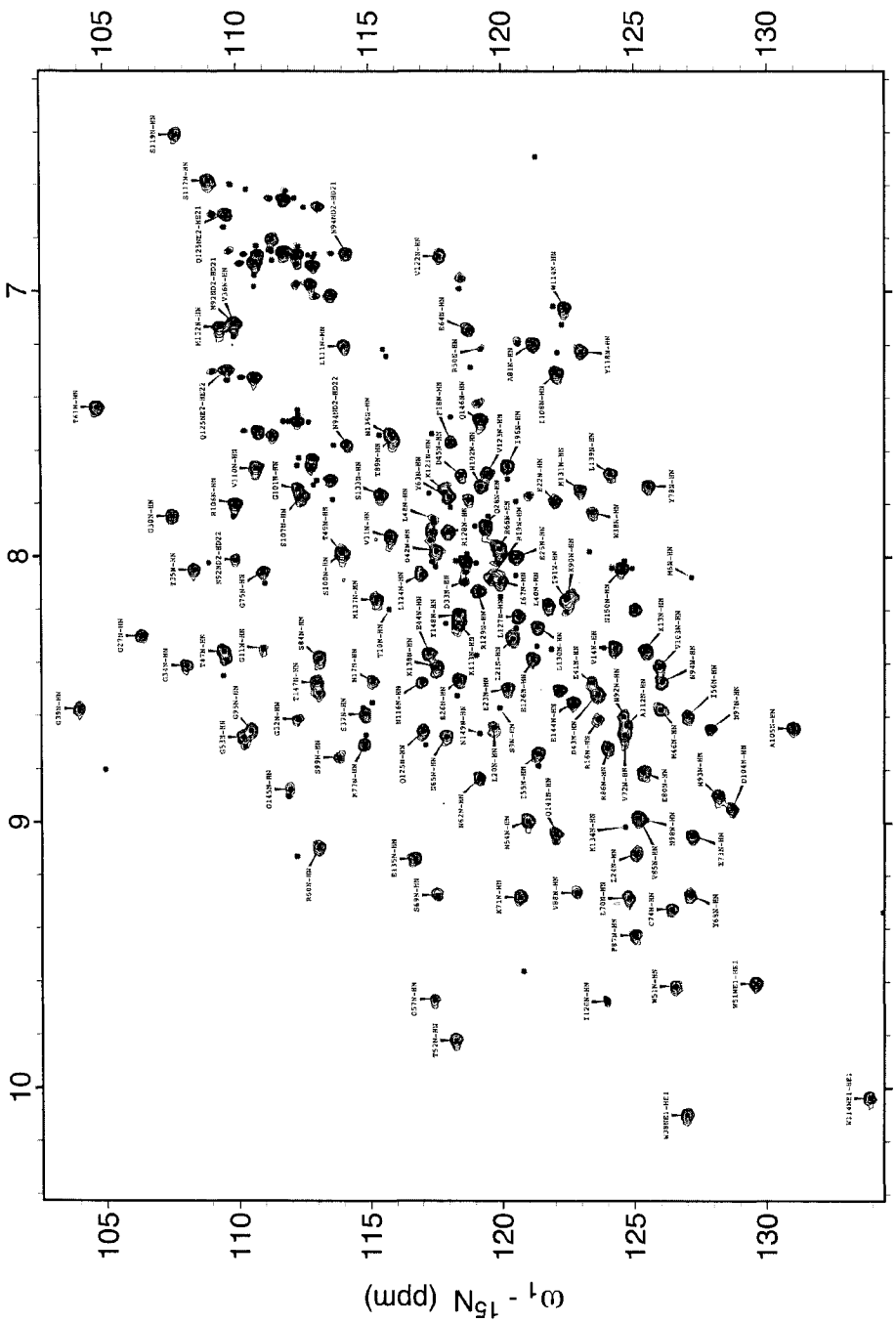

Figure 2.1: ^{1}H-^{15}N HSQC NMR Spectrum for hMms2.

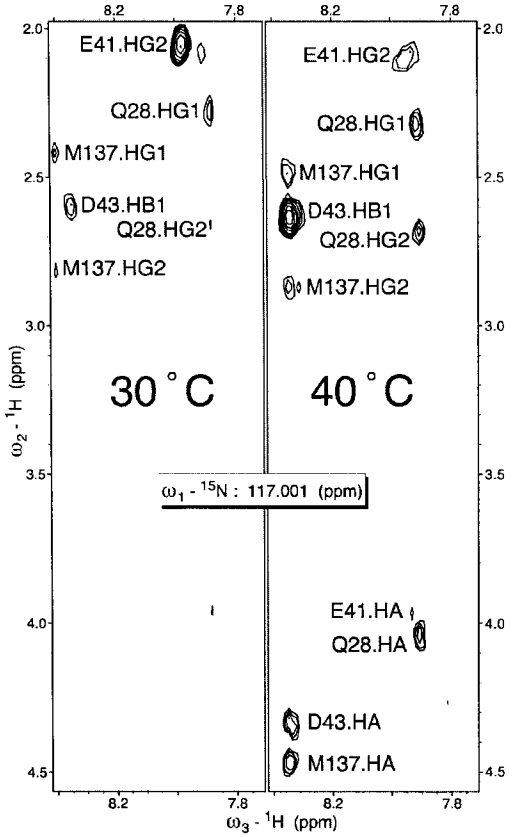

Figure 2.2: **Temperature dependence of H(CC)CONNH NMR spectra.** Comparison of slices from HCCCONNH spectra of Ub-bound [*U*-^{15}N; *U*-^{13}C]–Mms2 at 30 °C (left) and 40 °C (right).

Attempts to assign the chemical shifts of bound Ub by saturating [*U*-^{15}N; *U*-^{13}C]-Ub with a fourfold excess of hMms2 were unsuccessful due to protein precipitation. Therefore, a 4:1 [*U*-^{15}N; *U*-^{13}C]-Ub / unlabelled hMms2 sample was used to collect NMR spectra for chemical shift assignment of Ub at 30 °C. These conditions allowed nearly complete assignment of all Ub backbone and side chain atoms, given that Ub is mostly unbound.

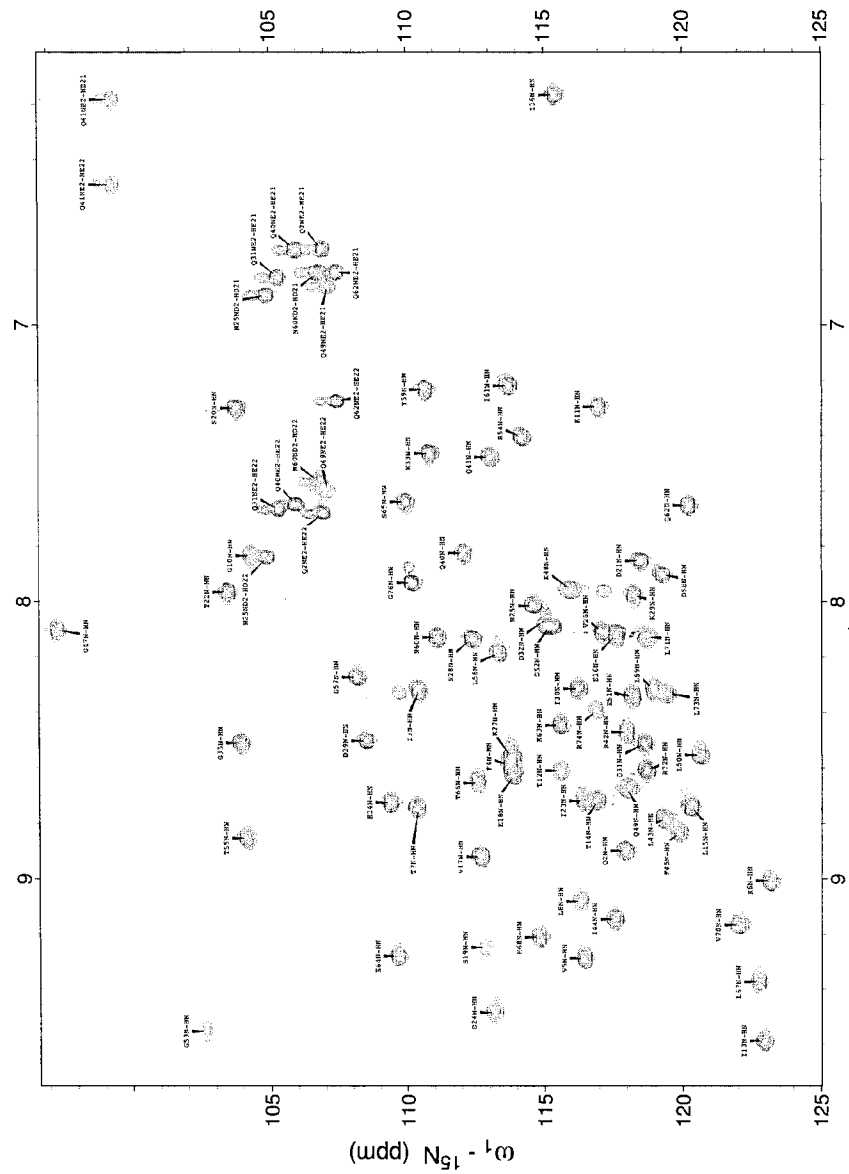

Figure 2.3: ^{1}H-^{15}N HSQC NMR Spectrum for Ub.

	Ub	*hMms2*
Distance Restraints		
Total	583	578
Intraresidue	248	206
Medium ($1 \leq \|i-j\| \leq 4$)	233	224
Long ($\|i-j\| > 4$)	102	148
^{13}C Chemical Shift Restraints	41	54
ϕ Dihedral Restraints	33	19
Total Restraints	657	651
Average Restraints per Residue	8.6	4.3
Restraint Violations	< 0.1	< 1.5
Ramachandran Plot		
Allowed Region	85.4%	72.2%
Generously Allowed Region	7.8%	17.1%
Disallowed Region	6.9%	10.7%
Mean Global RMSD (Å)		
backbone atoms	2.58 ± 0.55	8.25 ± 1.63
heavy atoms	3.21 ± 0.40	22.01 ± 5.21

Table 2.1: **Characteristics of the Preliminary Solution Structures for hMms2 bound to Ub and Free Ub.**

2.3.2 Description of the structures

The secondary structure of Ub is similar to that seen in the crystallographically determined structure [1UBQ], as shown in Figure 2.4. The α-helices are well defined, whereas the β-sheet is not as well defined. However, secondary structural elements determined using the chemical shift index (CSI) [40] are similar to those from the crystal structure. The lowest energy structure superimposes onto the crystallographically determined structure with a main chain rmsd of 2.56 Å. The largest deviations occur in the loop regions corresponding to residues 7-12 and 34-41, as well as the C-terminal residues 72-76. These poorly defined regions have low numbers of distance restraints per residue, and for these regions, main chain ^{15}N NMR relaxation experiments indicate that loop residues 7-12 and the C-terminal residues are the most flexible regions of Ub (BMRB accession number 6470) [37].

It is not surprising that the preliminary solution structure of hMms2 bound to Ub

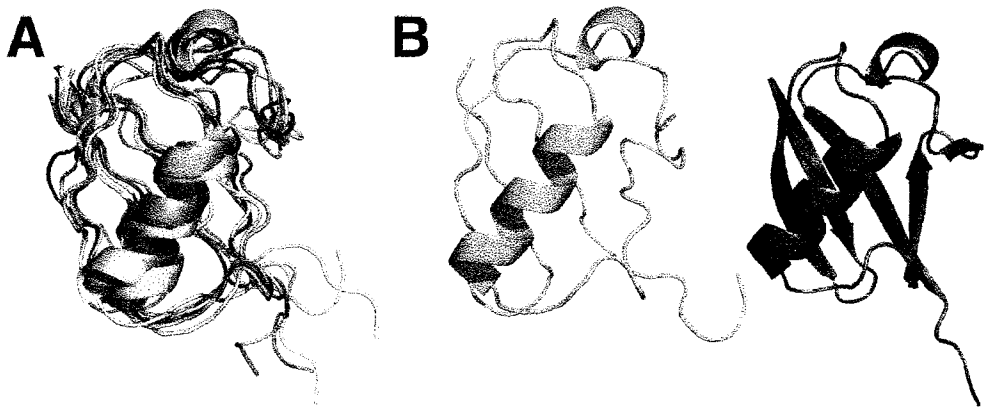

Figure 2.4: **Preliminary solution state structure of Ub.** (A) Ensemble of the lowest energy structures of Ub shown in the cartoon representation. (B) Comparison between the lowest energy solution structure (green) and the crystal structure (blue) of Ub [1UBQ] in the cartoon representation.

is poorly defined given the small number of intramolecular restraints used. The canonical secondary structure is poorly defined, however the CSI [40] predicts similar secondary structure to that observed in the crystallographically determined structure [1J74] [30]. The tertiary structure is poorly defined, most likely due to incomplete assignment of the side chain atoms, and subsequently, incomplete assignment of long-range NOEs.

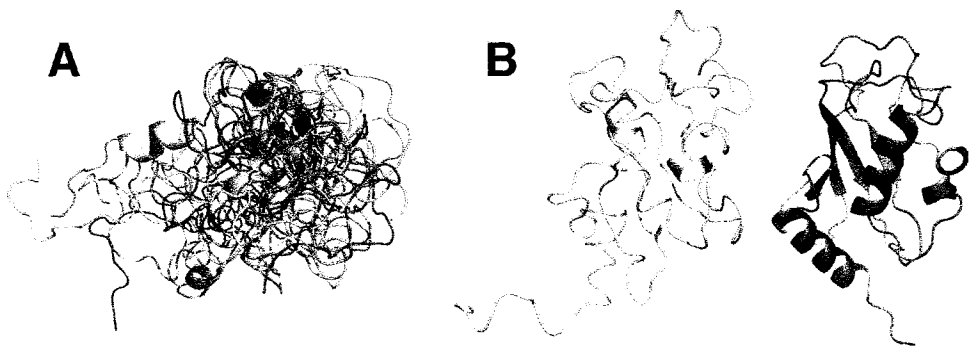

Figure 2.5: **Preliminary solution state structure of hMms2 bound to Ub.** (A) Ensemble of the lowest energy hMms2 structures shown in the cartoon representation. (B) Comparison between the lowest energy solution structure (green) and the crystal structure (blue) of hMms2 [1J74], shown in the cartoon representation.

2.4 Conclusion

In the present study we have compiled a database of chemical shifts for Ub-bound hMms2 and Ub (Appendix B.1). Complete side chain chemical shift assignment of hMms2 was hindered largely because of the size of the complex, which resulted in few assignments for the non-methyl side chains. The chemical shifts of Ub, on the other hand, were assigned almost completely, due to the fact that Ub was mostly unbound, and thus not subject to the slower tumbling rate of the fully bound complex.

Attempts to solve the solution state structure of hMms2 in the bound state were not successful due to a lack of chemical shift data for the side chains. For this reason, we have employed NMR methodologies that are focused on chemical shift assignment of methyl protons in combination with the NOE data driven program HADDOCK [10] to determine a high-resolution structure of the hMms2-Ub complex. The details of the structure determination form the basis of the next chapter.

Bibliography

[1] A. Bax, G. M. Clore, and A. M. Gronenborn. H-1-H-1 Correlation Via Isotropic Mixing of C-13 Magnetization, a New 3-Dimensional Approach for Assigning H-1 and C-13 Spectra of C-13-Enriched Proteins. *J Magn Reson*, 88:425–431, 1990.

[2] Yinon Ben-Neriah. Regulatory functions of ubiquitination in the immune system. *Nat Immunol*, 3:20–26, 2002.

[3] Stacey Broomfield, Barbara L. Chow, and Wei Xiao. *MMS2*, encoding a ubiquitin-conjugating-enzyme-like protein, is a member of the yeast error-free postreplication repair pathway. *Proc Natl Acad Sci U S A*, 95:5678–5683, 1998.

[4] A. T. Brunger, P. D. Adams, G. M. Clore, W. L. DeLano, P. Gros, R. W. Grosse-Kunstleve, J. S. Jiang, J. Kuszewski, M. Nilges, N. S. Pannu, Read R. J., L. M. Rice, T. Simonson, and G. L. Warren. Crystallography & NMR system: A new software suite for macromolecular structure determination. *Acta Crystallogr D Biol Crystallogr*, 54:905–921, 1998.

[5] J. Cavanagh, A. G. Palmer, P. E. Wright, and M. Rance. Sensitivity Improvement in Proton-Detected 2-Dimensional Heteronuclear Relay Spectroscopy. *J Magn Reson*, 91:429–436, 1991.

[6] Nei-Li Chan and Christopher P. Hill. Defining polyubiquitin chain topology. *Nat Struct Biol*, 8:650–652, 2001.

[7] Frank Delaglio, S. Grzesiek, G.W. Vuister, G. Zhu, J. Pfeifer, and A. Bax. NMRPipe: a multidimensional spectral processing system based on UNIX pipes. *J Biomol NMR*, 6:277–293, 1995.

[8] Warren L. DeLano. DeLano Scientific, San Carlos, CA, USA, 2002.

[9] Li Deng, Chen Wang, Erika Spencer, Liyong Yang, Amy Braun, Jianxin You, Clive Slaughter, Cecile Pickart, and Zhijian J. Chen. Activation of the IκB Kinase Complex by TRAF6 Requires a Dimeric Ubiquitin-Conjugating Enzyme Complex and a Unique Polyubiquitin Chain. *Cell*, 103:351–361, 2000.

[10] Cyril Dominguez, Rolf Boelens, and Alexandre M. J. J. Bonvin. HADDOCK: A Protein-Protein Docking Approach Based on Biochemical or Biophysical Information. *J Am Chem Soc*, 125:1731–1737, 2003.

[11] K. H. Gardner, R. Konrat, M. K. Rosen, and L. E. Kay. An (H)C(CO)NH-TOCSY pulse scheme for sequential assignment of protonated methyl groups in otherwise deuterated N-15,C-13-labeled proteins. *J Biomol NMR*, 8:351–356, 1996.

[12] Michael H. Glickman and Aaron Ciechanover. The Ubiquitin-Proteasome Proteolytic Pathway: Destruction for the Sake of Construction. *Physiol Rev*, 82:373–428, 2002.

[13] Tom D. Goddard and Donald G. Kneller. SPARKY 3.

[14] Kaisa Haglund, Pier Paolo Di Fiore, and Ivan Dikic. Distinct monoubiquitin signals in receptor endocytosis. *Trends Biochem Sci*, 28:598–603, 2003.

[15] Linda Hicke. Protein regulation by monoubiquitin. *Nat Rev Mol Cell Biol*, 2:195–201, 2001.

[16] Linda Hicke, Heidi L. Schubert, and Christopher P. Hill. Ubiquitin-binding domains. *Nat Rev Mol Cell Biol*, 6:610–621, 2005.

[17] Carsten Hoege, Boris Pfander, George-Lucian Moldovan, George Pyrowolakis, and Stefan Jentsch. *RAD6*-dependent DNA repair is linked to modification of PCNA by ubiquitin and SUMO. *Nature*, 419:135–141, 2002.

[18] Roseanne M. Hofmann and Cecile M. Pickart. Noncanonical *MMS2*-Encoded Ubiquitin-Conjugating Enzyme Functions in Assembly of Novel Polyubiquitin Chains for DNA Repair. *Cell*, 96:645–653, 1999.

[19] Bruce A. Johnson and Richard R. Blevins. NMRView: A computer program for the visualization and analysis of NMR data. *J Biomol NMR*, 4:603–614, 1994.

[20] L. E. Kay, M. Ikura, R. Tschudin, and A. Bax. 3-Dimensional Triple-Resonance Nmr-Spectroscopy of Isotopically Enriched Proteins. *J Magn Reson*, 89:496–514, 1990.

[21] Lewis E. Kay, Paul Keifer, and Tim Saarinen. Pure Absorption Gradient Enhanced Heteronuclear Single Quantum Correlation Spectroscopy with Improved Sensitivity. *J Am Chem Soc*, 114:10663–10665, 1992.

[22] Lewis E. Kay, Guang Yi Xu, Alex U. Singer, D.R. Muhandiram, and Julie D. Forman-Kay. A Gradient-Enhanced HCCH-TOCSY Experiment for Recording Side-Chain 1H and 13C Correlations in H2O Samples of Proteins. *J Magn Reson B*, 101:333–337, 1993.

[23] Roman A. Laskowski, Malcolm W. MacArthur, David S. Moss, and Janet M. Thorton. PROCHECK: A program to check the stereochemical quality of protein structures. *J Appl Cryst*, 26:283–290, 1993.

[24] T.M. Logan, E.T. Olejniczak, R.X. Xu, and S.W. Fesik. A general method for assigning NMR spectra of denatured proteins using 3D HC(CO)NH-TOCSY triple resonance experiments. *J Biomol NMR*, 3:225–231, 1993.

[25] B. A. Lyons and G. T. Montelione. An Hccnh Triple-Resonance Experiment Using C-13 Isotropic Mixing for Correlating Backbone Amide and Side-Chain Aliphatic Resonances in Isotopically Enriched Proteins. *J Magn Reson B*, 101:206–209, 1993.

[26] Sean McKenna, Jing Hu, Trevor Moraes, Wei Xiao, Michael J. Ellison, and Leo Spyracopoulos. Energetics and Specificity of Interactions within Ub·Uev·Ubc13 Human Ubiquitin Conjugation Complexes. *Biochemistry*, 42:7922–30, 2003.

[27] Sean McKenna, Trevor Moraes, Landon Pastushok, Christopher Ptak, Wei Xiao, Leo Spyracopoulos, and Michael J. Ellison. An NMR-based Model of the Ubiquitin-bound Human Ubiquitin Conjugation Complex Mms2·Ubc13. The structural basis for lysine 63 chain catalysis. *J Biol Chem*, 278:13151–13158, 2003.

[28] Sean McKenna, Leo Spyracopoulos, Trevor Moraes, Landon Pastushok, Christopher Ptak, Wei Xiao, and Michael J. Ellison. Noncovalent Interaction between Ubiquitin and the Human DNA Repair Protein Mms2 Is Required for Ubc13-mediated Polyubiquitination. *J Biol Chem*, 276:40120–40126, 2001.

[29] Takaaki Miura, Werner Klaus, Bernard Gsell, Chikara Miyamoto, and Hans Senn. Characterization of the binding interface between ubiquitin and class I human ubiquitin-conjugating enzyme 2b by multidimensional heteronuclear NMR spectroscopy in solution. *J Mol Biol*, 290:213–228, 1999.

[30] Trevor F. Moraes, Ross A. Edwards, Sean McKenna, Landon Pastushok, Wei Xiao, J. N. Mark Glover, and Michael J. Ellison. Crystal structure of the human ubiquitin conjugating enzyme complex, hMms2-hUbc13. *Nat Struct Biol*, 8:669–673, 2001.

[31] D. R. Muhandiram and L. E. Kay. Gradient-Enhanced Triple-Resonance 3-Dimensional Nmr Experiments with Improved Sensitivity. *J Magn Reson B*, 103:203–216, 1994.

[32] Dario Neri, Thomas Szyperski, Gottfried Otting, Hans Senn, and Kurt Wuthrich. Stereospecific Nuclear Magnetic-Resonance Assignments of the Methyl-Groups of Valine and Leucine in the DNA-Binding Domain of the 434-Repressor by Biosynthetically Directed Fractional ^{13}C Labeling. *Biochemistry*, 28:7510–7516, 1989.

[33] S. M. Pascal, D. R. Muhandiram, T. Yamazaki, J. D. Forman-Kay, and L. E. Kay. Simultaneous Acquisition of ^{15}N-Edited and ^{13}C-Edited NOE Spectra of Proteins Dissolved in H_2O. *J Magn Reson B*, 103:197–201, 1994.

[34] S Sambrook, E.F. Fritch, and T. Maniatis. *Molecular Cloning: A Laboratory Manual.* Cold Spring Harbor Laboratory Press, New York, NY, 1989.

[35] Joshua D. Schnell and Linda Hicke. Non-traditional functions of ubiquitin and ubiquitin-binding proteins. *J Biol Chem*, 278:35857–35860, 2003.

[36] Carolyn M. Slupsky, Cyril M. Kay, Fernando C. Reinach, Lawrence B. Smillie, and Brian D. Sykes. Calcium-Induced Dimerization of Troponin-C - Mode of Interaction and Use of Trifluoroethanol as a Denaturant of Quaternary Structure. *Biochemistry*, 34:7365–7375, 1995.

[37] Nico Tjandra, Scott E. Feller, Richard W. Pastor, and Ad Bax. Rotational Diffusion Anisotropy of Human Ubiquitin from ^{15}N NMR Relaxation. *J Am Chem Soc*, 117:12562–12566, 1995.

[38] G. W. Vuister and A. Bax. Resolution Enhancement and Spectral Editing of Uniformly C-13-Enriched Proteins by Homonuclear Broad-Band C-13 Decoupling. *J Magn Reson*, 98:428–435, 1992.

[39] Chen Wang, Li Deng, Mei Hong, Giridhar R. Akkaraju, Jun-Ichiro Inoue, and Zhijian J. Chen. TAK1 is a ubiquitin-dependent kinase of MKK and IKK. *Nature*, 412:346–351, 2001.

[40] D. S. Wishart, B. D. Sykes, and F. M. Richards. The Chemical Shift Index: A Fast and Simple Method for the Assignment of Protein Secondary Structure through NMR Spectroscopy. *Biochemistry*, 31:1647–1651, 1992.

[41] Michael Wittekind and Luciano Mueller. HNCACB, a High-Sensitivity 3D NMR Experiment to Correlate Amide-Proton and Nitrogen Resonances with the Alpha- and Beta-Carbon Resonances in Proteins. *J Magn Reson B*, 101:201–205, 1993.

[42] Wei Xiao, Stanley L. Lin, Stacey Broomfield, Barbara L. Chow, and Ying-Fei Wei. The products of the yeast *MMS2* and two human homologs (*hMMS2* and *CROC-1*) define a structurally and functionally conserved Ubc-like protein family. *Nucleic Acids Res*, 26:3908–3914, 1998.

[43] Toshio Yamazaki, Weontae Lee, Cheryl H. Arrowsmith, D.R. Muhandiram, and Lewis E. Kay. A suite of triple resonance experiments for the backbone assignment of 15N, 13C, 2H labeled proteins with high sensitivity. *J Am Chem Soc*, 116:11655–11666, 1994.

[44] Daiwen W. Yang, Yu Zheng, Dingjiang Liu, and Daniel F. Wyss. Sequence-specific assignments of methyl groups in high-molecular weight proteins. *J Am Chem Soc*, 126:3710–3711, 2004.

[45] O. W. Zhang, L. E. Kay, J. P. Olivier, and J. D. Forman-Kay. Backbone ^{1}H and ^{15}N Resonance Assignments of the N-Terminal SH3 Domain of Drk in Folded and Unfolded States Using Enhanced-Sensitivity Pulsed-Field Gradient NMR Techniques. *J Biomol NMR*, 4:845–858, 1994.

Chapter 3

Structural Basis for Non-Covalent Interaction Between Ubiquitin and the Ubiquitin Conjugating Enzyme Variant Human Mms2

3.1 Introduction

Structural characterization of a protein-protein complex can be a daunting task when there are insufficient experimental NMR distance restraints to produce a *de novo* structure. Data-driven docking is a technique that is designed to predict the structures of complexes that are difficult to study by conventional NMR or crystallographic techniques. Typical complexes that fall into this category include integral-membrane or membrane-associated proteins, proteins that bind their cognate ligands weakly, and those that are short lived. In the case of solution state NMR, structure determination of large complexes is also hampered

by line-broadening effects that make complete chemical shift assignment difficult to obtain. Given that *ab initio* docking is an unsolved problem, protocols have been developed for docking proteins of known structure using minimal amounts of experimental data. Examples of such data include mutagenesis, chemical cross-linking, and NMR-derived data such as chemical shift maps, pseudocontact shifts, and dipolar couplings (reviewed in [19]).

Traditional docking approaches typically begin with unbiased docking of constituents during rigid body docking, followed by a refinement stage with experimental data [19]. Data-driven docking, on the other hand, imposes experimental restraints during both rigid body docking and refinement. The advantage of this approach is that sampling of "near-correct" structures is higher than for traditional docking, however this method is also more sensitive to misinterpreted, or incorrect, experimental data [19].

Large conformational changes in docking partners present a major challenge to solving the protein docking problem. If conformational changes are too large, then docking predictions will likely fail [19]. Furthermore, the accuracy of predicted structures is compromised when the accompanying data is ambiguous, such as that from chemical shift maps or mutagenesis. However, if the experimental data is unambiguous, as in the case of intermolecular NOEs, then the predictions are significantly improved [18].

Due to the difficulties in obtaining a *de novo* structure of the hMms2-Ub complex, we implemented the HADDOCK (High Ambiguity Driven protein-protein Docking) protocol to dock the proteins in the presence of intermolecular NOE restraint data [5]. HADDOCK uses the CNS (crystallography and NMR systems) [2] simulated annealing engine for docking and refinement, and structures are scored according to their intermolecular energies (given by the sum of electrostatic, van der Waals, and experimental restraint energy terms). HADDOCK also allows both side chain and main chain flexibility during the refinement phase of the

structure calculation [5]. Allowing for protein flexibility during docking is known to increase the quality of the structures predicted from the calculation [18]. Using HADDOCK, we have characterized the interaction between hMms2 and Ub at high resolution, and explored the biological implications of this model in the context of the Ub-hMms2-hUbc13 complex.

3.2 Materials and Methods

3.2.1 Protein expression and purification

Protein expression protocols for [*U*-^{15}N; *U*-^{13}C]-hMms2, unlabelled hMms2, [*U*-^{15}N; *U*-^{13}C]-Ub, [*U*-^{15}N]-Ub, and unlabelled Ub are detailed in Chapter 2.2.1.

3.2.2 NMR spectroscopy

All NMR spectra were obtained using either Varian Unity INOVA 500 or 600 MHz NMR spectrometers. For [*U*-^{15}N; *U*-^{13}C]-hMms2 + Ub and [*U*-^{15}N; *U*-^{13}C]-Ub + hMms2, NMR samples were 600 μL for standard 5 mm i.d. NMR tubes, and 300 μL for SHIGEMI microcell NMR tubes, and contained 9:1 H_2O/D_2O with 50 mM phosphate (pH 7.5) 150 mM NaCl, 1 mM DTT, 1 mM DSS, 3 μL of 100x stock protease inhibitor cocktail I (Calbiochem catalog #539131), with ~0.5 mM hMms2 and ~2.0 mM Ub. For [*U*-^{15}N; *U*-^{13}C]-Ub, samples were 300 μL in SHIGEMI microcell NMR tubes with sample conditions same as above, with the exception that the protein concentrations used were ~2.0 mM Ub and ~0.5 mM hMms2. For [*U*-^{15}N]-Ub, the sample used for titration with hMms2 was 600 μL for a standard 5 mm i.d. NMR tube with sample conditions the same as above, with the exception that the protein concentrations used were ~0.25 mM Ub, and 0, ~0.25, ~0.5, ~0.75, and ~1 mM hMms2.

Titration of [U-^{15}N]-Ub with hMms2 - Four 38 μL aliquots of ~3.6 mM hMms2 were titrated into ~0.25 mM [*U*-^{15}N]-Ub at 30 °C, and a 2D ^{1}H-^{15}N-HSQC NMR spectrum was acquired at each titration point. Average chemical shift perturbations for each resonance were calculated using a previously described method [6]. Average chemical shift changes that were greater than one standard deviation from the mean were considered significant.

Ub-hMms2 Intermolecular NOEs - ^{1}H-^{1}H NOEs between Ub and hMms2 were identified by analyzing ^{13}C, ^{15}N F_1-filtered, F_3-edited NOESY experiments [23] collected for two NMR samples at 30 °C, one containing 1:4 [*U*-^{13}C; *U*-^{15}N]-hMms2:unlabelled Ub and the other containing 1:4 [*U*-^{13}C; *U*-^{15}N]-Ub:unlabelled hMms2. Intermolecular NOE restraints were set to lower and upper bounds of 1.8 and 5.0 Å, respectively. NOE assignment was accomplished using the program Sparky [7].

Structure Determination - Protein docking for the hMms2-Ub complex was performed with the HADDOCK (High Ambiguity Driven protein-protein Docking) protocol [5], using the crystal structures of hMms2 (1J74) and Ub (1UBQ), and intermolecular NOEs as restraints. The starting structures were fixed as rigid bodies, except for residues in and around the binding face, for which full flexibility was allowed. Out of 200 rigid body docking trials, the top 50 lowest energy structures underwent structural refinement. The ten lowest energy structures from the protocol were subjected to a final refinement in explicit solvent. The energy difference between the highest energy selected structure and the lowest energy omitted structure is 1.67 kcal/mol (the difference between the lowest and highest energy selected structures is 5.72 kcal/mol). The quality of the structural ensemble was assessed using the program Procheck [9]. Changes in accessible surface area for hMms2 and Ub upon binding were calculated using the program STC [10].

Molecular Graphics - Protein structure graphics (Figures 3.3-3.8) were produced using the program Pymol [3].

RCSB PDB Accession Code - The hMms2-Ub structure has been deposited in the Protein Data Bank under the accession code 1ZGU.

3.3 Results

3.3.1 Titration of [*U*-^{15}N]-Ub with hMms2

Backbone amide $^{1}H_{N}$ and ^{15}N chemical shift changes for [*U*-^{15}N]- hMms2 upon titration with Ub have been reported previously [12]. In this study, $^{1}H_{N}$ and ^{15}N chemical shift changes for [*U*-^{15}N]-Ub upon titration with hMms2 were determined (Figure 3.1). Only thirteen of 71 observable backbone amide $^{1}H_{N}$-^{15}N chemical shifts exhibit a significant change. On this basis, we assume that structural changes for Ub upon binding hMms2 are small. This assumption was also made with respect to the structure of hMms2 upon Ub binding on the basis of our previous work [11].

3.3.2 Ub-hMms2 Intermolecular NOEs

Intermolecular contacts between hMms2 and Ub were identified using ^{13}C, ^{15}N F_1-filtered, F_3-edited NOESY experiments for each of hMms2 and Ub (Figure 3.2). The interface was initially characterized by assigning methyl-methyl NOEs between the two proteins. Non-methyl and non-aromatic side chain protons for hMms2 were assigned with the aid of spectra collected at 40 °C and were subsequently assigned in the intermolecular NOE spectra. A total of 51 intermolecular NOEs were assigned, and of these, 27 were methyl-methyl NOEs.

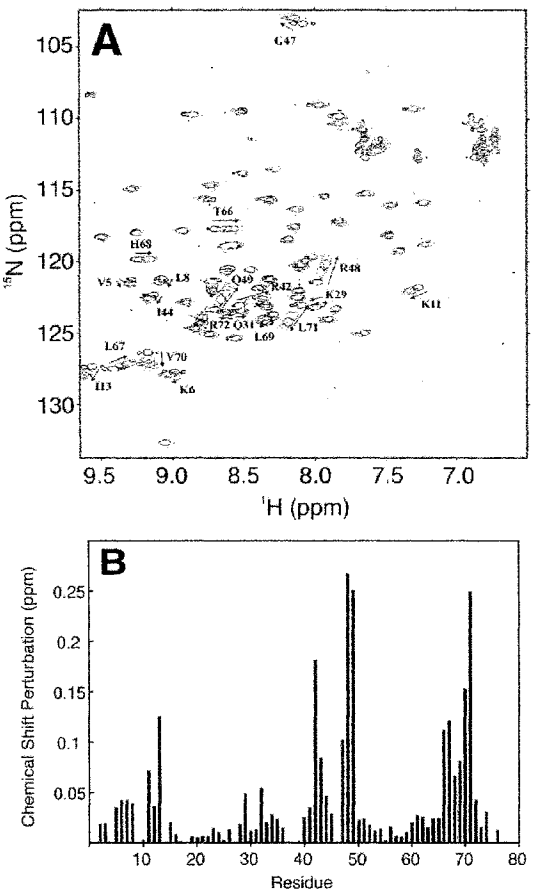

Figure 3.1: **^{15}N-Ub backbone amide chemical shift changes during titration of hMms2.** (A) Superposition of Ub ^{1}H-^{15}N HSQC spectra collected for various approximate values of [hMms2]/[Ub] ratios: orange (0:1), purple (1:1), violet (2:1), blue (3:1), and green (4:1). Only those cross-peaks that were affected by complex formation are labelled. (B) Plot of weighted average chemical shift perturbations by residue number, as given by $\Delta_{av} = \sqrt{\frac{\Delta\delta_{NH}^2 + \frac{\Delta\delta_N^2}{25}}{2}}$ [6].

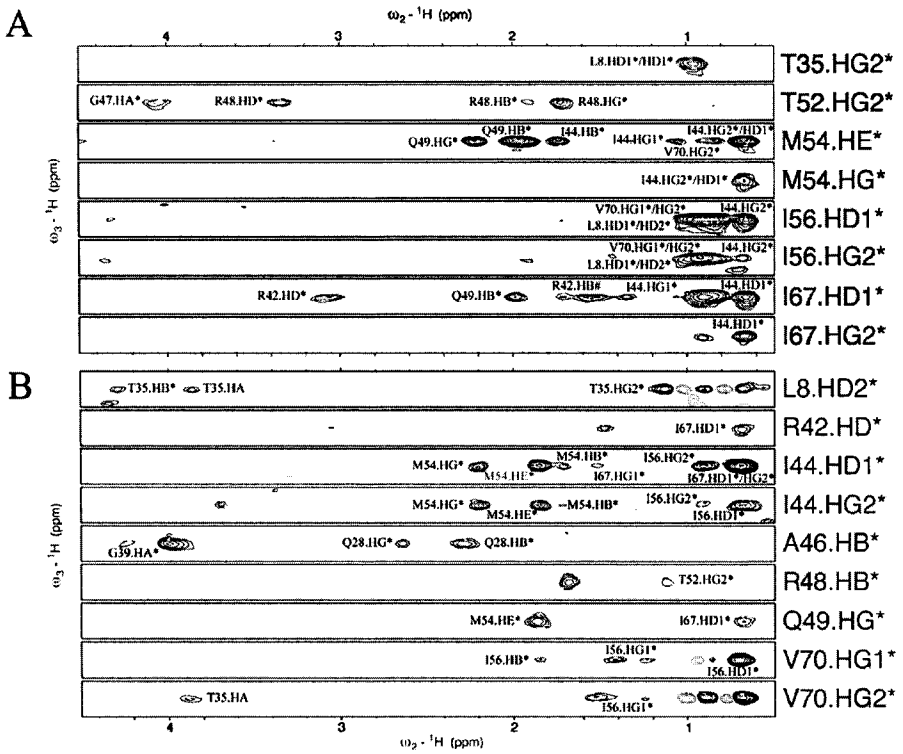

Figure 3.2: **Strips taken from the ^{13}C, ^{15}N F_1-filtered, F_3-edited NOESY experiments.** Intermolecular ^1H-^1H NOEs, or close contacts ranging from 1.8 – 5.0 Å between [*U*-^{13}C; *U*-^{15}N]-hMms2 and Ub are shown in (A), and NOE contacts between [*U*-^{13}C; *U*-^{15}N]-Ub and hMms2 are shown in (B). Unlabelled peaks were unassigned due to ambiguity or lack of chemical shift data.

3.3.3 Description of the structure

The structures of hMms2 and Ub in the complex are very similar to the free structures of the individual proteins, superimposing with backbone rmsds of 0.81 ± 0.13 Å and 0.77 ± 0.21 Å for hMms2 and Ub, respectively. This is due in large part to the fact that only regions that were involved in intermolecular NOEs, and adjacent regions, were unconstrained. In the family of ten structures, there are no NOE violations greater than 0.1 Å, the backbone rmsd value is 0.97 ± 0.14 Å to the average structure, the side chain heavy atom rmsd is 1.18 ± 0.12 Å (Figure 3.3), and 89.6% / 9.8% of residues are in the most favored / additionally allowed regions of the Ramachandran plot. In the family of ten structures generated using the HADDOCK protocol, hMms2 and Ub bury 296 ± 42 and 288 ± 23 $Å^2$ of polar accessible surface area respectively, as well as 412 ± 33 and 406 ± 43 $Å^2$ of nonpolar surface area, respectively.

3.4 Discussion

3.4.1 Description of the interface between Ub and hMms2

The structure of the hMms2-Ub complex presented here indicates that strands 1 – 3 from the single β-sheet face of hMms2 are involved in binding to strands 1 and 3 – 5 of the single β-sheet face of Ub. The binding interface of Ub is comprised in part by the hydrophobic residues Leu8, Ile44, and Val70 (Figure 3.4). Indeed, several intermolecular NOEs are observed between the methyl protons of these residues, and protons of hMms2 (Figure 3.2). These residues are also involved in interactions between Ub and the Ub-binding proteins CUE [8] [14] and UIM [16]. At the periphery of the interface there is a potential salt bridge between Glu41 O_γ of hMms2 and Arg48 H_η of Ub, which is ~5 Å away.

Figure 3.3: **Ensemble of ten structures for the hMms2-Ub complex generated using the HADDOCK protocol.** The backbone atoms of hMms2 are shown as a blue cartoon, and the backbone atoms of Ub are shown as a red cartoon. Lys63 of Ub is shown in green in the stick representation.

The side chain of Ub-Ile44 is involved in close contacts with a hydrophobic patch formed by hMms2 residues Met54, Ile56, and Ile67, and is almost completely buried by these residues (Figure 4). Additional NOE contacts are observed between Val70 and Leu8 of Ub and Ile56 of hMms2. The side chain of Ile67 of hMms2 forms close contacts with Ub residues Ile44, Arg42, and Gln49. At the periphery of the binding interface, Thr52 of hMms2 and Arg48 of Ub are in close contact. Further contacts at the periphery of the binding interface include Thr35 of hMms2 and Leu8 and Val70 of Ub, and Ala46 of Ub to Gly39 and Gln28 of hMms2.

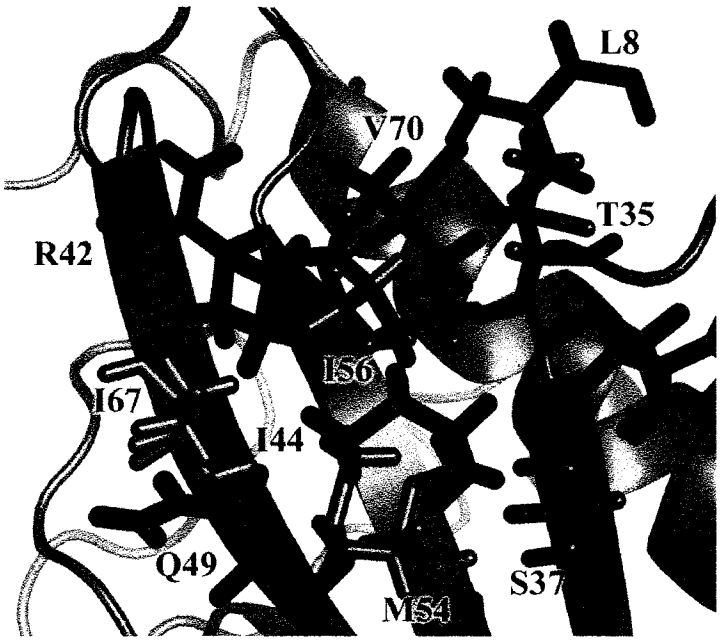

Figure 3.4: **Intermolecular interactions at the hMms2-Ub binding interface.** The backbone atoms of hMms2 are shown in the cartoon representation (blue), with side chains that interact with Ub shown in the stick representation. Ub residues for which intermolecular NOEs to hMms2 are observed are shown in the stick representation (red).

The total buried surface area in the hMms2-Ub interaction is 1402 ± 72 Å^2. This value is higher than for other reported ubiquitin binding domain interactions (1120 ± 66 Å^2 for CUE [1OTR] and 1054 ± 66 Å^2 UIM [1Q0W], using the first ten structures from each

ensemble), with a corresponding smaller K_D (98 $\pm$ 15 μM compared to 155 $\pm$ 9 μM for the CUE-Ub and 277 $\pm$ 8 μM for the UIM-Ub interactions [8] [16]).

3.4.2 Implications for catalysis of Lys63-linked polyubiquitin chains

Lys63-linked polyubiquitin chains play important functional roles within eukaryotic cells, and the Mms2-Ubc13 complex is the enzyme responsible for catalysis of these chains. A superposition of the structure of hMms2 within the hMms2-Ub complex presented herein and the structure of hMms2 within the hMms2-hUbc13 heterodimer determined previously [1J7D], positions Lys63 of Ub proximal to the binding interface between hMms2 and hUbc13 (Figure 3.6). In this orientation, the ϵ-amino group of Lys63 is 12 $\pm$ 1 Å away from the active site cysteine of hUbc13.

In order to better assess the biological impact of the hMms2-Ub structure presented herein, we have docked Ub to the hMms2-hUbc13 protein complex employing the HADDOCK protocol as described for the Ub-hMms2 complex, and using only Ub-hMms2 intermolecular NOEs measured in the absence of hUbc13 (see Methods). Using this approach, all of the intermolecular distance restraints are satisfied when hUbc13 is included in the docking protocol (there are no NOE violations greater than 0.1 Å). The intermolecular NOE energy when hUbc13 is present in the docking protocol is (14 $\pm$ 8) $\times$ 10^{-3} kcal/mol compared to (9.0 $\pm$ 0.6) $\times$ 10^{-3} kcal/mol in the absence of hUbc13. In the family of ten structures calculated in the presence of hUbc13, the ϵ-amino nitrogen of Ub-Lys63 is 9 $\pm$ 2 Å from the active site cysteine of hUbc13 (Figure 3.7A). In this orientation, the ϵ-amino group of Ub-Lys63 is predominantly involved in hydrogen bonds with either the backbone carbonyl of Pro120 or Leu121 of hUbc13, and is positioned at the mouth of a cleft that leads directly to the active site of hUbc13 (Figure 3.7B). The ensemble of structures shown

in Figure 3.7A is consistent with the following experimental observations. The backbone amide $^{1}H_{N}$-^{15}N chemical shift changes for hMms2 induced by Ub binding in the presence and absence of hUbc13 suggest that the surface of hMms2 involved in Ub binding is similar [12]. Furthermore, comparison of the ensemble of Ub-hMms2-hUbc13 structures shown in Figure 3.7A to the ensemble of Ub-hMms2 structures shown in Figure 3.3 indicates that the increase in buried surface area when hUbc13 is present is not large (hMms2 buries 1402 $\pm$ 72 Å^2 and hMms2-hUbc13 buries 1738 $\pm$ 86 Å^2, upon interaction with Ub). These small changes in buried surface area are consistent with the observation that we have not detected chemical shift changes in $^{1}H_{N}$-^{15}N HSQC NMR spectra of [*U*-^{15}N]-hUbc13 upon addition of acceptor Ub in the presence and absence of hMms2 [12]. Finally, the affinity of acceptor Ub is not radically greater (K_D = 28 $\pm$ 6 μM) than that for hMms2 alone (K_D = 98 $\pm$ 15 μM) (3 $\pm$ 1 fold greater) [11].

There are significant differences between the structure of the hMms2-Ub complex presented here and our previous model for the Ub2-hMms2-hUbc13 tetramer that was developed solely on the basis of backbone amide $^{1}H_{N}$-^{15}N chemical shift mapping [12] (Figure 3.5). While the structure determined herein buries the same amount of surface area as the previously determined chemical shift based model (1402 $\pm$ 72 Å^2, compared to 1368 Å^2), the structural differences are highlighted by the fact that the previous model is not consistent with our NOE data. Of the 51 distance restraints, 20 are violated by over 1 Å, and six restraints are violated by 3-5 Å.

Interestingly, hUbc13-Asp81 has been shown to be critical for the synthesis of Lys63-linked di-Ub chains [20]. For example, mutation of Asp81 to Ala results in impairment of catalysis, whereas mutation to Arg abolishes di-Ub formation. On the basis of these mutational studies, it has been suggested that the catalytic role of hUbc13-D81 is to position

Figure 3.5: **Comparison of the hMms2-Ub Structure with the Chemical Shift-Based Model.** The structure of hMms2-Ub determined in the present study (blue cartoon) is superimposed on the chemical shift-based model (grey cartoon) through the backbone atoms of hMms2. Differences in binding modes account for a ~7 Å displacement between the ϵ-nitrogens of Lys63 for each Ub (shown as sticks).

Ub-Lys63 within the active site [20]. If we assume that the role of hUbc13-D81 is to position Lys63, and impose a distance restraint of 2.5 ± 0.5 Å between the ϵ-amino nitrogen of Ub-Lys63 and either of the side chain carboxyl oxygen atoms of hUbc13-D81 during docking of Ub with the hMms-hUbc13 heterodimer using the HADDOCK protocol (as implemented for the hMms2-Ub structure), then all of the NOE distance restraints between hMms2 and Ub measured in the absence of hUbc13 are satisfied (intermolecular NOE energy of $(17 \pm 10) \times 10^{-3}$ kcal/mol), with no violations greater than 0.3 Å, and only one violation greater than 0.1 Å in the family of ten structures.

In light of this analysis, it is of interest to compare this model for the interaction of Ub-Lys63 with the active site of hUbc13 with the crystallographically determined structure of the E2 Ubc9 in complex with its substrate RanGAP1 [1]. Ubc9 is a SUMO E2 enzyme that attaches the ubiquitin-like modifier SUMO to Lys526 of RanGAP1, and this process is important in nucleocytoplasmic transport. Figure 3.8A shows the superposition of Ubc9 (in complex with RanGAP1, 1KPS) superimposed on hUbc13 (in complex with hMms2, 1J7D). There are key amino acid differences in the active site of hUbc13 compared to Ubc9. Leu121 in hUbc13 is equivalent to Ala129 in Ubc9, but the side chains of these residues occur in very different positions in comparison to other active site residues such as Cys87 (hUbc13) and Cys93 (Ubc9), Asn79 (hUbc13) and Asn85 (Ubc9). In addition, the bulky aromatic side chain of Tyr87 in Ubc9 replaces Asp81 of hUbc13, a residue important for catalysis [20]. Figure 3.8B shows the superposition between Ubc9 and hUbc13 within the acceptor Ub-hMms2-hUbc13 structure closest to the average structure, determined using HADDOCK docking as described above with the assumption that hUbc13-Asp81 is responsible for positioning Ub-Lys63. As shown in Figure 3.8B, if approach of substrate Ub-Lys63 to the active site cysteine of hUbc13 is similar to that for Ubc9, it would be involved in a steric

clash with Leu121. For Ubc9 on the other hand, given the active site orientation shown in Figure 3.8A, the substrate lysine cannot approach the active site cysteine from directly above due to steric clashes with Ubc9-Tyr87 and Ubc9-Ala129. The structural differences between the active sites of Ubc9 and hUbc13 may be important in the specific recognition and correct positioning of substrate lysine residues destined for SUMO conjugation rather than ubiquitination.

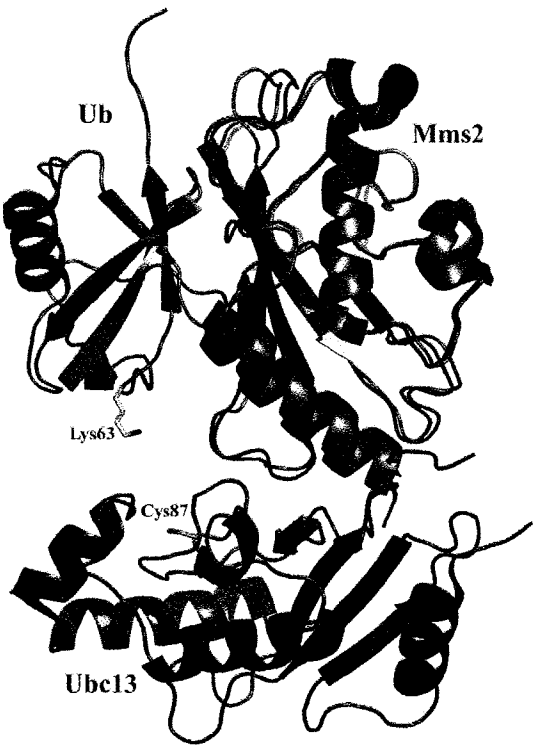

Figure 3.6: **Superposition of hMms2-Ub on the crystallographically determined structure of hMms2-hUbc13.** The backbone atoms of the lowest energy hMms2-Ub structure determined in the present study (violet cartoon), are superimposed on the backbone atoms of the hMms2-hUbc13 structure (1j7d), (red-blue cartoon). Lys63 of Ub and the active site cysteine of hUbc13 are shown in green in the stick representation.

Recently, it has been demonstrated that mutation of either of the side chains Ub-Ile44 and yeast Mms2-Ile57 (equivalent to hMms2-Ile67) to alanine results in a 10- to 20-fold inhibition of Lys63-linked polyubiquitin chain synthesis, suggesting that the acceptor Ub

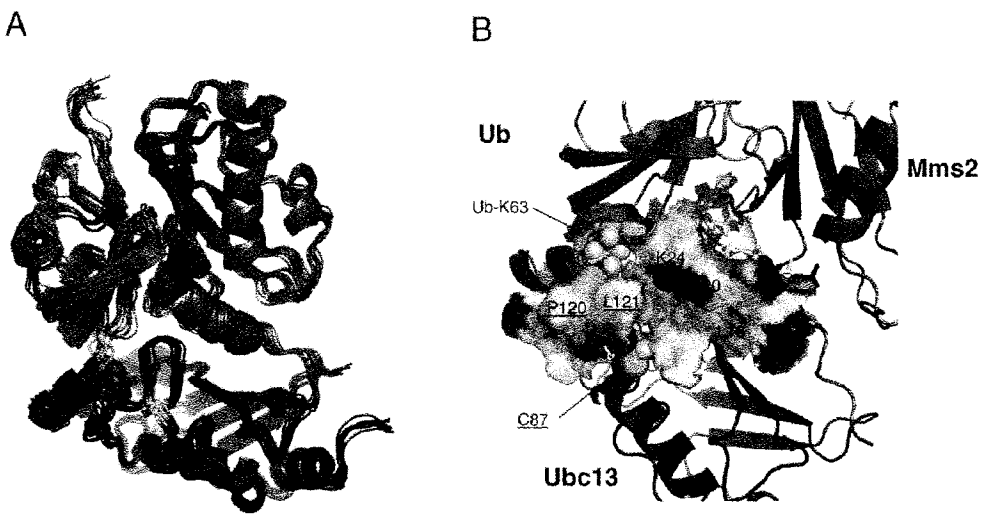

Figure 3.7: **Model for the acceptor Ub-hMms2-hUbc13 ternary complex generated using the HADDOCK protocol.** (A) Ensemble of ten structures calculated in the same fashion as the ensemble of Ub-hMms2 structures shown in Figure 3.3 with the exception that the coordinates of hUbc13 were included. The backbone atoms of hUbc13, hMms2, and Ub are shown as red, blue, and gold cartoons, respectively. (B) Surface representation of the active site cleft for the hMms2-hUbc13 heterodimer. Polar atoms of the surface of the active site are colored in white, negatively charged atoms are colored red, positively charged atoms are colored blue, and hydrophobic atoms are colored yellow. Labels for residues from hUbc13 are indicated in underline. The atoms of Ub-Lys63 and hUbc13-Cys87 are shown as spheres.

binding site on Mms2 is necessary for *in vivo* chain assembly [17]. In the present work, we have demonstrated a direct interaction between Ub-Ile44 and hMms2-Ile67. In addition, the position of Ub-Lys63 within the hMms2-Ub structure is consistent with proposed mechanisms of Lys63-linked chain catalysis. Thus, the structural basis for the functional data reported by Pickart and coworkers [17] is a direct disruption of the Ub-Ile-44 hMms2-Ile67 interaction, leading to impaired Lys63 chain catalysis.

Finally, the close proximity of Ub Arg48 to the binding interface in the hMms2-Ub complex suggests that Lys48 of the wild type Ub could potentially be excluded as a site for canonical Lys48-linked chain formation. However, in the present structure, as in the Tsg101-Ub structure [15] (*vide infra*), Arg/Lys48 is involved in contacts at the periphery of the interface, and remains partly solvent exposed.

3.4.3 Comparison to other Ub-binding protein complexes

Recently, the structure of the UEV domain of Tsg101 (Vps23p in yeast), has been solved in complex with Ub by X-ray crystallography [15]. Interestingly, the structural basis of the Tsg101-Ub interaction is distinct from that of hMms2-Ub. Whilst both UEV domains bind to a similar hydrophobic surface on Ub, Tsg101 does not bind *via* the single β-sheet face as observed for the hMms2-Ub interaction. Tsg101 binds Ub through the loop of an extended β-tongue motif, which consists of strands 1 and 2 of the UEV domain. This difference is not entirely surprising, given Tsg101 and Mms2 play very different functional roles in eukaryotic cells. Furthermore, from an evolutionary standpoint, the UEV domain of Tsg101 is further diverged from the canonical E2 fold than Mms2 [13]. Uev1a, a UEV involved in NF-κB activation [4] [21], is a close relative of hMms2 [22]. Both Uev1a and hMms2 form a stable heterodimer with hUbc13 in order to catalyze the formation of Lys63-

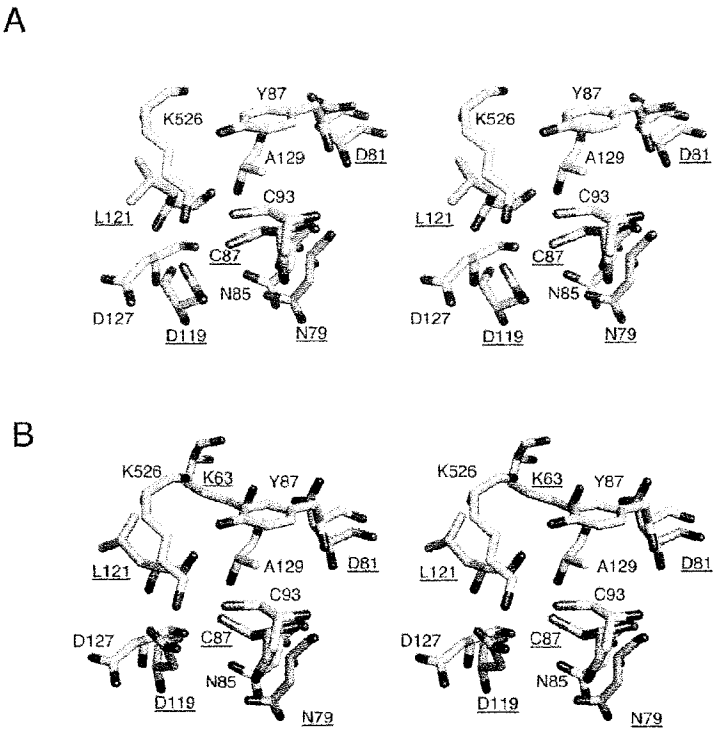

Figure 3.8: **Comparison of the structures of Ubc9 and hUbc13.** (A) Divergent stereo view of the structure of Ubc9 (in complex with RanGAP1, [1KPS]) superimposed on the structure of hUbc13 (in complex with hMms2, [1J7D]). (B) Divergent stereo view of the structure of Ubc9 (in complex with RanGAP1, [1KPS]) superimposed on the model of the ternary complex of acceptor Ub-hMms2-hUbc13 determined herein using intermolecular NOEs between hMms2 and Ub and assuming that hUbc13-Asp81 is involved in hydrogen bonding interactions with Ub-Lys63. The side chain carbon atoms of Ubc9/RanGAP1 are shown in light blue and those for hUbc13/Ub are shown in green. Labels indicating hUbc13 residues are shown in underline.

linked polyubiquitin chains [4]. hUev1a shares 92% core sequence identity with hMms2 [22], and adopts a nearly identical fold (data unpublished). Thus, it is reasonable to expect that the Uev1a-Ub interaction is similar to that for hMms2-Ub, particularly considering the fact that the putative Ub binding site of hUev1a is identical in sequence to hMms2.

3.4.4 Conclusion

In the current study we have used solution state NMR spectroscopy to produce a structure of the hMms2-Ub complex. The binding interface involves many close contacts between the side chains of Met54, Ile56, and Ile67 on hMms2, and Ile44, Val70, and Leu8 on Ub. The structure is consistent with a recent study by Pickart and co-workers [17] that demonstrates the necessity of both Ile67 of hMms2 and Ile44 of Ub in Lys63 chain assembly.

Bibliography

[1] V. Bernier-Villamor, D. A. Sampson, M. J. Matunis, and C. D. Lima. Structural basis for E2-mediated SUMO conjugation revealed by a complex between ubiquitin-conjugating enzyme Ubc9 and RanGAP1. *Cell*, 108:345–356, 2002.

[2] A. T. Brunger, P. D. Adams, G. M. Clore, W. L. DeLano, P. Gros, R. W. Grosse-Kunstleve, J. S. Jiang, J. Kuszewski, M. Nilges, N. S. Pannu, Read R. J., L. M. Rice, T. Simonson, and G. L. Warren. Crystallography & NMR system: A new software suite for macromolecular structure determination. *Acta Crystallogr D Biol Crystallogr*, 54:905–921, 1998.

[3] Warren L. DeLano. DeLano Scientific, San Carlos, CA, USA, 2002.

[4] Li Deng, Chen Wang, Erika Spencer, Liyong Yang, Amy Braun, Jianxin You, Clive Slaughter, Cecile Pickart, and Zhijian J. Chen. Activation of the IκB Kinase Complex by TRAF6 Requires a Dimeric Ubiquitin-Conjugating Enzyme Complex and a Unique Polyubiquitin Chain. *Cell*, 103:351–361, 2000.

[5] Cyril Dominguez, Rolf Boelens, and Alexandre M. J. J. Bonvin. HADDOCK: A Protein-Protein Docking Approach Based on Biochemical or Biophysical Information. *J Am Chem Soc*, 125:1731–1737, 2003.

[6] D. S. Garrett, Y. J. Seok, A. Peterkofsky, G. M. Clore, and A. M. Gronenborn. Identification by NMR of the binding surface for the histidine-containing phosphocarrier protein HPr on the N-terminal domain of enzyme I of the Escherichia coli phosphotransferase system. *Biochemistry*, 36:4393–4398, 1997.

[7] Tom D. Goddard and Donald G. Kneller. SPARKY 3.

[8] Richard S. Kang, Cynthia M. Daniels, Smitha A. Francis, Susan C. Shih, William J. Salerno, Linda Hicke, and Ishwar Radhakrishnan. Solution Structure of a CUE-Ubiquitin Complex Reveals a Conserved Mode of Ubiquitin Binding. *Cell*, 113:621–630, 2003.

[9] Roman A. Laskowski, Malcolm W. MacArthur, David S. Moss, and Janet M. Thorton. PROCHECK: A program to check the stereochemical quality of protein structures. *J Appl Cryst*, 26:283–290, 1993.

[10] P. Lavigne, J. R. Bagu, R. Boyko, L. Willard, C. F. Holmes, and B. D. Sykes. Structure-based thermodynamic analysis of the dissociation of protein phosphatase-1 catalytic subunit and microcystin-LR docked complexes. *Protein Sci*, 9:252–264, 2000.

[11] Sean McKenna, Jing Hu, Trevor Moraes, Wei Xiao, Michael J. Ellison, and Leo Spyracopoulos. Energetics and Specificity of Interactions within Ub·Uev·Ubc13 Human Ubiquitin Conjugation Complexes. *Biochemistry*, 42:7922–30, 2003.

[12] Sean McKenna, Trevor Moraes, Landon Pastushok, Christopher Ptak, Wei Xiao, Leo Spyracopoulos, and Michael J. Ellison. An NMR-based Model of the Ubiquitin-bound Human Ubiquitin Conjugation Complex Mms2·Ubc13. The structural basis for lysine 63 chain catalysis. *J Biol Chem*, 278:13151–13158, 2003.

[13] Owen Pornillos, Steven L. Alam, Rebecca L. Rich, David G. Myszka, Darrell R. Davis, and Wesley I. Sundquist. Structure and functional interactions of the Tsg101 UEV domain. *Embo J*, 21:2397–2406, 2002.

[14] Gali Prag, Saurav Misra, Eudora A. Jones, Rodolfo Ghirlando, Brian A. Davies, Bruce F. Horazdovsky, and James H. Hurley. Mechanism of Ubiquitin Recognition by the CUE Domain of Vps9p. *Cell*, 113:609–620, 2003.

[15] Wesley I. Sundquist, Heidi L. Schubert, Brian N. Kelly, Gina C. Hill, James M. Holton, and Christopher P. Hill. Ubiquitin Recognition by the Human TSG101 Protein. *Mol Cell*, 13:783–789, 2004.

[16] Kurt A. Swanson, Richard S. Kang, Svetoslava D. Stamenova, Linda Hicke, and Ishwat Radhakrishnan. Solution structure of Vps27 UIM-ubiquitin complex important for endosomal sorting and receptor downregulation. *Embo J*, 22:4597–4606, 2003.

[17] C. Tsui, A. Raguraj, and C. M. Pickart. Ubiquitin binding site of the ubiquitin E2 variant (UEV) protein Mms2 is required for DNA damage tolerance in the yeast RAD6 pathway. *J Biol Chem*, 280:19829–19835, 2005.

[18] A. D. J. van Dijk, S. J. de Vries, C. Dominguez, H. Chen, H.-X. Zhou, and A. M. J. J. Bonvin. Data-Driven Docking: HADDOCK's Adventures in CAPRI. *Proteins*, 60:232–238, 2005.

[19] Aalt D. J. van Dijk, Rolf Boelens, and Alexandre M. J. J. Bonvin. Data-driven docking for the study of biomolecular complexes. *FEBS J*, 272:293–312, 2004.

[20] Andrew P. VanDemark, Roseanne M. Hofmann, Colleen Tsui, Cecile M. Pickart, and Cynthia Wolberger. Molecular Insights into Polyubiquitin Chain Assembly: Crystal Structure of the Mms2/Ubc13 Heterodimer. *Cell*, 105:711–720, 2001.

[21] Chen Wang, Li Deng, Mei Hong, Giridhar R. Akkaraju, Jun-Ichiro Inoue, and Zhijian J. Chen. TAK1 is a ubiquitin-dependent kinase of MKK and IKK. *Nature*, 412:346–351, 2001.

[22] Wei Xiao, Stanley L. Lin, Stacey Broomfield, Barbara L. Chow, and Ying-Fei Wei. The products of the yeast *MMS2* and two human homologs (*hMMS2* and *CROC-1*) define a structurally and functionally conserved Ubc-like protein family. *Nucleic Acids Res*, 26:3908–3914, 1998.

[23] C. Zwahlen, P. Legault, S. J. F. Vincent, J. Greenblatt, R. Konrat, and L. E. Kay. Methods for measurement of intermolecular NOEs by multinuclear NMR spectroscopy: Application to a bacteriophage lambda N-peptide/boxB RNA complex. *J Am Chem Soc*, 119:6711–6721, 1997.

Chapter 4

Chemical Shift Mapping of Ubc13 Interactions with the RING Domain from Traf6

4.1 Introduction

The post-translational addition of ubiquitin (Ub) to a target protein plays a pivotal role in the regulation of cell processes in eukaryotes [5] [3] [13]. In the first step of this process, ubiquitin is activated by a ubiquitin-activating enzyme (E1) to form an E1-Ub thiolester intermediate. Ub is then transferred to a ubiquitin-conjugating enzyme (E2), and subsequently localized to a target peptide through the action of a ubiquitin ligase (E3). In the classical pathway, polyubiquitin chains are built up by the formation of isopeptide linkages between the C-terminus of one Ub, and the side chain of Lys48 of the previous Ub. Polyubiquitin chains built with this topology serve to target proteins to the 26S proteasome for degradation [13].

In addition to the classical pathway of polyubiquitin chain synthesis, many variant pathways exist as well. One of these is involved in the formation of polyubiquitin chains linked through Lys63, and proteins modified with these variant tags have been implicated in non-proteolytic pathways, such as DNA repair [4] [18] [17] and NF-κB activation [9] [28].

Lys63-linked polyubiquitin chains are covalently assembled by a protein heterodimer consisting of an E2 and a ubiquitin E2 variant, or UEV. UEVs are structurally similar to E2s, but lack the canonical active site cysteine residue that is necessary to catalyze isopeptide bond formation with the C-terminus of Ub. In yeast, the E2 Ubc13 forms a heterodimer with the E2 variant Uev1a to form poly-ubiquitin chains that function in NF-κB activation [9] [1]. One of the targets of this modification is TNF Receptor-Associated Factor 6 (TRAF6), which also acts as the E3 for this process [9]. Following antigen receptor stimulation, TRAF6 oligomerizes [30] and polyautoubiquitinates itself [28]. The variant polyubiquitin chains are then recognized by the TAB (Tak1-Binding) family of proteins through novel zinc finger (NZF) domains [19]. The TABs promote the autophosphorylation and activation of TAK1 (TGFβ-activating kinase), which in turn activates the IKK (IκB Kinase) complex [28]. The IKK complex consists of two catalytic subunits, α and β, and a regulatory subunit, known as NEMO. TAK1 phosphorylation of IKKβ activates the IKK complex, allowing it to phosphorylate IκB, the inhibitor of NF-κB. Once free of its inhibitor, NF-κB translocates to the nucleus where it upregulates the transcription of genes involved in immune response activation [6].

In the current model for Lys63-Ub chain synthesis, the UEV interacts non-covalently with an "acceptor" Ub, such that Lys63 is oriented towards the thiolester bond between Ubc13 and the "donor" ubiquitin. While no structures exist to describe either of the Uev1a-Ubc13 or Uev1a-Ub interactions, these are inferred by analogy to the Mms2-Ubc13 model

discussed in the previous chapter. The binding surface of Ubc13 employed in interaction with Traf6 has been predicted based on the structure of the E2-E3 pair c-cbl-UbcH7 [31], and is thought to comprise the N-terminal region of Ubc13: an interface which is distinct from both the Mms2 binding site and Ub conjugation site [24]. In this study, we have assigned the chemical shifts for hUbc13, and determined the binding surface for interaction with the RING domain from Traf6 using chemical shift perturbation analysis. We have also employed the HADDOCK algorithm to produce a low resolution structure of hUbc13 bound to Traf6.

4.2 Materials and Methods

4.2.1 Protein expression and purification

hUbc13

[*U*-^{15}N; *U*-^{13}C]-hUbc13 K92R was expressed in *E. coli* strain BL21(DE3)-RIL according to the protocol of Marley *et al.* [23]. 1 L of LB containing 50 μg/mL ampicillin and 25 μg/mL chloramphenicol was inoculated with a single colony and grown at 37 °C with aeration to A_{600} ~0.8. Cells were harvested by centrifugation and resuspended in 1 L of prewarmed M9 media lacking carbon and nitrogen sources, immediately harvested by centrifugation and resuspended in 500 mL of M9 salts containing ~50 μg/mL ampicillin, ~25 μg/mL chloramphenicol, 6 g/L [^{13}C]C_6-glucose, and 1 g/L [^{15}N]ammonium sulfate. Cells were incubated at 37 °C for 2 hours, induced with 0.4 mM IPTG, and incubated for an additional 9 hours.

Cells were harvested by centrifugation, and the cell pellets were resuspended in ~70 mL lysis buffer (140 mM NaCl, 2.7 mM KCl, 10 mM Na_2HPO_4, 1.8 mM KH_2PO_4, 100 μg/mL

DNase I, 1 mM DTT, 10 mM $MgSO_4$, 0.5% protease inhibitor cocktail II (Calbiochem catalog #538132)). Cells were lysed by two passes through a French press and the lysate was clarified by centrifugation. The supernatant was then filtered through a Millipore steriflip 0.45 μm vacuum filtration device. The filtered lysate was loaded onto a GSTprep FF 16/10 column equilibrated in pH 7.4 buffer containing 140 mM NaCl, 2.7 mM KCl, 10 mM Na_2HPO_4 and 1.8 mM KH_2PO_4. GST-fusion protein was eluted from the column with buffer containing 50 mM TrisHCl, 10 mM reduced glutathione, pH 8.0. Fractions eluting with glutathione buffer were collected, pooled, and buffer exchanged by passage through three HiPrep 26/10 desalting columns equilibrated with pH 7.0 buffer containing 50 mM TRIS, 250 mM NaCl, 1 mM EDTA, and 2 mM DTT. The flow-through was collected and concentrated to ~5 mL. 10 μL (20 units) of PreScission protease was added to the concentrated protein and the cleavage reaction was allowed to proceed for 24 hours at 4 °C. The cleaved protein was then purified with a GSTprep FF 16/10 column as described above for the intact fusion protein. The flow-through was collected and further purified by loading the protein solution onto a HiLoad 26/60 Superdex 75 column equilibrated with buffer containing 50 mM sodium phosphate, 250 mM NaCl, and 2 mM DTT, pH 7.0. The peak fractions eluting from 185–210 mL were pooled and concentrated for NMR studies.

Expression and purification of unlabelled hUbc13 K92R was accomplished in a similar fashion as unlabelled hMms2 (see Chapter 2.2.1), except that induction time was reduced to 7 hours, and the HiLoad 26/60 Superdex 75 column was equilibrated with buffer containing 50 mM sodium phosphate, 250 mM NaCl, and 2 mM DTT, pH 7.0.

Traf6 RING domain

[U-^{15}N]-Traf6 RING domain was prepared in a similar fashion as [U-^{15}N; U-^{13}C]-hUbc13 K92R, except that no [^{13}C]C_6-glucose was added to the M9 media, all buffers used were free of EDTA, and size exclusion chromatography was performed with a HiLoad 26/60 Superdex 30 column.

Expression and purification of unlabelled Traf6 RING domain was accomplished in a similar fashion as unlabelled hMms2 (see Chapter 2.2.1), except that all buffers used were free of EDTA, and size exclusion chromatography was performed with a HiLoad 26/60 Superdex 30 column.

4.2.2 NMR spectroscopy

All NMR spectra were obtained on a Varian Unity INOVA 600 NMR spectrometer. NMR samples were 600 μL for standard 5 mm i.d. NMR tubes, and 300 μL for SHIGEMI microcell NMR tubes, and contained 9:1 H_2O/D_2O with 50 mM phosphate (pH 7.5) 150 mM NaCl, 1 mM DTT, 1 mM DSS, 3 μL of 100x stock protease inhibitor cocktail I (Calbiochem catalog #539131), with ~0.5 mM hUbc13.

Chemical shift assignment of hUbc13 - The main chain atoms of hUbc13 were unambiguously assigned using a combination of the HNCACB [29] [26] and CBCA(CO)NNH [15] experiments at 30 °C. Side chain atoms were assigned using the H(CC)TOCSY(CO)NNH and (H)CCTOCSY(CO)NNH experiments [22] [21] [11], and the HCCH-TOCSY experiment [2] [20]. All spectra were processed using the program NMRPipe [7], and chemical shift assignment was accomplished using the program Sparky [14]. All assigned chemical shifts are tabulated in Appendix B.2.

Titration of [U-^{15}N; U-^{13}C]-hUbc13 with Traf6 - Three aliquots of Traf6 were titrated

into ~0.2 mM [U-^{15}N; U-^{13}C]-hUbc13 at 30 °C, and a 2D ^{1}H-^{15}N-HSQC NMR spectrum was acquired at each titration point. Protein concentrations were determined by amino acid analysis, and the Traf6/Ubc13 molar ratios were calculated to be 0, 0.6, 2.2, and 7.2. Average chemical shift perturbations for each assigned resonance were calculated using a previously described method [12]. Average chemical shift changes that were greater than one standard deviation from the mean were considered significant.

Titration of [U-^{15}N]-Traf6 with hUbc13 - A 2D ^{1}H-^{15}N-HSQC NMR spectrum was acquired for ~0.1 mM [U-^{15}N]-Traf6 in the presence and absence of ~0.4 mM hUbc13. Average chemical shift perturbations for each resonance were calculated using a previously described method [12]. Average chemical shift changes that were greater than one standard deviation from the mean were considered significant.

Protein-Protein Docking - Protein docking for the hUbc13-Traf6 complex was performed using the HADDOCK (High Ambiguity Driven protein-protein Docking) protocol [10] with the structure of hUbc13 determined within the hMms2-Ubc13 complex [1J7D], the structure of the RING domain from Traf6 determined by solution state NMR spectroscopy (unpublished data), and ambiguous interaction restraints (AIRs) determined through chemical shift mapping. AIRs consisted of all possible interactions between the residues in hUbc13 that experienced significant chemical shift perturbation upon titration with Traf6, and every residue in the Traf6 RING domain that displays significant chemical shift perturbation upon titration with hUbc13, provided these residues have a fractional side chain solvent exposure of at least 30%. The starting structures were fixed as rigid bodies, except for residues in and around the interface of hUbc13 and Traf6, for which side chain flexibility was allowed. Out of 1000 rigid body docking trials, the top 150 lowest energy structures underwent structural refinement, and the 15 lowest energy refined structures were subjected

to a final refinement in explicit solvent.

Molecular Graphics - Protein structure graphics were produced using the program Pymol [8].

4.3 Results and Discussion

4.3.1 Titration of [*U*-^{15}N; *U*-^{13}C]-hUbc13 with Traf6

Backbone amide $^{1}H_{N}$ and ^{15}N chemical shift changes for [*U*-^{15}N; *U*-^{13}C]-hUbc13 upon titration with Traf6 are shown in Figure 4.1A and 4.1B. Only nine of 116 observable backbone amide $^{1}H_{N}$-^{15}N chemical shifts exhibit a significant change, suggesting that conformational changes in hUbc13 upon binding Traf6 are minimal. The interaction between hUbc13 and Traf6 is likely to be weak (high μM range) given the high Traf6/hUbc13 ratio (7.2:1) that is required to perturb hUbc13 $^{1}H_{N}$-^{15}N chemical shifts, as well as the linear change in hUbc13 $^{1}H_{N}$-^{15}N chemical shifts upon titration.

The chemical shift analysis indicates that the Traf6 binding surface on hUbc13 consists primarily of helix-α1 and the N-terminal region of helix-α3 (Figure 4.1C). Importantly, this binding surface is distinct from the hMms2 binding site [25], and the proposed donor ubiquitin binding site described by Hamilton *et al.* [16].

4.3.2 Titration of [*U*-^{15}N]-Traf6 with hUbc13

Backbone amide $^{1}H_{N}$ and ^{15}N chemical shift changes for [*U*-^{15}N]-Traf6 upon titration with hUbc13 are shown in Figure 4.2A and 4.2B. Ten of the 46 observable backbone amide $^{1}H_{N}$-^{15}N chemical shifts exhibit a significant change. The hUbc13 binding surface on Traf6 is shown in Figure 4.2C.

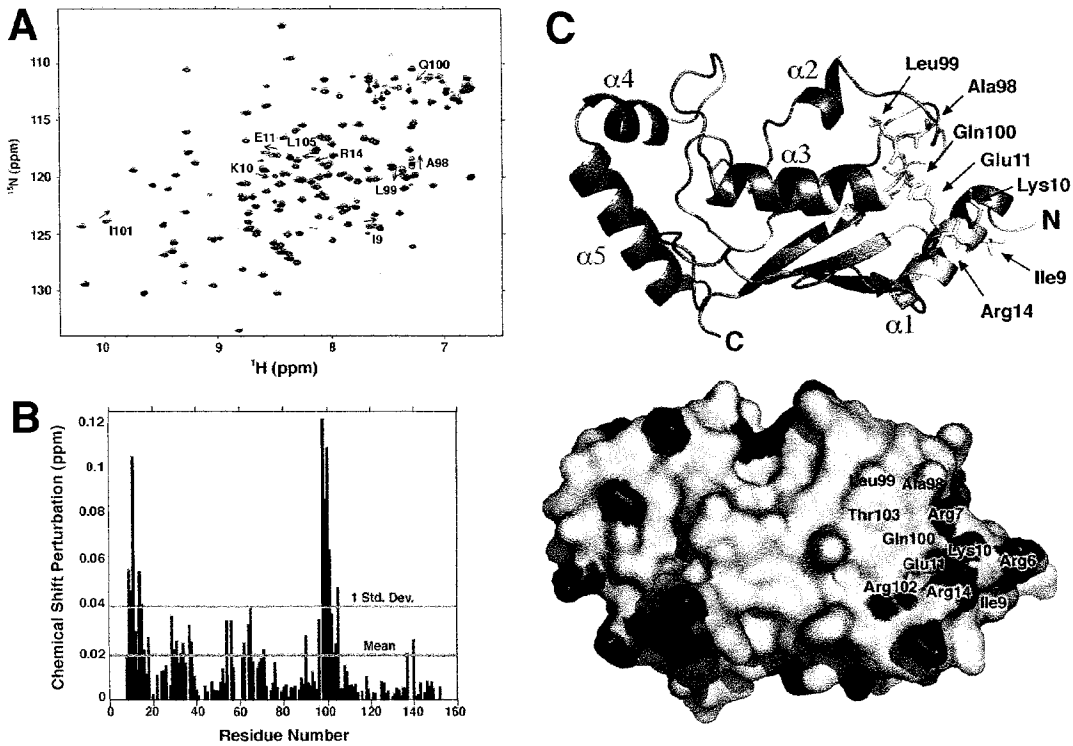

Figure 4.1: **hUbc13 backbone amide chemical shift changes upon titration with Traf6 RING domain.** (A) Superposition of ^{1}H-^{15}N HSQC NMR spectra of hUbc13 collected for various [Traf6]/[Ubc13] ratios: black (0:1), red (0.6:1), magenta (2.2:1), blue (7.2:1). Only those cross-peaks that were affected by complex formation are labelled. (B) Per residue plot of weighted average chemical shift perturbations given by $\Delta_{av} = \sqrt{\frac{\Delta\delta_{NH}^2 + \frac{\Delta\delta_N^2}{15}}{2}}$ [12] for 7.2:1 [Traf6]/[hUbc13]. The mean and cutoff for one standard deviation from the mean are included. (C) Cartoon (top) and surface (bottom) representation of hUbc13. In the cartoon representation, residues that experience chemical shift perturbation greater than one standard deviation from the mean upon titration of Traf6 are colored in yellow and shown as sticks. In the surface representation, positively charged atoms are colored in blue, negatively charged atoms are colored in red, aliphatic atoms from hydrophobic residues (Ala, Ile, Leu, Val, Phe, Tyr, Met, Pro) are colored in yellow, and atoms from polar residues are colored in white. Surface exposed residues around the Traf6 binding face are labeled.

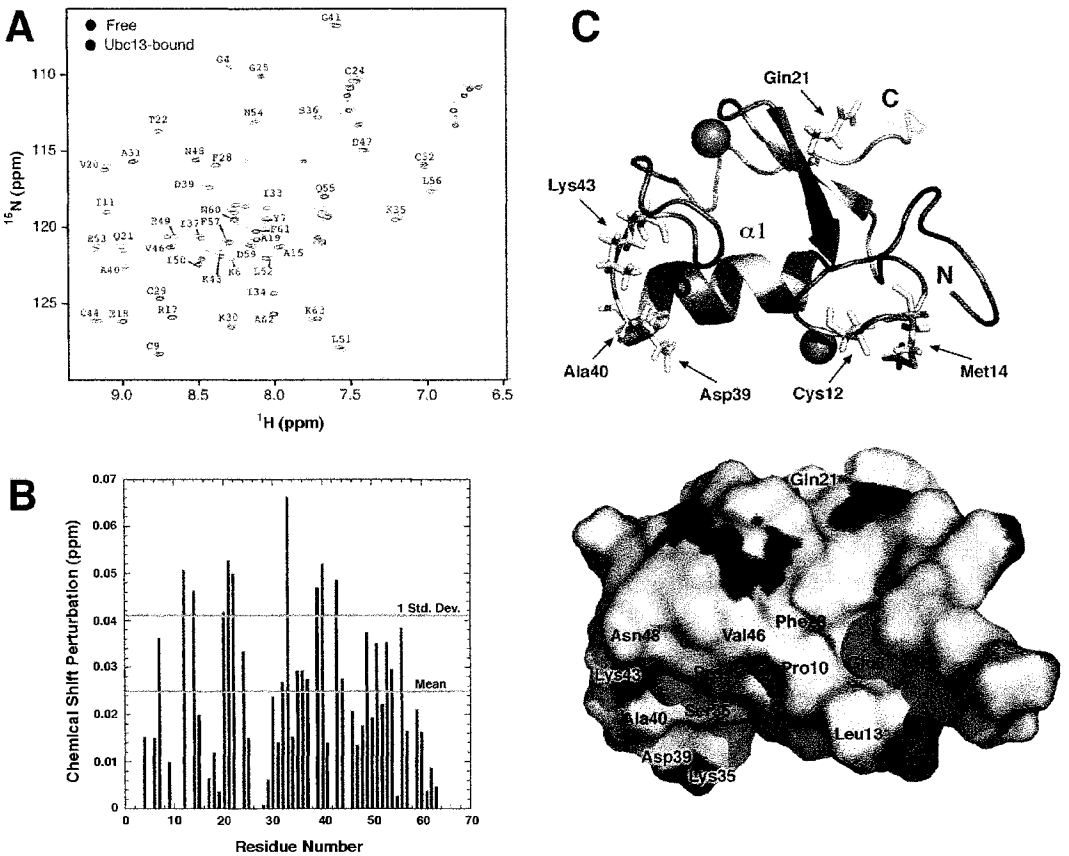

Figure 4.2: **Traf6 backbone amide chemical shift changes upon titration with hUbc13.** (A) Superposition of ^{1}H-^{15}N HSQC NMR spectra of Traf6 RING domain collected for Traf6 alone (red) and ~1:4 Traf6:hUbc13 (blue). (B) Per residue plot of weighted average chemical shift perturbations given by $\Delta_{av} = \sqrt{\frac{\Delta\delta^2_{NH} + \frac{\Delta\delta^2_{N}}{15}}{2}}$ [12]. The mean and cutoff for one standard deviation from the mean are included. (C) Cartoon (top) and surface (bottom) representation of Traf6. In the cartoon representation, residues that experience chemical shift perturbation greater than one standard deviation from the mean upon titration of Traf6 are colored in yellow and shown as sticks, and zinc ions are shown as grey spheres. In the surface representation, positively charged atoms are colored in blue, negatively charged atoms are colored in red, aliphatic atoms from hydrophobic residues (Ala, Ile, Leu, Val, Phe, Tyr, Met, Pro) are colored in yellow, and atoms from polar residues are colored in white. Surface exposed residues around the hUbc13 binding face are labeled.

4.3.3 Docking of Traf6 onto hUbc13

The structure of the E2-RING complex between UbcH7 and c-Cbl has previously been solved using x-ray crystallography [31] and indicates that c-Cbl binds to UbcH7 through an interface composed of helix-α1 and the loop region adjacent to C-terminal to the helix-α1 (Figure 4.3A). To investigate possible binding modes, the HADDOCK protocol was employed to dock Traf6 onto Ubc13 using AIR restraints determined through chemical shift mapping.

The top fifteen lowest energy structures superimpose with a backbone rmsd value of 0.81 $\pm$ 0.34 Å (Figure 4.3B). The binding mode is distinct from that revealed by the structure of UbcH7 bound to the RING domain of c-Cbl [31] (Figure 4.3A), though it should be stressed that restraints used in the Traf6 model were based on ambiguous data and the structure may not be accurate. In the model presented here, the hUbc13 binding site on Traf6 consists of the N-terminus, the β-strand composed of residues 9–14, and the loop composed of residues 41–47. The Traf6 binding site on hUbc13 consists of the N-terminal α-helix, loop residues 62–64, and residues 96–103 (Figure 4.3B). The difference in binding modes between the UbcH7-c-Cbl structure and our hUbc13-Traf6 model is perhaps not surprising considering the absence of a key residue in the Traf6 RING domain. The UbcH7-c-Cbl interaction involves a highly conserved Trp residue (Trp408), which corresponds to Ser36 in the Traf6 RING domain. In addition, the interface in our model involves Met14 from loop 1 of the Traf6 RING domain, which corresponds to Glu387 in the RING domain of c-Cbl [31].

In contrast to the hMms2-Ub structure described in Chapter 3, our model of the hUbc13-Traf6 interaction is based solely on chemical shift mapping data rather than directly observed intermolecular NOEs. While this data is sufficient to produce low resolution models, HADDOCK blind docking trials have shown that structures generated using ambiguous data

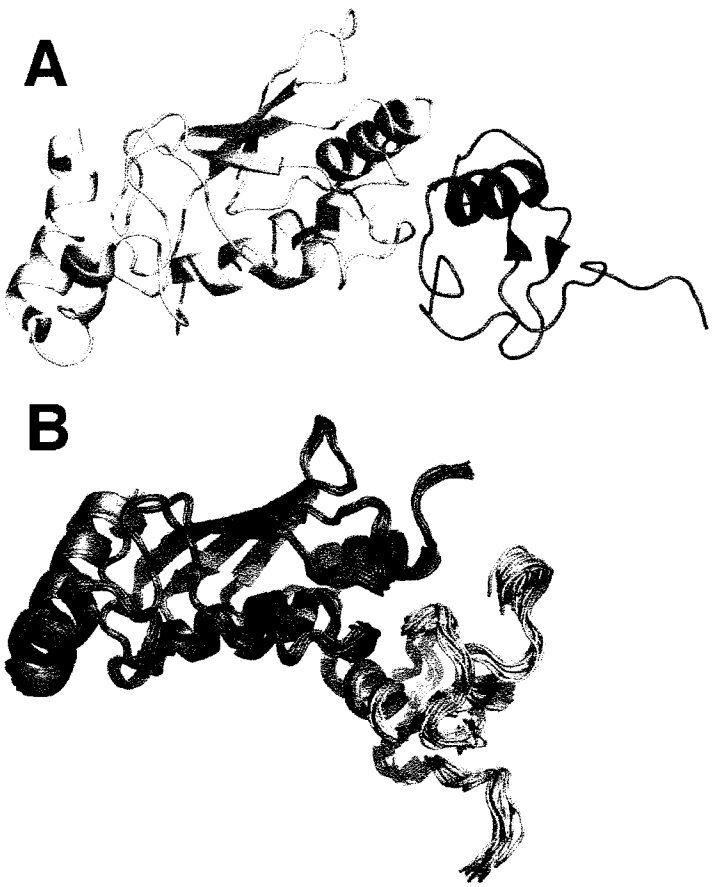

Figure 4.3: **Comparison between the structures of UbcH7-c-Cbl and hUbc13-Traf6.** (A) Cartoon representation of UbcH7 (green) in complex with the RING domain from c-Cbl (purple) [1FBV]. (B) Ensemble of the top twenty-five lowest NOE energy structures generated using the HADDOCK protocol. The backbone atoms of hUbc13 are shown as a blue cartoon, and the backbone atoms of the RING domain of Traf6 are shown as a green cartoon.

are not always accurate [27]. Therefore the preliminary hUbc13-Traf6 model presented here must be cautiously considered.

4.4 Conclusion

The main chain and side chain chemical shifts for hUbc13 have been assigned using high resolution solution state NMR spectroscopy (Appendix B.2). The binding interface of hUbc13 and Traf6 has been determined through NMR chemical shift mapping, and we have used HADDOCK to generate a model of hUbc13 bound to the RING domain of Traf6. The model suggests that the binding mode is distinct from the interaction between UbcH7 and c-Cbl [31].

Bibliography

[1] Parker L. Andersen, Honglin Zhou, Landon Pastushok, Trevor Moraes, Sean McKenna Barry Ziola, Michael J. Ellison, Vishva M. Dixit, and Wei Xiao. Distinct regulation of Ubc13 functions by the two ubiquitin-conjugating enzyme variants Mms2 and Uev1A. *J Cell Biol*, 170:745–755, 2005.

[2] A. Bax, G. M. Clore, and A. M. Gronenborn. H-1-H-1 Correlation Via Isotropic Mixing of C-13 Magnetization, a New 3-Dimensional Approach for Assigning H-1 and C-13 Spectra of C-13-Enriched Proteins. *J Magn Reson*, 88:425–431, 1990.

[3] Yinon Ben-Neriah. Regulatory functions of ubiquitination in the immune system. *Nat Immunol*, 3:20–26, 2002.

[4] Stacey Broomfield, Barbara L. Chow, and Wei Xiao. *MMS2*, encoding a ubiquitin-conjugating-enzyme-like protein, is a member of the yeast error-free postreplication repair pathway. *Proc Natl Acad Sci U S A*, 95:5678–5683, 1998.

[5] Nei-Li Chan and Christopher P. Hill. Defining polyubiquitin chain topology. *Nat Struct Biol*, 8:650–652, 2001.

[6] Zhijian J. Chen. Ubiquitin signalling in the NF-κB pathway. *Nat Cell Biol*, 7:758–765, 2005.

[7] Frank Delaglio, S. Grzesiek, G.W. Vuister, G. Zhu, J. Pfeifer, and A. Bax. NMRPipe: a multidimensional spectral processing system based on UNIX pipes. *J Biomol NMR*, 6:277–293, 1995.

[8] Warren L. DeLano. DeLano Scientific, San Carlos, CA, USA, 2002.

[9] Li Deng, Chen Wang, Erika Spencer, Liyong Yang, Amy Braun, Jianxin You, Clive Slaughter, Cecile Pickart, and Zhijian J. Chen. Activation of the IκB Kinase Complex by TRAF6 Requires a Dimeric Ubiquitin-Conjugating Enzyme Complex and a Unique Polyubiquitin Chain. *Cell*, 103:351–361, 2000.

[10] Cyril Dominguez, Rolf Boelens, and Alexandre M. J. J. Bonvin. HADDOCK: A Protein-Protein Docking Approach Based on Biochemical or Biophysical Information. *J Am Chem Soc*, 125:1731–1737, 2003.

[11] K. H. Gardner, R. Konrat, M. K. Rosen, and L. E. Kay. An (H)C(CO)NH-TOCSY pulse scheme for sequential assignment of protonated methyl groups in otherwise deuterated N-15,C-13-labeled proteins. *J Biomol NMR*, 8:351–356, 1996.

[12] D. S. Garrett, Y. J. Seok, A. Peterkofsky, G. M. Clore, and A. M. Gronenborn. Identification by NMR of the binding surface for the histidine-containing phosphocarrier protein HPr on the N-terminal domain of enzyme I of the Escherichia coli phosphotransferase system. *Biochemistry*, 36:4393–4398, 1997.

[13] Michael H. Glickman and Aaron Ciechanover. The Ubiquitin-Proteasome Proteolytic Pathway: Destruction for the Sake of Construction. *Physiol Rev*, 82:373–428, 2002.

[14] Tom D. Goddard and Donald G. Kneller. SPARKY 3.

[15] Stephan Grzesiek and Ad Bax. Correlating Backbone Amide and Side Chain Resonances in Larger Proteins by Multiple Relayed Triple Resonance NMR. *J Am Chem Soc*, 114:6291–6293, 1992.

[16] Katherine S. Hamilton, Michael J. Ellison, Kathryn R. Barber, R. Scott Williams, John T. Huzil, Sean McKenna, Christopher Ptak, Mark Glover, and Gary S. Shaw. Structure of a Conjugating Enzyme-Ubiquitin Thiolester Intermediate Reveals a Novel Role for the Ubiquitin Tail. *Structure*, 9:897–904, 2001.

[17] Carsten Hoege, Boris Pfander, George-Lucian Moldovan, George Pyrowolakis, and Stefan Jentsch. *RAD6*-dependent DNA repair is linked to modification of PCNA by ubiquitin and SUMO. *Nature*, 419:135–141, 2002.

[18] Roseanne M. Hofmann and Cecile M. Pickart. Noncanonical *MMS2*-Encoded Ubiquitin-Conjugating Enzyme Functions in Assembly of Novel Polyubiquitin Chains for DNA Repair. *Cell*, 96:645–653, 1999.

[19] Atsuhiro Kanayama, Rashu B. Seth, Lijun Sun, Chee-Kwee Ea, Mei Hong, Abdullah Shaito, Yu-Hsin Chiu, Li Deng, and Zhijian J. Chen. TAB2 and TAB3 Activate the NF-κB Pathway through Binding to Polyubiquitin Chains. *Mol Cell*, 15:535–548, 2004.

[20] Lewis E. Kay, Guang Yi Xu, Alex U. Singer, D.R. Muhandiram, and Julie D. Forman-Kay. A Gradient-Enhanced HCCH-TOCSY Experiment for Recording Side-Chain 1H and 13C Correlations in H2O Samples of Proteins. *J Magn Reson B*, 101:333–337, 1993.

[21] T.M. Logan, E.T. Olejniczak, R.X. Xu, and S.W. Fesik. A general method for assigning NMR spectra of denatured proteins using 3D HC(CO)NH-TOCSY triple resonance experiments. *J Biomol NMR*, 3:225–231, 1993.

[22] B. A. Lyons and G. T. Montelione. An Hccnh Triple-Resonance Experiment Using C-13 Isotropic Mixing for Correlating Backbone Amide and Side-Chain Aliphatic Resonances in Isotopically Enriched Proteins. *J Magn Reson B*, 101:206–209, 1993.

[23] J. Marley, M. Lu, and C. Bracken. A Method for Efficient Isotopic Labeling of Recombinant Proteins. *J Biomol NMR*, 20:71–75, 2001.

[24] Sean McKenna, Trevor Moraes, Landon Pastushok, Christopher Ptak, Wei Xiao, Leo Spyracopoulos, and Michael J. Ellison. An NMR-based Model of the Ubiquitin-bound Human Ubiquitin Conjugation Complex Mms2·Ubc13. The structural basis for lysine 63 chain catalysis. *J Biol Chem*, 278:13151–13158, 2003.

[25] Trevor F. Moraes, Ross A. Edwards, Sean McKenna, Landon Pastushok, Wei Xiao, J. N. Mark Glover, and Michael J. Ellison. Crystal structure of the human ubiquitin conjugating enzyme complex, hMms2-hUbc13. *Nat Struct Biol*, 8:669–673, 2001.

[26] D. R. Muhandiram and L. E. Kay. Gradient-Enhanced Triple-Resonance 3-Dimensional Nmr Experiments with Improved Sensitivity. *J Magn Reson B*, 103:203–216, 1994.

[27] A. D. J. van Dijk, S. J. de Vries, C. Dominguez, H. Chen, H.-X. Zhou, and A. M. J. J. Bonvin. Data-Driven Docking: HADDOCK's Adventures in CAPRI. *Proteins*, 60:232–238, 2005.

[28] Chen Wang, Li Deng, Mei Hong, Giridhar R. Akkaraju, Jun-Ichiro Inoue, and Zhijian J. Chen. TAK1 is a ubiquitin-dependent kinase of MKK and IKK. *Nature*, 412:346–351, 2001.

[29] Michael Wittekind and Luciano Mueller. HNCACB, a High-Sensitivity 3D NMR Experiment to Correlate Amide-Proton and Nitrogen Resonances with the Alpha- and Beta-Carbon Resonances in Proteins. *J Magn Reson B*, 101:201–205, 1993.

[30] Jill Wooff, Landon Pastushok, Michelle Hanna, Yu Fu, and Wei Xiao. The TRAF6 RING finger domain mediates physical interaction with Ubc13. *FEBS L*, 566:229–233, 2004.

[31] Ning Zheng, Ping Wang Philip D. Jeffrey, and Nicola P. Pavletich. Structure of a c-Cbl-UbcH7 Complex: RING Domain Function in Ubiquitin-Protein Ligases. *Cell*, 102:533–539, 2000.

Chapter 5

Conclusions and Future Directions

5.1 Conclusions

The primary focus of this dissertation is determining the manner in which the Mms2-Ubc13 heterodimer recruits acceptor ubiquitin for Lys63-linked polyubiquitin chain synthesis. Solution state NMR spectroscopy was employed to measure intermolecular distance restraints between hMms2 and Ub. These data were used within a docking algorithm to produce a structure for the hMms2-Ub complex that is consistent with previously determined functional data. Through additional docking onto hMms2-hUbc13, the intermolecular distance restraints indicate that the role of hMms2 is to position acceptor Ub such that the side chain of Lys63 is poised at the mouth of a channel that leads into the active site of Ubc13, where the C-terminus of the donor ubiquitin is covalently attached through a thioester bond to the active site cysteine of hUbc13. Notably, the hMms2-Ub interface involves the hydrophobic patch on Ub (L8, I44, V70) that has been implicated in numerous other interactions with ubiquitin binding motifs. Furthermore, imposing a distance restraint between Lys63 of Ub and Asp81 of Ubc13 allows Lys63 to come within catalytic distance of active

site, without violating any of the observed intermolecular NOEs measured between Ub and hMms2 in the absence of hUbc13.

In addition to research regarding the catalyic mechanism of E2-UEV enzymes, the interaction between hUbc13 and its cognate E3 ligase Traf6 was investigated using NMR chemical shift mapping. The Traf6 binding site on hUbc13 appears to be distinct from both the hMms2 binding site, and the donor ubiquitin conjugation site. The structure of the complex between Traf6 and hUbc13 was investigated using a docking algorithm in combination with NMR chemical shift data. While the hUbc13-Traf6 structure has yet to be unambiguously defined, the model suggests a mode of binding that is distinct from those characterized in the literature.

5.2 Future Directions for Protein Ubiquitination Research

The field of protein ubiquitination encompasses a vast range of research opportunities given the wide variety of biological outcomes for ubiquitinated proteins. In the following section, future directions pertinent to the focus of research described in this dissertation, and some additional intriguing results are discussed.

5.2.1 Questions concerning polyubiquitination during post-replicative DNA repair

(i) The manner in which Lys63-linked chains are attached to PCNA is an intriguing problem. Given the model shown in Figure 5.1, some type of scaffolding must exist in order to bridge the distance between the Ubc13-RING binding site and the substrate, bound to the C-terminus of the acceptor ubiquitin. Scaffolding is common in RING-mediated ubiquitination (examples given in Chapter 1.6.2), though in the case of hMms2-hUbc13 it

is not known if there is a protein scaffold. The scaffolding may comprise only RAD5, or both RAD5 and RAD18. RAD5 and RAD18 have been shown to associate with PCNA in a yeast two-hybrid screen [3], and a model where both proteins combine to form a scaffold could explain targeting of hMms2-hUbc13 to synthesize Lys63-linked polyUb chains.

Furthermore, it has yet to be determined whether PCNA ubiquitination requires any additional post-translational modifications, such as phosphorylation, as a pre-requisite to ubiquitination. As discussed in Chapter 1.6.3, there are precedents for cross-talk between ubiquitination and other post-translational modification signalling pathways.

(ii) From a biological perspective, a key problem involves the manner in which polyubiquitinated PCNA promotes DNA template swapping. The factors responsible for recognition of polyubiquitin chains are not known, and may be mediated by NZF domains similar to those found in the TAB family of proteins [5]. Elucidation of the structural basis for template swapping will most likely require a variety of structural techniques, such as NMR spectroscopy, x-ray crystallography, and cryo-electron microscopy.

5.2.2 Questions concerning the role of polyubiquitination for NF-κB activation

(i) Bcl10 activation of NF-κB has been shown to involve the Lys63-linked polyubiquitination of NEMO by the Uev1a-Ubc13 complex [11] [1], but the purpose of this modification and the link to NF-κB activation are unclear. Further questions include the identity of the E3 ligase involved in NEMO polyubiquitination, and whether or not NEMO polyubiquitination requires ATM-triggered monoubiquitination in the nucleus. Perhaps polyubiquitin chain extension requires the presence of a mono-ubiquitin tag, much like how PCNA polyubiquitination requires monoubiquitination by RAD6/RAD18 [3]. If this is the case, it is not

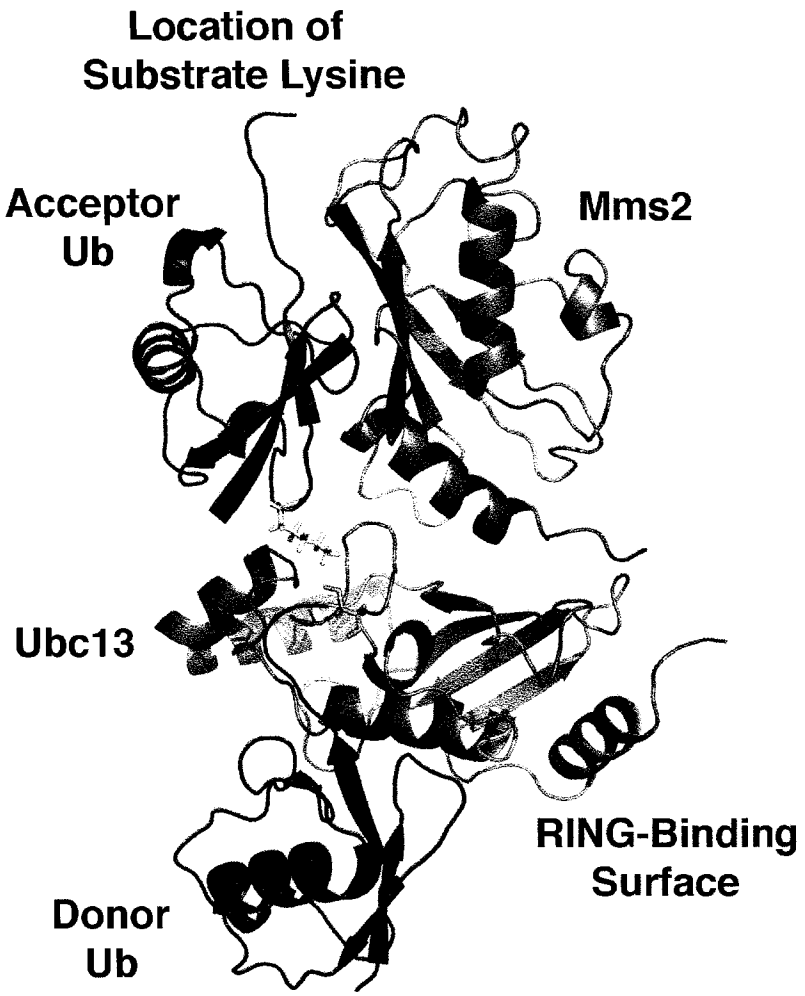

Figure 5.1: **Model of the Ub_2-Mms2-Ubc13 Tetramer.** Cartoon representation of acceptor Ub (red, top)-hMms2-hUbc13 (blue) structure calculated with an additional distance restraint between Ub Lys63 (green) and Ubc13 Cys87 (violet), as determined in Chapter 3. The donor Ub (red, bottom) is positioned relative to Ubc13 in an analogous manner to the Ubc1-Ub structure determined by Hamilton *et al.* [2]. The proposed RING domain-binding surface, inferred by analogy to the Traf6 binding site on Ubc13 determined in Chapter 4, is colored in yellow. Location of the substrate lysine residue is noted.

clear which of the two monoubiquitin tags on NEMO are extended.

(ii) Similar to polyubiquitination in the PRR pathway, the nature of the E3 scaffolding for the auto-ubiquitination of TRAF6 is unknown. Since this is an auto-ubiqutination event, TRAF6 must bridge the gap on its own. Perhaps the heterodimer is involved: Does TRAF6 make additional contacts to Uev1a? The possibility that the N-terminal tail of Uev1a is involved in TRAF6 binding has not been excluded. This could explain why TRAF6 binding to Ubc13 alone appears to be weak on the basis of the NMR experiments in Chapter 4. Clearly, a better understanding of the overall structure of TRAF6 will help to answer these questions.

5.2.3 Questions concerning the Uev-Ubc13 heterodimer

(i) Ubc13 is subject to modification by the attachment of ISG15, a Ubl modifier, to Lys92. This modification has the effect of inhibiting thiolester bond formation between Ubc13 and Ub [12]. Ubc13 autoubiquitinates at Lys92 *in vitro*, and the K92R mutation does not affect K63-linked chain formation or interaction with Mms2 [7]. Modification by ISG15 suggests cross-talk between the ubiquitination and ISGylation pathways. The relationship between these two pathways is a major unresolved question.

(ii) It has been observed that both Mms2 and Ubc13 are cytosolic proteins, and only enter the nucleus when DNA damage occurs [9]. The role of Mms2 in the nucleus has been well characterized [1], but Mms2 has no known role in the cytoplasm. One possible explanation is that relocation of Mms2 acts as an inhibitory mechanism against DNA PRR. Another hypothesis, proposed by Andersen *et al.* [1], is that Mms2 and Uev1a regulate each other by competing for binding with Ubc13. This theory has yet to be substantiated, but may explain why Uev1a, which has no known roles outside of the cytoplasm, has been

observed in the nucleus as well [1].

5.2.4 Additional ubiquitination questions

(i) A recent surprising observation is the phosphorylation of yeast Ub at Ser57, a residue that is both poorly conserved (absent in humans) and non-essential for yeast survival [8]. The role of this modification in yeast is unknown.

(ii) Mixed Ubiquitin and NEDD8 chains (His_{10}-NEDD8-Ub_3) have been observed to bind the proteasome as efficiently as Ub_4 *in vitro* [10], and the *in vivo* existence and biological function of these chains is currently unknown.

In the search for novel polyubiquitin linkages, it is typical to test for functional activity in ubiquitin mutants that lack the capability to produce any other type of chain. For example, to test for involvement of Lys63-linked chains in PRR, every Lys residue in ubiquitin has been simultaneously mutated to Arg, except for Lys63, and assayed for activity [4]. While this method unambiguously defines the dominant linkage involved in the pathway, this approach also occludes insight into mixed topology chains. Currently, the only evidence for mixed chains is the observation that UbcH5 produces heteropolymers consisting of Lys29 and Lys48 linkages *in vitro* [6]. Whether or not heteropolymers exist *in vivo* is unknown.

5.3 Closing

Protein ubiquitination is a fascinating topic, considering the variety of cellular responses that it regulates, and the conservation of this system across the eukaryotic kingdom. In the grand scheme of things, this thesis provides but a small piece to the ubiquitination puzzle, but I am confident in the work that I have done, and proud to have had the opportunity to contribute to the research in this field.

Bibliography

[1] Parker L. Andersen, Honglin Zhou, Landon Pastushok, Trevor Moraes, Sean McKenna Barry Ziola, Michael J. Ellison, Vishva M. Dixit, and Wei Xiao. Distinct regulation of Ubc13 functions by the two ubiquitin-conjugating enzyme variants Mms2 and Uev1A. *J Cell Biol*, 170:745–755, 2005.

[2] Katherine S. Hamilton, Michael J. Ellison, Kathryn R. Barber, R. Scott Williams, John T. Huzil, Sean McKenna, Christopher Ptak, Mark Glover, and Gary S. Shaw. Structure of a Conjugating Enzyme-Ubiquitin Thiolester Intermediate Reveals a Novel Role for the Ubiquitin Tail. *Structure*, 9:897–904, 2001.

[3] Carsten Hoege, Boris Pfander, George-Lucian Moldovan, George Pyrowolakis, and Stefan Jentsch. *RAD6*-dependent DNA repair is linked to modification of PCNA by ubiquitin and SUMO. *Nature*, 419:135–141, 2002.

[4] Roseanne M. Hofmann and Cecile M. Pickart. Noncanonical *MMS2*-Encoded Ubiquitin-Conjugating Enzyme Functions in Assembly of Novel Polyubiquitin Chains for DNA Repair. *Cell*, 96:645–653, 1999.

[5] Atsuhiro Kanayama, Rashu B. Seth, Lijun Sun, Chee-Kwee Ea, Mei Hong, Abdullah Shaito, Yu-Hsin Chiu, Li Deng, and Zhijian J. Chen. TAB2 and TAB3 Activate the NF-κB Pathway through Binding to Polyubiquitin Chains. *Mol Cell*, 15:535–548, 2004.

[6] Lucy D. Mastrandrea, Jianxin You, Edward G. Niles, and Cecile M. Pickart. E2/E3-mediated Assembly of Lysine 29-linked Polyubiquitin Chains. *J Biol Chem*, 274:27299–27306, 1999.

[7] Sean McKenna, Leo Spyracopoulos, Trevor Moraes, Landon Pastushok, Christopher Ptak, Wei Xiao, and Michael J. Ellison. Noncovalent Interaction between Ubiquitin and the Human DNA Repair Protein Mms2 Is Required for Ubc13-mediated Polyubiquitination. *J Biol Chem*, 276:40120–40126, 2001.

[8] Junmin Peng, Daniel Schwartz, Joshua E Elias, Carson C Thoreen, Dongmei Cheng, Gerald Marsischky, Jeroen Roelofs, Daniel Finley, and Steven P Gygi. A proteomics approach to understanding protein ubiquitination. *Nat Biotechnol*, 21:921–926, 2003.

[9] Helle D. Ulrich and Stefan Jentsch. Two RING finger proteins mediate cooperation between ubiquitin-conjugating enzymes in DNA repair. *Embo J*, 19:3388–3397, 2000.

[10] Frank G. Whitby, Gang Xia, Cecile M. Pickart, and Christopher P. Hill. Crystal Structure of the Human Ubiquitin-like Protein NEDD8 and Interactions with Ubiquitin Pathway Enzymes. *J Biol Chem*, 273:34983–34991, 1998.

[11] Honglin Zhou, Ingrid Wertz, Karen O'Rourke, Mark Ultsch, Somasekar Seshagiri, Michael Eby, Wei Xiao, and Vishva M. Dixit. Bcl10 activates the NF-κB pathway through ubiquitination of NEMO. *Nature*, 427:167–171, 2004.

[12] Weiguo Zou, Vladimir Papov, Oxana Malakhova, Keun Il Kim, Chinh Dao, Jun Li, and Dong-Er Zhang. ISG15 modification of ubiquitin E2 Ubc13 disrupts its ability to form thioester bond with ubiquitin. *Biochem Biophys Res Commun*, 336:61–68, 2005.

Appendix A

Deity v2.2.5: A Tcl/Tk module for NMRview

A.1 The Purpose of Deity

Deity is a Tcl/Tk script written to add functionality to the software program NMRview [1]. The script loads a window that contains three different modules described below. Pop-up instructions on how to use each module can be displayed simply by clicking on the module name (Figure A.1).

The first module, termed "Gremlin", deals with peak deletion. It deletes selected peak assignments without corrupting the peak list, taking advantage of the built-in *nv_peak del-region* NMRview command, which removes from the peak list **all** picked peaks selected between the two crosshairs in the spectral window. This feature is especially useful when dealing with noisy spectra.

The second module, termed "Zodiac", searches the selected peak list for assignments matching the query term, and returns the reference number from the peak list. This func-

tionality is useful for searching reference spectra when assigning peaks for the current data set.

The third module, termed "Evangelist", allows the user to save the selected peak list and the assigned chemical shift list with a single button. This functionality is useful for instances where users forget to save each data file upon terminating the program. It also provides an alternative to using NMRview STAR files, that save entire sessions, which have been reported by some users to be easily corruptible.

To run Deity, the user must first source the code by typing "source deity.tcl" in the console window of NMRview, and then type "deity" to run the code. It should be noted that this script was written prior to NMRviewJ, and may not work properly due to changes in the compiled code. It was built and tested on Mac OS X and Unix machines using NMRview 5.2.2.

Figure A.1: **Deity in Action.** Deity running on the Mac OS X platform.

A.1.1 Deity Code

```
################
# Deity v2.2.5 by Mike Lewis #
################
#
```

```
#Modules:
# Gremlin v1.5 : Unassigns peaks in the current peak list
# Zodiac v0.8 : Searches current peak list for assigned residues
# Evangelist v1.3 : Saves chemical shifts and current peak list
#

#Calls up the Deity window
proc deity {} {

    global candidate

    toplevel .deity -bg #2a3854
    wm title .deity "Deity"
    wm geometry .deity 206x173

    button .deity.voice -bg #2a3854 -fg gold -borderwidth 2 \
        -font {Helvetica -14 bold} \
        -text {Deity v2.2.5} -command DareToQuestionDeity
    place .deity.voice \
        -x 3 -y 3 -width 90 -height 25

    SummonTheGremlin
    CallUponZodiac
    PresentEvangelist
}

proc DareToQuestionDeity {} {
    set result [tk_dialog .aboutdeity "Deity v2.2.5 by Mike Lewis" \
        "Deity is a plugin for nmrview to make life easier. The modules that encompass it
were written to perform menial tasks, but are valuable tools.\n\nClicking on the title of any
module will bring up a dialog box with instructions on how to use it." \
        info 0 OK]
}


#########
# Gremlin v1.5 #
#########

#Calls up Gremlin module
proc SummonTheGremlin {} {

    frame .deity.gremlin -borderwidth 1 -width 75 -height 60 -relief groove -bg #007608
    button .deity.gremlin.gibblegabble -borderwidth 1 -fg gold -bg #007608 \
        -font {Helvetica -8} -text Gremlin -relief groove -activebackground #007608 \
        -command AskGizmo
    button .deity.gremlin.doom -font {Helvetica -13} -text "Zap!" -justify center \
        -bg black -activebackground black -fg gold \
        -activeforeground red -relief raised -command BringDoomToPeak
```

```
    button .deity.gremlin.massdoom -font {Helvetica -10} -text "Zap\nAll" -justify center\
        -bg black -activebackground black -fg gold \
        -activeforeground red -relief raised -command RainDoomUponAll

    place .deity.gremlin \
        -x 3 -y 30
    place .deity.gremlin.gibblegabble \
        -x 3 -y 0 -width 35 -height 15
    place .deity.gremlin.doom \
        -x 35 -y 20 -width 35 -height 35
    place .deity.gremlin.massdoom \
        -x 3 -y 20 -width 25 -height 35
}

#Unassigns current peak
proc BringDoomToPeak {} {
    global curr_list curr_peak
    for {set i 1} {$i<=3} {incr i} {
        nv_peak elem [lindex [nv_peak label $curr_list] [expr $i-1]].L $curr_list.$curr_peak ?
    }
}

#Unassigns all peaks within cursor box
proc RainDoomUponAll{} {
    nv_peak delregion
}

#Brings up info box
proc AskGizmo {} {
    set result [tk_dialog .aboutgremlin "Gremlin v1.5" \
        "Gremlin provides an easy way to unassign peaks.\n\nClicking on the \"Zap!\"
button will unassign the peak currently selected in the peak window.\n(Note that the peak
window won't update automatically)\n\nClicking on the \"Zap All\" button will unassign
all visible peaks within the cursor box from the current peak list." \
        questhead 0 OK]
}


#########
# Zodiac v0.8 #
#########

#Calls up the Zodiac module
proc CallUponZodiac {} {

    frame .deity.zodiac -borderwidth 1 -width 200 -height 77 -relief groove -bg #900a4a
    button .deity.zodiac.constellation -borderwidth 1 -fg gold -bg #900a4a \
        -font {Helvetica -8} -text Zodiac -relief groove -activebackground #900a4a \
        -command ConsultStarChart
```

```
    entry .deity.zodiac.atomos -fg black -bg white -relief sunken
    entry .deity.zodiac.anotheratomos -fg black -bg white -relief sunken
    button .deity.zodiac.barhop -font {Helvetica -12} -text "Search" -justify center \
        -bg black -activebackground black -fg gold \
        -activeforeground red -relief raised -command WhatsYourSign
    label .deity.zodiac.maker -text "Match?" -bg #900a4a
    entry .deity.zodiac.horoscope -fg gold -bg #900a4a -relief sunken

    place .deity.zodiac \
        -x 3 -y 93
    place .deity.zodiac.constellation \
        -x 3 -y 0 -width 33 -height 15
    place .deity.zodiac.atomos \
        -x 5 -y 20 -width 60 -height 20
    place .deity.zodiac.anotheratomos \
        -x 70 -y 20 -width 60 -height 20
    place .deity.zodiac.barhop \
        -x 140 -y 18 -width 50 -height 24
    place .deity.zodiac.maker \
        -x 20 -y 50
    place .deity.zodiac.horoscope \
        -x 70 -y 50 -width 60 -height 20
}

#Searches current peak list for user-specifed residues
proc WhatsYourSign {} {

    global curr_list

    set labels [nv_peak label $curr_list]
    set dim1name [lindex $labels 0]
    set dim2name [lindex $labels 1]

    set lineone [.deity.zodiac.atomos get]
    set linetwo [.deity.zodiac.anotheratomos get]
    puts $lineone
    puts $linetwo

    .deity.zodiac.horoscope delete 0 10
    .deity.zodiac.horoscope insert 1 "None"

    foreachpeak candidate $curr_list {
        set first [nv_peak elem $dim1name.L $curr_list.$candidate]
        set second [nv_peak elem $dim2name.L $curr_list.$candidate]
        if {$first != $lineone —— $second != $linetwo} {continue}

        .deity.zodiac.horoscope delete 0 10
        .deity.zodiac.horoscope insert 1 "#$candidate"
    }
```

```
}

#Brings up info box
proc ConsultStarChart } {
    set result [tk_dialog .aboutzodiac "Zodiac v0.8" \
        "Zodiac searches the selected peak list for a specified assignment.\n\nThe entry fields correspond to the x and y labels respectively, and the peak names must be typed in exactly.\n\n example: 101.HN 101.N\n\nThen press the \"Search\" button, and the matching peak number will appear in the \"Match?\" field.\n\nZodiac still has trouble matching to ambiguously assigned peaks." \
        questhead 0 OK]
}


##########
# Evangelist v1.3 #
##########

#Calls up Evangelist module
proc PresentEvangelist {} {

    global healppm
    global healxpk

    frame .deity.evangelist -borderwidth 1 -width 122 -height 60 -relief groove -bg #3c1eac
    button .deity.evangelist.stage -borderwidth 1 -fg gold -bg #3c1eac \
        -font {Helvetica -8} -text Evangelist -relief groove -activebackground #3c1eac \
        -command InquireAboutTheFaith
    checkbutton .deity.evangelist.afflictedppm -text "ppm.out" -borderwidth 2 -fg gold \
        -font {Helvetica -10} -selectcolor gold -bg #2a3854 -activebackground #2a3854 \
        -variable ::healppm -anchor w -activeforeground gold
    checkbutton .deity.evangelist.afflictedxpk -text ".xpk" -borderwidth 2 -fg gold \
        -font {Helvetica -10} -selectcolor gold -bg #2a3854 -activebackground #2a3854 \
        -variable ::healxpk -anchor w -activeforeground gold
    button .deity.evangelist.prayer -font {Helvetica -12} -text "Save" -justify center \
        -bg black -activebackground black -fg gold \
        -activeforeground red -relief raised \
        -command InvokePowersThatBe

    place .deity.evangelist \
        -x 81 -y 30
    place .deity.evangelist.stage \
        -x 68 -y 0 -width 51 -height 15
    place .deity.evangelist.afflictedppm \
        -x 5 -y 10 -width 60 -height 17
    place .deity.evangelist.afflictedxpk \
        -x 5 -y 35 -width 60 -height 17
    place .deity.evangelist.prayer \
        -x 76 -y 19 -width 36 -height 36
```

```
}

#Saves specified output files
proc InvokePowersThatBe {} {

    global curr_list

    if {$::healppm} {
        writeppm
        puts "Chemical shifts saved."
    }
    if {$::healxpk} {
        writepks
        puts "$curr_list.xpk saved."
    }

    puts "\n"
}

#Brings up info box
proc InquireAboutTheFaith {} {
    set result [tk_dialog .aboutdeity "Evangelist v1.3" \
        "Evangelist saves your data with a single click.\n\nUse the check boxes to turn on
which data files you want saved, and then press \"Save\" to write them to disk.\n\nNote
that when \"xpk\" is checked, Evangelist will NOT save every read peak list; It will only
save the currently selected one." \
        questhead 0 OK]
}


##########
# Version History #
##########
#
# 2.2.5 - Evangelist updated to v1.3
#         - Removed the "save state" button (it wasn't doing anything anyways)
#         - Clarified the instructions with respect to saving data lists
#
# 2.2.1 - Evangelist updated to v1.2.1
#     - Clarified the instructions with respect to saving peak lists
#
# 2.2 - Dialog boxes have been updated, and the Evangelist dialog box has been added
#     - Zodiac upgraded to v0.8
#     - Evangelist updated to v1.2
#         - Checkbuttons are now dynamic
#
# 2.1b - Deity is now more user-friendly
#         - Code is more organized and easier to follow
#         - Clicking on any title now brings up a dialog box complete with instructions
```

```
#     - Gremlin updated to v1.5
#         - Added the "Zap All" button
#     - Evangelist updated to v1.1a
#         - Evangelist now gives better feedback
#
# 2.0a - Evangelist 1.0a introduced
#
# 1.5b - Gremlin upgraded to v1.0
#     - Zodiac v0.8b introduced
#
# 1.0b - First release
#     - Gremlin v1.0b introduced
#


#######
# Bug List #
#######
#
#Zodiac:
#     - Can't match to ambiguous assignments
#
```

Bibliography

[1] Bruce A. Johnson and Richard R. Blevins. NMRView: A computer program for the visualization and analysis of NMR data. *J Biomol NMR*, 4:603–614, 1994.

Appendix B

NMR Chemical Shift Data Tables and BMRB Submissions

B.1 hMms2-Ub Data Submission

B.1.1 hMms2 bound to Ub at 30 °C

Main chain amide ^{15}N, $^{1}H_N$ and various carbon chemical shifts

Residue	^{15}N	$^{1}H_N$	$^{13}C_\alpha$	$^{13}C_\beta$	$^{13}C_\gamma$	$^{13}C_\delta$	$^{13}C_\epsilon$
S5			58.549				
M6	127.071	8.078	57.313				
A7			51.850	19.941			
V8			62.366				
S9	119.898	8.575	58.206				
T10	115.731	8.211	61.912	69.784	21.595		
G11	110.944	8.365	45.423				
V12			62.225	32.887	21.049, 20.498		
K13	125.528	8.364	55.997				

V14	124.348	8.364	59.949	33.095	21.344, 20.771		
R16	123.645	8.611					
N17	115.126	8.467	57.031				
F18	118.105	7.534	60.823	38.863			
R19	119.645	8.076	57.689				
L20	119.656	8.656	58.540		28.301	26.422, 23.881	
L21	120.425	8.287	58.231	41.556	26.921	25.442, 23.274	
E22	121.962	7.791	60.061				
E23	120.208	8.498	61.630				
L24	125.055	9.118	58.884	42.829	27.370	24.751, 25.943	
E25	120.514	7.996	59.727				
E26	118.387	8.455	60.104				
G27	106.397	8.294	45.362				
Q28	119.424	7.892	60.154				
K29	117.356	7.917	57.295				
G30	107.560	7.848	46.489				
V31	115.837	7.926	62.619	32.781	21.663, 20.504		
G32	112.200	8.611	45.301				
D33	118.603	8.097	53.827				
G34	108.060	8.410	45.186				
T35	108.410	8.058	64.276	70.186	22.780		
V36	109.892	7.112	59.056	35.731	22.271, 19.018		
S37	114.804	8.591	57.624				
W38	123.407	7.832	57.679				
G39	104.001	8.571	45.419				
L40	121.732	8.176	55.059	42.730	26.685	25.234, 23.094	
E41	123.394	8.470	59.255				
D42	117.568	7.975	52.823				

D43	123.626	8.508	56.115				
E44	117.250	8.362	56.239				
D45	118.420	7.684	53.540				
M46	126.038	8.581	56.593		32.496		17.426
T47	109.500	8.352	62.440	70.209	21.675		
L48	117.407	7.844	56.464	39.949		27.086, 24.692	
T49	113.951	7.976	66.010	69.376	21.282		
R50	119.252	7.212	57.239				
W51	126.529	9.621	56.798				
T52	118.240	9.818	59.368	70.608	20.696		
G53	110.205	8.679	43.886				
M54	120.925	8.992	54.446				18.179
I55	121.361	8.738	60.354	44.729	27.546, 18.072	16.287	
I56	126.976	8.600	59.471	36.950	28.035, 17.617	12.828	
G57	117.452	9.671	44.900				
P59			62.658				
R60	113.053	9.086	57.441				
T61	104.745	7.432	60.185	74.564	22.340		
N62	119.171	8.829	53.844				
Y63	118.057	7.771	56.596				
E64	118.787	7.143	57.920				
N65	117.873	8.669	55.329				
R66	119.887	7.961	56.188				
I67	119.980	8.094	60.801	38.807	27.445, 18.189	13.248	
Y68	127.031	9.270	58.579			134.177	119.617
S69	117.588	9.271	57.887	64.597			
L70	124.795	9.287	55.975	46.427	29.408	25.707, 26.888	
K71	120.696	9.276	55.355				

V72	124.635	8.668	60.608	35.473	21.652, 20.195		
E73	127.126	9.047	54.723				
C74	126.317	9.318	58.268				
G75	110.942	8.056	45.675				
P76			65.027				
K77	114.792	8.702	54.885				
Y78	125.553	7.734	57.678				
P79			63.897				
E80	125.323	8.805	58.485				
A81	121.148	7.195	48.172	20.599			
P83			61.675				
S84	113.113	8.379	57.276				
V85	125.119	8.977	61.382	34.694	22.749, 21.595		
R86	123.916	8.714	54.327				
F87	125.028	9.427	60.163				
V88	122.796	9.263	64.785	32.764	20.919, 22.214		
T89	115.912	7.556	63.455	70.840	23.219		
K90	122.552	8.143	58.830				
I91	122.377	8.161	60.381	41.721	30.598, 14.156	14.226	
N92	124.580	8.595	50.880				
M93	128.147	8.893	56.479				18.736
N94	126.046	8.470	56.470				
G95	110.477	8.642	45.083				
I96	120.187	7.656	58.985	36.799	30.711, 18.817	13.311	
N97	127.803	8.642	55.155				
N98	125.445	8.986	55.487				
S99	113.773	8.748	59.894				
S100	113.987	7.986	57.328				

G101	112.259	7.736	46.195				
M102	119.248	7.730	56.706				16.643
V103	125.941	8.411	62.587	32.225	22.718, 22.506		
D104	128.602	8.945	53.665				
A105	130.996	8.642	54.940	19.332			
R106	109.908	7.797	58.046				
S107	112.419	7.772	59.661				
I108	122.036	7.307	55.357	37.402	26.560, 17.740	9.842	
P109			67.426				
V110	110.680	7.665	64.478	31.392	21.092 ($^{13}C_{\gamma 1}$)		
L111	114.009	7.210	56.154	41.758	27.296	25.269, 22.891	
A112	124.661	8.637	54.954	19.088			
K113	118.359	8.248	53.651				
W114	122.300	7.057	59.616				
Q115	123.808	5.175	52.394				
N116	116.986	8.470	54.090				
S117	108.927	6.579	57.506				
Y118	123.055	7.227	53.792				
S119	107.720	6.406	56.396				
I120	123.965	9.665	67.075	37.946	28.823, 16.649	11.919	
K121	117.849	7.743	59.828				
V122	117.629	6.854	65.776	32.657	20.445, 23.166		
V123	119.486	7.683	67.029	31.393	21.251, 24.334		
L124	116.966	8.067	58.269	40.660	26.583	27.750, 22.500	
Q125	117.021	8.650	59.308				
E126	121.203	8.375	58.743				
L127	120.619	8.223	58.564	42.159		26.746, 23.513	
R128	118.018	7.902	59.329				

R129	119.095	8.132	59.686				
L130	121.338	8.266	57.702	41.407	27.451	26.442, 22.876	
M131	122.926	7.745	59.602				18.153
M132	109.361	7.131	55.504				
S133	115.429	7.765	58.634				
K134	124.646	9.015	60.099				
E135	116.646	9.122	58.863				
N136	115.781	7.535	54.249				
M137	115.241	8.159	60.302				
K138	117.564	8.414	54.182				
L139	124.020	7.680	53.713				
P140			62.640				
Q141	122.063	9.043	52.495				
P143			63.136				
E144	122.699	8.546	57.817				
G145	111.930	8.870	45.368				
Q146	119.205	7.483	56.330				
T147	112.954	8.472	59.767	72.253	21.756		
Y148	118.355	8.214	60.283				
N149	119.250	8.663	53.500				
N150	124.498	8.037	54.967				

Main chain amide ^{15}N, ^{1}H$_{N}$ and various hydrogen chemical shifts

Residue	^{15}N	$^{1}H_N$	$^{1}H_\alpha$	$^{1}H_\beta$	$^{1}H_\gamma$	$^{1}H_\delta$	$^{1}H_\epsilon$
S5			4.530	3.882			
M6	127.071	8.078					
A7				1.502			
S9	119.898	8.575	4.559	3.962			

T10	115.731	8.211	4.355	4.280	0.203		
G11	110.944	8.365	3.982				
V12			4.090	2.019	0.902, 0.898		
K13	125.528	8.364	4.353	1.704	1.317, 1.408	1.599	2.924
V14	124.348	8.364	4.408	2.051	1.020, 0.967		
R16	123.645	8.611					
N17	115.126	8.467	4.359	2.829			
F18	118.105	7.534	4.365	3.196, 3.308			
R19	119.645	8.076	4.432				
L20	119.656	8.656				1.186, 0.883	
L21	120.425	8.287	4.361	1.599, 1.998		0.910, 0.965	
E22	121.962	7.791	4.282	2.287	2.159, 2.468		
E23	120.208	8.498	4.399				
L24	125.055	9.118				0.966, 0.953	
E25	120.514	7.996	4.130		2.328, 2.471		
E26	118.387	8.455					
G27	106.397	8.294					
Q28	119.424	7.892					
K29	117.356	7.917					3.025
G30	107.560	7.848					
V31	115.837	7.926	4.226	2.093	1.074, 0.951		
G32	112.200	8.611	3.934				
D33	118.603	8.097					
G34	108.060	8.410					
T35	108.410	8.058	3.893	4.142	1.155		
V36	109.892	7.112	5.340	2.267	0.916, 0.999		
S37	114.804	8.591					
W38	123.407	7.832	5.838				10.100

G39	104.001	8.571					
L40	121.732	8.176	3.614	1.106, 1.117	0.896	0.462, -0.105	
E41	123.394	8.470					
D42	117.568	7.975					
D43	123.626	8.508	4.313	2.599			
E44	117.250	8.362	4.254	1.904	2.151, 2.290		
D45	118.420	7.684	4.659				
M46	126.038	8.581	4.381	2.131	2.571		2.086
T47	109.500	8.352	4.518	4.436	1.295		
L48	117.407	7.844	3.663			0.980, 0.912	
T49	113.951	7.976	4.479	3.962	1.149		
R50	119.252	7.212				3.208	
W51	126.529	9.621	5.040				9.608
T52	118.240	9.818	5.304	4.112	1.166		
G53	110.205	8.679	5.554				
M54	120.925	8.992	5.804	2.180	2.230		1.886
I55	121.361	8.738	4.754	1.558	0.821 ($^1H_{\gamma 2}$)	0.800	
I56	126.976	8.600	4.732	1.893	1.458, 1.300, 0.937 ($^1H_{\gamma 2}$)	0.721	
G57	117.452	9.671					
R60	113.053	9.086	3.912			3.271	
T61	104.745	7.432	4.917	1.355			
N62	119.171	8.829					
Y63	118.057	7.771					
E64	118.787	7.143	3.584		2.357, 2.139		
N65	117.873	8.669	4.200	2.537, 2.827			
R66	119.887	7.961	4.386				
I67	119.980	8.094		1.625	0.923, 0.753	0.703	
Y68	127.031	9.270	4.609			7.101	6.796

S69	117.588	9.271	5.367	3.828, 3.989			
L70	124.795	9.287	5.197			0.403, -0.306	
K71	120.696	9.276	5.088		1.415		
V72	124.635	8.668	4.834	1.835	0.669, 0.659		
E73	127.126	9.047	5.446	2.126, 1.942			
C74	126.317	9.318	4.054				
G75	110.942	8.056	4.364				
K77	114.792	8.702	4.554		1.373		
Y78	125.553	7.734					
E80	125.323	8.805	4.276		2.271, 2.388		
A81	121.148	7.195	4.544	1.136			
S84	113.113	8.379	4.650	3.833			
V85	125.119	8.977	4.820	1.698	0.654, 0.728		
R86	123.916	8.714	5.095				
F87	125.028	9.427	4.493				
V88	122.796	9.263	4.267	1.979	1.129, 0.994		
T89	115.912	7.556	4.261	4.278	1.537		
K90	122.552	8.143			1.286		
I91	122.377	8.161			0.031 ($^1H_{\gamma 2}$)	-0.281	
N92	124.580	8.595					
M93	128.147	8.893	4.040				1.845
N94	126.046	8.470	4.390	2.623, 3.043			
G95	110.477	8.642	3.714				
I96	120.187	7.656	4.530		0.614 ($^1H_{\gamma 2}$)	0.641	
N97	127.803	8.642					
N98	125.445	8.986		3.007			
S99	113.773	8.748		3.994			
S100	113.987	7.986					

G101	112.259	7.736	4.185				
M102	119.248	7.730	4.325		2.543		2.071
V103	125.941	8.411	4.310		0.711, 0.983		
D104	128.602	8.945	4.570				
A105	130.996	8.642	3.918	1.419			
R106	109.908	7.797	3.977			3.229	
S107	112.419	7.772	4.427	3.927			
I108	122.036	7.307	4.748	2.155	0.870 ($^1H_{\gamma 2}$)	0.651	
V110	110.680	7.665	4.031	1.968	0.746 ($^1H_{\gamma 1}$)		
L111	114.009	7.210	4.808			0.878, 0.939	
A112	124.661	8.637	4.010	1.477			
K113	118.359	8.248	4.647		1.365		2.973
W114	122.300	7.057					10.036
Q115	123.808	5.175	4.239				
N116	116.986	8.470					
S117	108.927	6.579	4.200				
Y118	123.055	7.227	4.443				
S119	107.720	6.406	5.129	3.729			
I120	123.965	9.665			0.239 ($^1H_{\gamma 2}$)	-0.764	
K121	117.849	7.743					
V122	117.629	6.854	3.553	1.854	0.450, 0.909		
V123	119.486	7.683	3.372	2.261	0.781, 1.167		
L124	116.966	8.067	3.855			1.001, 0.587	
Q125	117.021	8.650	3.806				
E126	121.203	8.375	4.299				
L127	120.619	8.223	3.991			0.641, 0.819	
R128	118.018	7.902	3.822				
R129	119.095	8.132					

L130	121.338	8.266	4.107			1.010, 0.933	
M131	122.926	7.745	3.738				1.240
M132	109.361	7.131	4.408		2.572, 2.695		
S133	115.429	7.765	4.451	4.180			
K134	124.646	9.015					3.032
E135	116.646	9.122	4.139	1.990	2.271		
N136	115.781	7.535	5.310				
M137	115.241	8.159					
K138	117.564	8.414	4.589	1.644, 2.057	1.385		
L139	124.020	7.680					
Q141	122.063	9.043	4.593				
E144	122.699	8.546	4.064		2.217, 2.278		
G145	111.930	8.870	3.724, 4.208				
Q146	119.205	7.483	4.449	1.890	2.289, 2.451		
T147	112.954	8.472	5.132	4.411	1.167		
Y148	118.355	8.214					
N149	119.250	8.663	4.798	2.790, 2.904			
N150	124.498	8.037	4.504				

B.1.2 hMms2 bound to Ub at 40 °C

Main chain amide ^{15}N, $^{1}H_N$ and various carbon chemical shifts

Residue	^{15}N	$^{1}H_N$	$^{13}C_\alpha$	$^{13}C_\beta$	$^{13}C_\gamma$	$^{13}C_\delta$	$^{13}C_\epsilon$
A7				20.116			
T10					21.627		
V12			62.357	32.902	21.095, 20.433		
K13	125.522	8.32					
N17			56.936	37.108			

F18	117.943	7.472	60.791	38.836			
R19	119.804	8.049					
L20	119.487	8.628			28.458	26.42, 23.910	
L21			58.423	41.647	26.942	25.382 ($^{13}C_{\delta 1}$)	
E22	121.873	7.7904	60.120	29.540	36.875		
E23	120.146	8.467			37.859		
L24	124.927	9.072		42.816		24.744, 26.060	
E25	120.601		59.869	29.561	36.347		
E26	118.383	8.445	60.256	30.109	37.147		
G27	106.265	8.255	45.328				
Q28	119.310	7.868	58.113	28.925	34.438		
K29	117.223	7.910	57.336	33.264	25.485	29.330	42.470
G30	107.548	7.838	46.435				
V31	115.773	7.871			21.707 ($^{13}C_{\gamma 1}$)		
D33			53.950	41.197			
G34	107.936	8.371	45.190				
T35	108.172	8.008	64.177	70.251	22.736		
V36	109.975	7.114	59.256		22.265, 19.093		
S37	114.747	8.561		65.322			
W38	123.567	7.771	57.845	32.450			
G39	103.891	8.568	45.372				
L40	121.698	8.099				25.180, 23.120	
E41			59.284	30.500	36.959		
D42	117.550	7.942	53.072	42.877			
D43	123.422	8.450	56.099	40.821			
E44	117.332	8.339	56.400		36.804		
D45	118.523	7.677					
M46			56.558	32.037	32.474		17.398

T47	109.427	8.348			21.695		
L48			56.572	40.017		27.108, 24.759	
T49	113.858	7.984					
W51	126.445	9.583		30.535			
T52	118.127	9.773	59.386	70.753	20.585		
G53	110.339	8.684	43.918				
M54	120.766	8.993	54.455	38.099	32.041		18.213
I55	121.141	8.715			17.929 ($^{13}C_{\gamma 2}$)	16.189	
I56	126.956	8.564		36.828	28.071, 17.658	12.868	
G57	117.449	9.661					
P59			62.737	32.801	27.438		
R60	113.080	9.093	57.653	28.080	27.127	43.499	
T61	104.625	7.427	60.294	74.609	22.321		
N62	119.152	8.803	53.967	36.358			
Y63	117.948	7.758		38.758			
E64	118.846	7.133	57.906	30.812	35.520		
N65	117.986	8.637	55.317	38.157			
R66	119.718	7.954		31.559	28.546		
I67	119.959	8.056	60.888	38.837	27.496, 18.189	13.313	
Y68	126.826	9.230		40.980			
S69	117.525	9.214	57.999	64.667			
L70	124.740	9.266	55.887	46.461	29.167	25.727, 26.872	
K71	120.646	9.248	55.308	35.044	25.577	28.881	
V72	124.532	8.663	60.887		21.675, 20.092		
E73	127.159	9.035	54.410	32.066	36.907		
C74	126.309	9.300	58.433	27.894			
G75	110.955	8.036					
K77			54.805	32.580	25.513	28.910	

Y78	125.495	7.727					
P79			64.043	32.132			
E80	125.374	8.803	58.468	28.821	36.36		
A81	121.108	7.189					
P83			61.766				
S84	113.052	8.361	57.321	64.487			
V85	125.160	8.922	61.067	34.473	22.658, 21.542		
R86	123.974	8.702	54.335	34.239	26.648	44.106	
F87	124.994	9.398		39.612			
V88	122.589	9.225	64.778	32.868	20.904, 22.177		
T89	115.903	7.557		70.978	23.158		
K90	122.654	8.143		32.932	25.377	29.763	
I91	122.215	8.097		41.931	30.542, 14.098	14.218	
N92	124.517	8.579	51.008	38.809			
M93	127.941	8.836					18.629
N94			56.497	38.536			
G95	110.515	8.602	45.085				
I96	119.971	7.627	58.947		30.509, 18.669	13.389	
N97	127.653	8.638					
N98			55.512	39.027			
S99	113.728	8.727	59.830	64.339			
S100	113.820	7.937		67.140			
G101	112.139	7.755	46.132				
M102	119.189	7.696	56.831				16.680
V103	125.783	8.364	62.793		22.566 ($^{13}C_{\gamma 1}$)		
D104	128.580	8.895	53.969	40.973			
A105	130.767	8.565	55.007	19.335			
R106	110.091	7.795	58.076	30.062	27.206	43.261	

S107	112.367	7.757	59.720	64.961			
I108	121.933	7.288			17.771 ($^{13}C_{\gamma 2}$)	9.947	
P109			67.452	32.176	27.465		
V110	110.658	7.607	64.519	31.388	21.037 ($^{13}C_{\gamma 1}$)		
L111	114.099	7.180				25.319 ($^{13}C_{\gamma 1}$)	
A112			55.167	19.020			
K113	118.402	8.217	53.699	30.944	24.718	29.282	42.169
W114	122.282	7.039					
Q115			52.567	31.684	32.715		
N116	116.930	8.414	54.162	37.438			
S117	108.967	6.585	57.628	63.144			
Y118	122.907	7.213	53.810	35.286			
S119	107.797	6.411					
I120	123.966	9.661		13.988	28.825, 16.627	11.914	
K121			59.867				41.073
V122	117.665	6.820	65.845		20.411, 23.165		
V123	119.401	7.657	66.935	31.422	21.155, 24.291		
L124	116.942	8.028	58.476	40.857	26.593	27.637, 22.531	
Q125	117.062	8.623	59.287				
E126	121.096	8.370	58.790				
L127	120.446	8.194	58.568	42.145		26.704, 23.474	
R128	117.969	7.873	59.312			43.307	
R129	119.082	8.113	59.881	30.002	27.925		
L130	121.325	8.231	57.784	41.461	27.414	26.393, 22.965	
M131	122.715	7.727	59.442				18.199
M132	109.438	7.131	55.564	33.916	32.862		
S133	115.361	7.736					
K134			60.192	32.396	24.806	29.329	42.228

E135	116.637	9.114	59.006	28.944	36.418		
N136	115.534	7.522	54.290	41.129			
M137	115.427	8.133	60.407		30.961		
K138	117.427	8.343	54.397	31.962	25.233	29.043	42.297
L139	123.825	7.647					
P140				31.527	27.652		
Q141	121.723	8.930					
P143			63.098	32.046	27.949	49.953	
E144	122.632	8.499					
G145			45.358				
Q146	119.128	7.452	56.402	29.900	34.418		
T147	113.005	8.413	59.758	72.280	21.747		
Y148	118.411	8.209					
N149			53.480	39.171			
N150	124.488	7.991					

Main chain amide ^{15}N, ^{1}H$_{N}$ and various hydrogen chemical shifts

Residue	^{15}N	$^{1}H_N$	$^{1}H_\alpha$	$^{1}H_\beta$	$^{1}H_\gamma$	$^{1}H_\delta$	$^{1}H_\epsilon$
A7				1.496			
T10					1.220		
V12			4.118	2.050	0.915, 0.912		
K13	125.522	8.320					
N17			4.357	2.833			
F18	117.943	7.472	4.388	3.182, 3.307			
R19	119.804	8.049	4.439				
L20	119.487	8.628			1.918	1.193, 0.893	
L21			4.353	1.600, 2.016	1.965	0.920, 0.974	
E22	121.873	7.790	4.287	2.309, 2.487	2.189, 2.496		

E23	120.146	8.467	4.456				
L24	124.927	9.072				0.980, 0.967	
E25	120.601		4.183	2.371	2.358, 2.493		
E26	118.383	8.445	4.129	2.505	2.491, 2.758		
G27	106.265	8.255	3.993				
Q28	119.310	7.868	4.050	2.312	2.321, 2.694		
K29	117.223	7.910	4.515	2.002, 2.094	1.647, 1.765	1.775	3.067
G30	107.548	7.838	3.918, 3.978				
V31	115.773	7.871			1.082 ($^1H_{\gamma 1}$)		
D33			4.583	2.712, 3.117			
G34	107.936	8.371	2.967, 3.686				
T35	108.172	8.008	3.932	4.182	1.163		
V36	109.975	7.114	5.331	2.277	0.940, 1.010		
S37	114.747	8.561					
W38	123.567	7.771	5.857	3.107			10.074
G39	103.891	8.568	3.978, 4.274				
L40	121.698	8.099				0.465, -0.083	
E41			3.978	1.676, 1.823	2.101, 2.101		
D42	117.550	7.942	4.703	2.522, 2.774			
D43	123.422	8.450	4.339	2.633, 2.633			
E44	117.332	8.339	4.272	1.937, 2.231	2.187, 2.335		
D45	118.523	7.677					
M46			4.397	2.142, 2.217	2.582, 2.772		2.105
T47	109.427	8.348			1.300		
L48			3.688	2.302, 2.284	1.547	0.979, 0.926	
T49	113.858	7.984					
W51	126.445	9.583		3.103, 3.306			9.588
T52	118.127	9.773		4.138	1.184		

G53	110.339	8.684	3.356, 5.562				
M54	120.766	8.993	5.815	1.729, 1.812	2.241		1.890
I55	121.141	8.715			0.837 ($^1H_{\gamma 2}$)	0.804	
I56	126.956	8.564	4.782	1.886	1.298, 1.445, 0.948 ($^1H_{\gamma 2}$)	0.733	
G57	117.449	9.661					
P59			4.498	1.959, 2.427	2.095, 2.135	3.680, 3.724	
R60	113.080	9.093	3.939	1.649	2.051, 2.216	3.251, 3.311	
T61	104.625	7.427	4.921	4.558	1.361		
N62	119.152	8.803	4.753	2.632, 2.833			
Y63	117.948	7.758		2.650, 3.670			
E64	118.846	7.133	3.586	2.179, 2.372	2.386, 2.144		
N65	117.986	8.637	4.212	3.079			
R66	119.718	7.954					
I67	119.959	8.056	4.451	1.624	0.927, 1.539, 0.763 ($^1H_{\gamma 2}$)	0.711	
Y68	126.826	9.230		2.964, 3.066			
S69	117.525	9.214	5.366	3.834, 3.971			
L70	124.740	9.266	5.210	0.838, 1.363	0.916	0.409, -0.265	
K71	120.646	9.248	5.111	1.610, 1.979	1.436	1.781	2.931, 3.002
V72	124.532	8.663	4.867		0.667 ($^1H_{\gamma 2}$)		
E73	127.159	9.035	5.458		1.971, 2.163		
C74	126.309	9.300	4.079	1.931, 2.891			
G75	110.955	8.036					
K77			4.580	2.043	1.453	1.700	2.967
Y78	125.495	7.727					
P79			4.299			3.739	
E80	125.374	8.803	4.299		2.302, 2.417		
A81	121.108	7.189					
P83			4.848				

S84	113.052	8.361	4.659	3.850, 3.856			
V85	125.160	8.922	4.822	1.728	0.678, 0.742		
R86	123.974	8.702	5.108	1.720, 1.847	1.309, 1.688	3.095, 3.191	
F87	124.994	9.398					
V88	122.589	9.225	4.293	2.004	1.139, 1.002		
T89	115.903	7.557	4.296	1.554			
K90	122.654	8.143					
I91	122.215	8.097		1.543	1.531, 0.055	-0.259	
N92	124.517	8.579	5.258	2.693, 2.978			
M93	127.941	8.836					1.840
N94			4.450	2.656, 3.053			
G95	110.515	8.602	3.716, 4.285				
I96	119.971	7.627			0.623 ($^1H_{\gamma 2}$)	0.643	
N97	127.653	8.638					
N98			4.835	3.018, 3.082			
S99	113.728	8.727	4.824	4.029			
S100	113.820	7.937					
G101	112.139	7.755	3.226, 4.189				
M102	119.189	7.696	4.325		2.568		2.094
V103	125.783	8.364	4.204		0.734 ($^1H_{\gamma 1}$)		
D104	128.580	8.895	4.603	2.743, 3.010			
A105	130.767	8.565	3.934	1.434			
R106	110.091	7.795	4.008	1.931	1.754	3.236, 3.267	
S107	112.367	7.757	4.443	3.949			
I108	121.933	7.288			0.887 ($^1H_{\gamma 2}$)	0.659	
P109			4.252				
V110	110.658	7.607	4.038	1.969	0.750 ($^1H_{\gamma 1}$)		
L111	114.099	7.180				0.884 ($^1H_{\delta 1}$)	

A112			4.024	1.492			
K113	118.402	8.217	4.701		1.412		2.988
W114	122.282	7.039					10.021
Q115			4.259	0.386, 1.639	1.708		
N116	116.930	8.414	4.295	2.635, 2.760			
S117	108.967	6.585	4.201	3.638, 3.900			
Y118	122.907	7.213					
S119	107.797	6.411					
I120	123.966	9.661		0.750	-0.152, 1.451, 0.241 ($^1H_{\gamma 2}$)	-0.741	
K121							2.855
V122	117.665	6.820	3.553	1.882	0.464, 0.926		
V123	119.401	7.657	3.398	2.289	0.795, 1.176		
L124	116.942	8.028	3.858	1.322, 1.799	1.843	0.997, 0.601	
Q125	117.062	8.623					
E126	121.096	8.370	4.311				
L127	120.446	8.194	3.987	1.051, 2.089	1.845	0.653, 0.828	
R128	117.969	7.873					
R129	119.082	8.113	4.013	1.951, 2.027	1.568, 1.770	3.171, 3.289	
L130	121.325	8.231	4.137	1.476, 1.942	1.855	1.027, 0.947	
M131	122.715	7.727	3.783				1.245
M132	109.438	7.131	4.412	2.277	2.575, 2.714		
S133	115.361	7.736					
K134			4.076	1.900, 1.988	1.566	1.773	3.069
E135	116.637	9.114	4.164	1.997	2.277, 2.353		
N136	115.534	7.522	5.326	2.900, 3.699			
M137	115.427	8.133	4.462	2.187	2.473, 2.866		
K138	117.427	8.343	4.582	2.076	1.373, 1.466	1.700	2.995
L139	123.825	7.647					

P140			4.454				
Q141	121.723	8.930					
P143			4.351				
E144	122.632	8.499					
G145			3.756, 4.245				
Q146	119.128	7.452	4.470	1.867, 1.940	2.324, 2.471		
T147	113.005	8.413	5.139	4.418	1.178		
Y148	118.411	8.209					
N149			4.824	2.815, 2.946			
N150	124.488	7.991					

B.1.3 Ub at 30 °C

Main chain amide ^{15}N, ^{1}H$_{N}$ and various carbon chemical shifts

Residue	^{15}N	$^{1}H_N$	$^{13}C_\alpha$	$^{13}C_\beta$	$^{13}C_\gamma$	$^{13}C_\delta$	$^{13}C_\epsilon$
M1			54.573	33.307	30.699		17.674
Q2	122.968	8.899	55.093	30.664	34.615		
I3	115.420	8.320	59.532	42.125	25.138, 17.824	14.164	
F4	118.712	8.589	55.156	41.286		132.203, 132.203	131.134, 131.134
V5	121.468	9.289	60.421	34.252	22.279, 20.833		
K6	128.185	9.007	54.644	34.599	24.968	29.413	41.994
T7	115.391	8.745	60.459	70.508	21.536		
L8	121.347	9.083	57.474	41.803	27.372	25.442, 23.765	
T9	106.100	7.658	61.381	68.982	21.941		
G10	109.308	7.834	45.463				
K11	121.994	7.297	56.304	33.522	25.154	29.501	41.962
T12	120.583	8.610	62.292	69.808	21.973		
I13	127.962	9.589	60.063	40.910	27.063, 17.824	14.482	

T14	121.918	8.717	62.089	69.529	21.806		
L15	125.325	8.740	52.906	46.844	27.097	24.208, 24.193	
E16	122.646	8.120	54.921	29.990	35.679		
V17	117.707	8.921	58.531	36.402	22.224, 19.453		
E18	118.889	8.626	53.844	32.371	35.706		
S19	117.873	9.249	62.106	63.547			
S20	108.782	7.302	57.292	63.544			
D21	123.504	7.852	55.639	40.882			
T22	108.465	7.966	59.701	71.535	22.290		
I23	121.462	8.719	62.196	35.063	28.182, 18.196	9.613	
D24	118.207	9.486	56.979	39.855			
N25	119.633	8.014	55.959	38.785			
V26	122.133	8.108	67.737	30.907	23.622, 21.439		
K27	118.823	8.564	59.377	33.589	26.143	30.405	42.494
S28	117.384	8.134	62.493	62.493			
K29	123.264	7.977	59.847	33.316	26.488	30.175	42.470
I30	121.257	8.315	66.057	36.843	31.0190, 17.075	15.165	
Q31	123.658	8.513	60.077	27.781	33.894		
D32	119.997	8.070	57.460	40.969			
K33	115.850	7.465	58.265	34.166	25.309	28.934	42.248
E34	114.383	8.725	55.431	33.404	36.458		
G35	108.935	8.511	46.100				
I36	120.409	6.167	57.811	40.562	17.827, 27.145	13.593	
P37			61.659	31.809	28.264		
P38			66.124	32.887	27.781	51.103	
D39	113.500	8.503	55.753	39.868			
Q40	117.065	7.825	55.643	30.114	34.459		
Q41	118.054	7.478	56.619	31.580	33.525		

R42	123.015	8.471	55.113	31.732	27.049	43.632	
L43	124.361	8.783	53.065	45.774	26.590	26.590, 24.238	
I44	122.591	9.147	58.982	41.337	27.923, 17.564	12.973	
F45	124.882	8.831	56.456	43.651		132.194, 132.194	132.226, 132.226
A46	133.426	9.054	52.476	16.725			
G47	102.308	8.102	45.570				
K48	120.973	7.957	54.483	32.626			44.007
Q49	123.040	8.673	55.811	29.261	34.661		
L50	125.642	8.553	54.163	41.441	25.992	25.991, 19.781	
E51	123.241	8.343	56.124	32.019	36.621		
D52	120.174	8.089	56.574	40.839			
G53	107.667	9.555	45.360				
R54	119.204	7.405	54.465	32.521	27.508	42.890	
T55	109.149	8.854	59.923	72.353	22.326		
L56	118.361	8.185	58.812	40.225	26.632	23.294	
S57	113.170	8.274	60.990	62.568			
D58	124.276	7.901	57.431	40.366			
Y59	115.685	7.234	58.157	40.154		133.581, 133.581	118.626, 118.626
N60	116.123	8.129	54.146	37.389			
I61	118.725	7.220	62.426	36.860	28.290, 17.222	14.130	
Q62	125.229	7.652	53.633	31.710	33.489		
K63	120.586	8.447	57.857	32.735	23.937	30.034	42.133
E64	114.657	9.281	58.446	26.104	37.449		
S65	114.948	7.640	60.848	64.862			
T66	117.610	8.654	62.398	70.201	21.429		
L67	127.761	9.375	53.747	44.392	29.391	25.064, 24.851	
H68	119.829	9.213	56.320	32.659		119.916	137.738
L69	123.979	8.315	53.736	44.336	27.540	26.245	

V70	127.038	9.168	60.712	34.750	20.812, 21.447		
L71	123.704	8.129	53.991	42.893	27.518	25.100, 23.973	
R72	123.730	8.609	55.658	31.351	27.334	43.457	
L73	124.472	8.332	54.892	42.540	27.170	25.038, 23.438	
R74	121.916	8.394	56.357	30.871	26.945	43.341	
G75	111.059	8.445	45.337				
G76	115.189	7.932	46.057				

Main chain amide ^{15}N, ^{1}H$_{N}$ and various hydrogen chemical shifts

Residue	^{15}N	$^{1}H_N$	$^{1}H_\alpha$	$^{1}H_\beta$	$^{1}H_\gamma$	$^{1}H_\delta$	$^{1}H_\epsilon$
M1			4.234	2.193, 2.052	2.516, 2.049		1.666
Q2	122.968	8.899	5.284	1.867, 1.639	2.258, 1.923		
I3	115.420	8.320	4.160	1.770	1.077, 0.847, 0.604	0.569	
F4	118.712	8.589	5.624	3.072, 2.881		7.069, 7.069	7.235, 7.235
V5	121.468	9.289	4.831	1.926	0.689, 0.715		
K6	128.185	9.007	5.330	1.724, 1.415	1.505, 1.305	1.611, 1.611	2.924, 2.924
T7	115.391	8.745	4.984	4.831	1.179		
L8	121.347	9.083	4.337	1.948, 1.792	1.915	1.030, 0.952	
T9	106.100	7.658	4.445	4.615	1.257		
G10	109.308	7.834	4.363, 3.630				
K11	121.994	7.297	4.381	1.822, 1.728	1.422, 1.259	1.646, 1.646	2.933, 2.934
T12	120.583	8.610	5.075	3.967	1.069		
I13	127.962	9.589	4.511	1.886	1.461, 1.115, 0.865	0.712	
T14	121.918	8.7171	4.961	4.057	1.117		
L15	125.325	8.740	4.771	1.385, 1.228	0.726	0.778, 0.752	
E16	122.646	8.120	4.953	1.931, 1.848	2.244, 2.091		
V17	117.707	8.921	4.712	2.355	0.723, 0.421		
E18	118.889	8.626	4.856	2.204, 1.705	2.367, 2.251		

S19	117.873	9.249	3.975				
S20	108.782	7.302	4.426	4.180, 3.800			
D21	123.504	7.852	4.713	2.983, 2.567			
T22	108.465	7.966	4.973	4.763	1.251		
I23	121.462	8.719	3.611	2.432	1.854, 1.316, 0.785	0.564	
D24	118.207	9.486	4.198	2.635			
N25	119.633	8.014	4.513	3.205, 2.912			
V26	122.133	8.108	3.373	2.365	0.992, 0.678		
K27	118.823	8.564	4.638	2.107, 1.462		1.726, 1.726	2.650, 2.650
S28	117.384	8.134	4.238	4.137, 4.137			
K29	123.264	7.977	4.220	2.130, 1.945	1.859, 1.604	1.784, 1.460	3.178, 3.012
I30	121.257	8.315	3.516	2.373	2.020, 0.709, 0.686	0.875	
Q31	123.658	8.513	3.839	2.527, 2.007	2.305, 1.949		
D32	119.997	8.070	4.346	2.878, 2.769			
K33	115.850	7.465	4.325	2.046, 1.857	1.621, 1.621	1.728, 1.728	3.192, 3.137
E34	114.383	8.725	4.583	2.294, 1.692	2.177, 2.091		
G35	108.935	8.511	4.160, 3.936				
I36	120.409	6.167	4.442	1.446	0.927, 0.956, 1.110	0.781	
P37			4.658	2.438, 1.996	2.119, 2.068		
P38			4.120	2.280, 2.050	2.178, 1.641	3.767, 3.767	
D39	113.500	8.503	4.430	2.786, 2.670			
Q40	117.065	7.825	4.470	2.470, 1.849	2.428, 2.428		
Q41	118.054	7.478	4.226	1.917, 1.917	2.541, 1.672		
R42	123.015	8.471	4.521	1.748, 1.629	1.519, 1.449	3.131, 3.064	
L43	124.361	8.783	5.398	1.580, 1.169	0.778	0.778, 0.785	
I44	122.591	9.147	4.917	1.757	1.375, 1.081, 0.696	0.668	
F45	124.882	8.831	5.160	3.060, 2.795		7.350, 7.350	7.545, 7.545
A46	133.426	9.054	3.663	0.763			

G47	102.308	8.102	4.100, 3.408				
K48	120.973	7.957	4.651	1.938, 1.938			3.378, 3.378
Q49	123.040	8.673	4.570	1.998, 1.998	2.257, 2.257		
L50	125.642	8.553	4.074	1.505	1.453	0.502, -0.173	
E51	123.241	8.343	4.477	2.241, 1.981	2.435, 2.352		
D52	120.174	8.089	4.330	2.837, 2.489			
G53	107.667	9.555	4.129, 3.992				
R54	119.204	7.405	4.730		1.865, 1.626	3.170, 3.118	
T55	109.149	8.854	5.219	4.514	1.135		
L56	118.361	8.185	4.062	2.088, 1.277	0.767	0.755, 0.599	
S57	113.170	8.274	4.275	3.894, 3.798			
D58	124.276	7.901	4.300	2.991, 2.274			
Y59	115.685	7.234	4.657	3.465, 2.527		7.216, 7.216	6.868, 6.868
N60	116.123	8.129	4.349	3.308, 2.804			
I61	118.725	7.220	3.410	1.402	1.145, 0.459	0.381	
Q62	125.229	7.652	4.490	2.267, 1.913	2.390, 2.322		
K63	120.586	8.447	3.990	2.061, 1.912	1.505, 1.505	1.758, 1.758	3.059, 3.059
E64	114.657	9.281	3.353	2.523, 2.397	2.257, 2.257		
S65	114.948	7.640	4.652	3.909, 3.632			
T66	117.610	8.654	5.285	4.058	0.925		
L67	127.761	9.375	5.069	1.632, 1.632	1.770	0.664, 0.658	
H68	119.829	9.213	5.160	3.069, 2.914		6.982	7.916
L69	123.979	8.315	5.179	1.625, 1.108	1.343	0.759, 0.851	
V70	127.038	9.168	4.355	2.031	0.838, 0.927		
L71	123.704	8.129	5.046	1.712, 1.544	1.690	0.960, 0.887	
R72	123.730	8.609	4.311	1.805, 1.552	1.567, 1.516	3.174, 3.174	
L73	124.472	8.332	4.404	1.666, 1.589	1.671	0.918, 0.866	
R74	121.916	8.394	4.338	1.897, 1.813	1.671, 1.671	3.232, 3.232	

G75	111.059	8.445					
G76	115.189	7.932					

B.1.4 Intermolecular NOE restraints for the hMms2-Ub complex

For the following intermolecular restraints, segid 'A' corresponds to hMms2, and segid B corresponds to Ub.

assign (resid 28 and name HA and segid A) (resid 46 and name HB1 and segid B) 3.400 1.600 1.600 !

assign (resid 35 and name HA and segid A) (resid 8 and name HD21 and segid B) 3.400 1.600 1.600 !
assign (resid 35 and name HA and segid A) (resid 70 and name HG21 and segid B) 3.400 1.600 1.600 !
assign (resid 35 and name HB and segid A) (resid 8 and name HD11 and segid B) 3.400 1.600 1.600 !
assign (resid 35 and name HB and segid A) (resid 8 and name HD21 and segid B) 3.400 1.600 1.600 !
assign (resid 35 and name HG21 and segid A) (resid 8 and name HD11 and segid B) 3.400 1.600 1.600 !
assign (resid 35 and name HG21 and segid A) (resid 8 and name HD21 and segid B) 3.400 1.600 1.600 !

assign (resid 39 and name HA1 and segid A) (resid 46 and name HB# and segid B) 3.400 1.600 1.600 !
assign (resid 39 and name HA2 and segid A) (resid 46 and name HB# and segid B) 3.400 1.600 1.600 !

assign (resid 52 and name HG21 and segid A) (resid 48 and name HB# and segid B) 3.400 1.600 1.600 !
assign (resid 52 and name HG21 and segid A) (resid 48 and name HG# and segid B) 3.400 1.600 1.600 !
assign (resid 52 and name HG21 and segid A) (resid 48 and name HD# and segid B) 3.400 1.600 1.600 !
assign (resid 52 and name HG21 and segid A) (resid 47 and name HA# and segid B) 3.400 1.600 1.600 !

assign (resid 54 and name HB# and segid A) (resid 44 and name HG21 and segid B) 3.400 1.600 1.600 !
assign (resid 54 and name HB# and segid A) (resid 44 and name HD11 and segid B) 3.400 1.600 1.600 !
assign (resid 54 and name HG# and segid A) (resid 44 and name HD11 and segid B) 3.400 1.600 1.600 !
assign (resid 54 and name HG# and segid A) (resid 44 and name HG21 and segid B) 3.400 1.600 1.600 !
assign (resid 54 and name HE# and segid A) (resid 44 and name HB# and segid B) 3.400 1.600 1.600 !
assign (resid 54 and name HE# and segid A) (resid 44 and name HG11 and segid B) 3.400 1.600 1.600 !
assign (resid 54 and name HE# and segid A) (resid 44 and name HG12 and segid B) 3.400 1.600 1.600 !

assign (resid 54 and name HE# and segid A) (resid 44 and name HG21 and segid B) 3.400 1.600 1.600 !
assign (resid 54 and name HE# and segid A) (resid 44 and name HD11 and segid B) 3.400 1.600 1.600 !
assign (resid 54 and name HE# and segid A) (resid 49 and name HB# and segid B) 3.400 1.600 1.600 !
assign (resid 54 and name HE# and segid A) (resid 49 and name HG# and segid B) 3.400 1.600 1.600 !
assign (resid 54 and name HE# and segid A) (resid 70 and name HG21 and segid B) 3.400 1.600 1.600 !

assign (resid 56 and name HD11 and segid A) (resid 8 and name HD11 and segid B) 3.400 1.600 1.600 !
assign (resid 56 and name HD11 and segid A) (resid 8 and name HD21 and segid B) 3.400 1.600 1.600 !
assign (resid 56 and name HD11 and segid A) (resid 44 and name HG11 and segid B) 3.400 1.600 1.600 !
assign (resid 56 and name HD11 and segid A) (resid 44 and name HG21 and segid B) 3.400 1.600 1.600 !
assign (resid 56 and name HD11 and segid A) (resid 70 and name HG11 and segid B) 3.400 1.600 1.600 !
assign (resid 56 and name HD11 and segid A) (resid 70 and name HG21 and segid B) 3.400 1.600 1.600 !
assign (resid 56 and name HG21 and segid A) (resid 8 and name HD11 and segid B) 3.400 1.600 1.600 !
assign (resid 56 and name HG21 and segid A) (resid 8 and name HD21 and segid B) 3.400 1.600 1.600 !
assign (resid 56 and name HG21 and segid A) (resid 44 and name HG21 and segid B) 3.400 1.600 1.600 !
assign (resid 56 and name HG21 and segid A) (resid 44 and name HD11 and segid B) 3.400 1.600 1.600 !
assign (resid 56 and name HG21 and segid A) (resid 70 and name HG11 and segid B) 3.400 1.600 1.600 !
assign (resid 56 and name HG21 and segid A) (resid 70 and name HG21 and segid B) 3.400 1.600 1.600 !
assign (resid 56 and name HG11 and segid A) (resid 70 and name HG11 and segid B) 3.400 1.600 1.600 !
assign (resid 56 and name HG11 and segid A) (resid 70 and name HG21 and segid B) 3.400 1.600 1.600 !
assign (resid 56 and name HG12 and segid A) (resid 70 and name HG11 and segid B) 3.400 1.600 1.600 !
assign (resid 56 and name HG12 and segid A) (resid 70 and name HG21 and segid B) 3.400 1.600 1.600 !
assign (resid 56 and name HB# and segid A) (resid 70 and name HG11 and segid B) 3.400 1.600 1.600 !

assign (resid 67 and name HD11 and segid A) (resid 42 and name HB# and segid B) 3.400 1.600 1.600 !
assign (resid 67 and name HD11 and segid A) (resid 42 and name HD1 and segid B) 3.400 1.600 1.600 !
assign (resid 67 and name HD11 and segid A) (resid 42 and name HD2 and segid B) 3.400 1.600 1.600 !
assign (resid 67 and name HD11 and segid A) (resid 44 and name HG1# and segid B) 3.400 1.600 1.600 !
assign (resid 67 and name HD11 and segid A) (resid 44 and name HD11 and segid B) 3.400 1.600 1.600 !
assign (resid 67 and name HD11 and segid A) (resid 49 and name HB# and segid B) 3.400 1.600 1.600 !
assign (resid 67 and name HD11 and segid A) (resid 49 and name HG# and segid B) 3.400 1.600 1.600 !

assign (resid 67 and name HG21 and segid A) (resid 44 and name HD11 and segid B) 3.400 1.600 1.600 !

assign (resid 67 and name HG1# and segid A) (resid 44 and name HD11 and segid B) 3.400 1.600 1.600 !

B.2 hUbc13 Chemical Shifts at 30 °C

Main chain amide ^{15}N, $^{1}H_N$ and various carbon chemical shifts

Residue	^{15}N	$^{1}H_N$	$^{13}C_\alpha$	$^{13}C_\beta$	$^{13}C_\gamma$	$^{13}C_\delta$	$^{13}C_\epsilon$
R12			58.921	30.370		42.926	
I13	115.657	7.311	65.833	38.132	17.435	14.036	
I14	124.247	7.674	65.315	37.958	16.925	12.977	
K15	119.218	8.582	59.286	31.932	24.856	28.908	41.853
E16	118.129	8.487	61.389	31.595	38.573		
T17	115.958	8.329	68.253	68.244	21.001		
Q18	119.732	8.430	59.252	28.211	34.069		
R19	118.753	8.013	58.908	29.702	27.451	43.035	
L20	121.432	8.087	57.488	42.271	27.058	24.495	
L21	116.543	7.713	56.598	41.746	27.304	23.197, 25.242	
A22	120.049	7.845	53.840	19.771			
E23	118.153	8.008	53.056	30.344			
P24			63.018	32.651	27.275	50.270	
V25	125.714	9.382	60.130	33.126	21.843		
P26			64.234	31.555	27.821		
G27	111.961	8.563	45.596				
I28	120.216	8.258	57.462	40.491	26.674, 17.471	14.849	
K29	129.460	9.033	55.112	34.707	24.858	29.246	41.824
A30	127.121	8.375	51.192	21.522			
E31	120.623	8.483	52.778	32.746			
P32			61.500	31.286	26.834		

D33	123.956	8.722	54.625	43.598			
E34	124.503	8.700	58.749	29.951	36.192		
S35	113.782	8.603	59.178	64.167			
N36	119.808	7.935	52.857	38.733			
A37	126.129	8.475	53.801	19.105			
R38	111.202	7.659	57.237	30.149		42.354	
Y39	119.002	8.061	56.630	40.657			
F40	120.698	9.548	55.984	41.934			
H41	122.140	8.785	55.529	31.054			
V42	126.452	8.403	60.092	34.319	21.131, 22.136		
V43	127.641	9.291	61.202	34.771	21.236, 22.289		
I44	126.838	9.461	60.279	38.472	27.801, 16.452	14.039	
A45	130.162	8.477	51.512	19.097			
G46	110.540	9.259	44.338				
Q48			57.561	28.978	33.828		
D49	119.789	9.363	56.453	39.316			
S50	115.403	7.902	57.458	65.604			
P51			63.539	31.829	27.729	50.184	
F52	115.172	7.279	55.362	39.391			
E53	123.161	7.400	58.387	30.056	35.884		
G54	116.011	9.262	44.818				
G55	106.661	8.429	44.677				
T56	118.778	9.181	61.901	70.216	22.218		
F57	123.155	8.731	57.150	41.097			
K58	123.131	9.281	55.691	33.844	25.819	29.405	41.907
L59	124.389	9.513	54.870	45.799	28.220	25.391, 27.089	
E60	121.881	8.782	54.724	33.654	37.534		
L61	127.697	8.309	53.956	45.590		24.966, 27.099	

F62	126.516	9.380	54.913	42.924			
L63	126.943	8.370	50.058	29.458	25.518	21.910, 26.618	
E65			60.281	29.217	36.681		
E66	114.321	8.749	57.049	29.369	37.053		
Y67	124.915	8.285	58.335	39.583			
P68			64.124	33.232			
M69	125.492	9.037	57.163	30.614	33.004		16.752
A70	120.004	6.785	49.697	22.451			
A71	119.799	7.258	49.341	18.218			
P72			61.984	31.715	27.020		
K73	120.538	8.758	54.582	33.176			42.106
V74	122.625	8.652	59.589	34.749	21.528, 22.386		
R75	122.296	8.446	54.643	33.771		43.767	
F76	124.214	10.198	59.987	40.227			
M77	121.098	9.446	54.880	32.862			
T78	118.999	7.478	62.674	71.888	22.731		
K79	128.507	8.600	58.270	33.133	22.741	28.700	41.426
I80	119.975	8.111	60.380	40.925	13.885	12.828	
Y81	133.391	8.808	57.708	37.050			
H82	123.017	7.906	54.248	35.565			
P83			64.282	32.100	26.492	44.487	
N84	118.003	10.901	53.515	40.723			
V85	120.026	7.346	60.845	34.779	19.863, 20.921		
D86	125.993	8.455	52.542	41.791			
K87	115.345	8.248	58.525	32.229	24.919	29.434	42.051
L88	120.852	8.144	54.373	42.045	27.364	23.011, 24.926	
G89	109.471	8.355	46.020				
R90	121.259	8.574	56.955	29.910			

I91			60.269	40.905	18.183	15.388	
C92	128.230	8.789	57.669	26.604			
L93	125.941	7.270	53.632	46.336			
D94	129.256	9.305	58.116	39.040			
I95	116.455	8.389	64.103	38.173	18.153	15.332	
L96	113.358	7.267	53.889	41.310	27.155	25.552	
K97	122.880	7.880	56.151	32.856	24.718	29.313	41.924
D98	120.541	8.806	55.939	40.585			
K99	115.413	7.761	54.582	31.817	25.052	28.459	41.952
W100	120.769	7.344	59.265	29.924			
S101	120.703	5.463	54.550	64.991			
P102			63.852	31.688	27.193	52.621	
A103	119.128	7.348	52.891	18.895			
L104	119.227	7.389	54.135	41.499		22.228, 26.479	
Q105	111.173	7.132	53.819	32.475	34.230		
I106	123.917	9.982	66.741	37.557	17.796	13.373	
R107	117.755	9.261	60.468	30.418	27.481	42.843	
T108	113.087	7.121	66.108	68.914	22.850		
V109	122.756	7.806	67.020	31.431	21.814, 23.410		
L110	117.737	8.136	58.268	40.618	25.821		
L111	118.485	8.278	58.190	42.324	27.466		
S112	116.432	8.090	62.733	63.100			
I113	123.436	8.099	65.545	37.723	17.764	15.144	
Q114	119.793	8.033	60.395	30.396	34.316		
A115	120.422	8.177	54.879	17.965			
L116	120.176	7.665	56.397	42.573		24.771	
L117	119.327	7.681	58.048	41.246	27.170	22.580, 25.110	
S118	110.474	7.286	60.774	63.884			

A119	124.118	7.853	49.980	19.123			
P120			62.855	31.819	27.071	49.284	
N121	116.791	8.739	49.616	39.170			
P122			63.494	32.322	26.938		
D123	116.956	7.620	54.849	40.946			
D124	120.786	7.123	52.409	41.984			
P125			63.917	32.755	26.840	50.226	
L126	119.014	8.324	54.611	42.935	27.200	23.817, 24.625	
A127	123.266	7.627	51.996	18.791			
D129			56.895	39.536			
V130	122.141	7.805	65.366	31.678	20.734, 21.580		
A131	122.067	8.248	55.885	18.922			
E132	116.620	8.033	59.651	29.251	35.864		
Q133	120.359	7.771	58.717	28.388	33.782		
W134	120.666	8.467	61.386	28.668			
K135	112.864	7.927	58.332	33.155	24.904	28.72	41.605
T136	111.342	8.060	64.058	70.298	21.680		
N137	122.784	8.457	52.081	38.092			
E138	125.808	8.515	60.430	30.416	36.385		
A139	118.296	8.367	51.442	17.888			
Q140	117.57	7.319	57.714	28.942	34.170		
A141	125.561	7.996	55.036	17.145			
I142	117.529	8.146	65.271	37.666	16.956	13.547	
E143	119.175	7.475	59.395	28.966	35.867		
T144	120.212	8.286	66.666	68.277	20.124		
A145	125.032	8.665	55.904	18.657			
R146	121.727	8.696	59.776	30.396	27.674	43.45	
A147	125.015	8.391	55.559	17.661			

W148	119.388	9.742	61.052	29.117			
T149			68.225	68.183	22.507		
R150	120.138	7.615	58.923	30.060	27.524	43.278	
L151	117.074	7.998	57.215	42.797	26.585	23.410, 24.065	
Y152	112.407	8.060	57.597	40.668			
A153	121.815	8.070	51.119	21.731			
M154	116.776	7.647		34.307			
N156			53.511	38.596			
I157	124.463	7.577	62.751	39.413	18.142	13.627	

Main chain amide ^{15}N, $^{1}H_N$ and various hydrogen chemical shifts

Residue	^{15}N	$^{1}H_N$	$^{1}H_\alpha$	$^{1}H_\beta$	$^{1}H_\gamma$	$^{1}H_\delta$	$^{1}H_\epsilon$
R12			4.231				
I13	115.657	7.311	3.735	1.939	0.896	1.006	
I14	124.247	7.674	3.769	2.040	0.970, 1.598	0.913	
K15	119.218	8.582	4.171	1.974, 2.008	1.529, 1.617	1.734	3.003
E16	118.129	8.487	4.123				
T17	115.958	8.329	3.836	4.514	1.311		
Q18	119.732	8.430	4.034	2.314, 2.155	2.485, 2.706		
R19	118.753	8.013	4.176	2.013	1.811, 1.865	3.258	
L20	121.432	8.087	4.063	1.708, 1.926	1.828	0.713	
L21	116.543	7.713	4.298	1.640, 1.878	1.996	1.051, 0.977	
A22	120.049	7.845	4.329	1.558			
E23	118.153	8.008					
P24			4.731	2.517	2.006, 2.065	3.443, 3.590	
V25	125.714	9.382	4.256	1.994	0.998		
G27	111.961	8.563	3.757, 4.269				
I28	120.216	8.258	5.020	1.864	0.724	0.618	

K29	129.460	9.033	4.797	1.776, 1.880	1.402, 1.532	1.703	2.980
A30	127.121	8.375	5.344	1.235			
E31	120.623	8.483					
P32			4.130				
D33	123.956	8.722	4.454	2.272, 3.314			
E34	124.503	8.700	4.011	2.041	2.315		
S35	113.782	8.603	4.595	3.888			
N36	119.808	7.935	4.722	2.790, 3.068			
A37	126.129	8.475	4.171	1.431			
R38	111.202	7.659					
Y39	119.002	8.061	5.239	2.894			
F40	120.698	9.548	4.834	2.268, 2.899			
H41	122.140	8.785	4.930	3.137, 3.190			
V42	126.452	8.403	5.316	1.903	0.812		
V43	127.641	9.291	5.048	1.955	0.859		
I44	126.838	9.461	4.813	1.610	0.898	0.671	
A45	130.162	8.477	4.905	1.529			
G46	110.540	9.259					
Q48			4.073	2.046, 2.141			
D49	119.789	9.363	4.435	3.031			
S50	115.403	7.902					
P51			4.317				
F52	115.172	7.279	5.393	2.476, 3.954			
E53	123.161	7.400	3.701	2.302	2.337		
G54	116.011	9.262	4.433, 3.762				
G55	106.661	8.429	3.492, 4.487				
T56	118.778	9.181	4.560	3.855	1.084		
F57	123.155	8.731	4.625	2.882, 3.106			

K58	123.131	9.281	5.125	1.769, 1.953	1.463	1.720	2.986
L59	124.389	9.513	5.065	1.019, 1.295	1.070	0.199	
E60	121.881	8.782	4.973	2.101	2.109, 2.354		
L61	127.697	8.309	5.249	1.183, 1.484	1.343	0.319, 0.460	
F62	126.516	9.380	5.546	2.658, 2.772			
L63	126.943	8.370	4.330	1.572	1.329	0.539	
E65			3.740	2.022	2.344		
E66	114.321	8.749	4.323	1.875, 2.183	2.235, 2.360		
Y67	124.915	8.285					
P68			3.723				
M69	125.492	9.037	4.487	2.244	2.593, 2.787		2.111
A70	120.004	6.785	4.319	1.139			
A71	119.799	7.258					
P72			4.283				
K73	120.538	8.758	4.634				
V74	122.625	8.652	5.314	1.762	0.692		
R75	122.296	8.446	4.975	1.702, 1.847	1.498	3.122, 3.275	
F76	124.214	10.198	4.554	3.046, 3.420			
M77	121.098	9.446	4.689	1.725, 2.348	2.360, 2.609		
T78	118.999	7.478	4.497	4.077	1.726		
K79	128.507	8.600	4.118	1.202, 1.361	1.181, 1.331	0.494, 0.905	2.263
I80	119.975	8.111	4.818	1.619	0.167		
Y81	133.391	8.808	3.981	2.268			
H82	123.017	7.906					
P83			4.031	1.519	0.899		
N84	118.003	10.901	4.872	2.346, 3.425			
V85	120.026	7.346	4.984	1.489	0.757		
D86	125.993	8.455	4.841	3.503			

K87	115.345	8.248	4.396	2.018	1.578, 1.672	1.837	3.138
L88	120.852	8.144	4.585	1.825, 1.892	1.641	0.916	
G89	109.471	8.355	3.737, 4.795				
R90	121.259	8.574					
I91			4.674	1.523	0.665, 1.875	0.630	
C92	128.230	8.789	4.528	2.763, 2.920			
L93	125.941	7.270	4.709	1.366, 1.549		0.865, 0.914	
D94	129.256	9.305	4.343	2.699, 2.820			
I95	116.455	8.389	3.826	2.126	0.968, 1.356	0.954	
L96	113.358	7.267	4.607			0.859	
K97	122.88	7.880	4.580	1.887, 2.048	1.492, 1.567	1.766	3.039
D98	120.541	8.806	4.623	2.793			
K99	115.413	7.761	4.554				2.970
W100	120.769	7.344	3.698	2.869			
S101	120.703	5.463					
P102			4.416	1.871, 2.088			
A103	119.128	7.348	4.128	1.197			
L104	119.227	7.389	4.141	0.886, 1.073	1.345	0.730, 0.818	
Q105	111.173	7.132	5.040	2.608	2.246, 2.357		
I106	123.917	9.982	3.341	1.710	0.368, 0.470	0.312	
R107	117.755	9.261					
T108	113.087	7.121	3.924	4.388	1.359		
V109	122.756	7.806	3.472	2.440	1.163		
L110	117.737	8.136					
L111	118.485	8.278	3.993	1.582, 1.939	1.724	0.944	
S112	116.432	8.090	4.356	4.110, 3.890			
I113	123.436	8.099	3.513	1.696	0.619	0.566	
Q114	119.793	8.033	3.725	2.494	2.233		

A115	120.422	8.177	4.223	1.571			
L116	120.176	7.665	4.168			0.690	
L117	119.327	7.681	3.920	2.029, 1.246	1.524	0.467	
S118	110.474	7.286	4.461	4.015			
A119	124.118	7.853	4.864	1.273			
P120			4.183				
N121	116.791	8.739					
P122			4.045	1.940, 2.153	1.813		
D123	116.956	7.620	4.593	2.612, 2.768			
D124	120.786	7.123					
P125			4.220				
L126	119.014	8.324	4.499	1.556	1.525	0.836, 0.910	
A127	123.266	7.627	4.515	1.424			
D129			4.419	2.764, 2.852			
V130	122.141	7.805	3.651	1.913	0.629		
A131	122.067	8.248	3.892	1.627			
E132	116.62	8.033	4.095	2.134, 2.213	2.316, 2.359		
Q133	120.359	7.771					
W134	120.666	8.467					
K135	112.864	7.927	4.260	1.978			
T136	111.342	8.060	4.283	4.242	1.324		
N137	122.784	8.457	4.823	2.597, 3.010			
E138	125.808	8.515	3.606	2.322	2.106		
A139	118.296	8.367	3.949	1.412			
Q140	117.57	7.319	3.989	1.934	2.263		
A141	125.561	7.996	3.922	0.566			
I142	117.529	8.146	3.188	1.719	0.784, 0.899	0.790	
E143	119.175	7.475	3.987		2.321		

T144	120.212	8.286	3.807	3.670			
A145	125.032	8.665	4.344	1.798			
R146	121.727	8.696	4.377				3.200
A147	125.015	8.391	4.221	1.742			
W148	119.388	9.742					
T149			4.341	4.858	1.127		
R150	120.138	7.615	4.262	1.948	1.698, 1.868	3.252, 3.299	
L151	117.074	7.998	3.929	0.388, 0.974	1.212	0.565, 0.582	
Y152	112.407	8.060	5.087	2.741, 3.581			
A153	121.815	8.070	4.907	1.157			
M154	116.776	7.647					
N156			4.710	2.786, 2.903			
I157	124.463	7.577	4.097	1.862	0.888, 1.408	0.859	